Tailored recovery of nutrients from the anaerobic membrane bioreactor (AnMBR) resource recovery platform and their subsequent beneficial reuse

by

Arvind Damodara Kannan

B.Tech., Anna University, 2012
M.Tech., Anna University, 2014
M.S., Manhattan College, 2017

AN ABSTRACT OF A DISSERTATION

submitted in partial fulfillment of the requirements for the degree

DOCTOR OF PHILOSOPHY

Department of Civil Engineering
Carl R. Ice College of Engineering

KANSAS STATE UNIVERSITY
Manhattan, Kansas

2022

Abstract

Agriculture runoff, animal farming wastewater, and processed livestock wastes contain high concentrations of nutrients and organic matter. There is a great potential to recover the nitrogen and phosphorus from agriculture wastewater as stabilized sludge biosolids or value-added Recovered Nutrient Products (RNPs) in the form of ammonia nitrogen and/or phosphorus (P) mineral precipitates, using suitable treatment technology. This research aims to demonstrate tailored recovery of valuable macronutrients like Nitrogen and Phosphorus from anaerobic environmental biotechnology platforms such as Anaerobic Membrane Bioreactors (AnMBR) treating swine wastewater from confined animal feeding operations (CAFOs) for targeted reuse as fertilizer products. The first objective of this study was the recovery of ammonium (NH_4^+) from real swine wastewater and simulated AnMBR treated swine permeate using natural clinoptilolite. Batch experimental results showed a maximum adsorption capacity of 14 mg N/g clinoptilolite from synthetic swine permeate. Column experiments revealed that the breakthrough times for the real swine and synthetic swine wastewaters to be similar indicating that the wastewater matrix did not really have an effect on ammonia adsorption. Ion release profiles showed sodium to be the main counter ion for ammonium capture. The presence of potassium ion had the greatest impact on ammonia adsorption and the selectivity series was summarized to be Potassium (K^+) > Calcium (Ca^{2+}) > Sodium (Na^+) > Magnesium (Mg^{2+}).

The second objective was to identify the core microbial community in Anaerobic sludge for beneficial soil application as stabilized biosolids. Results revealed that the core of the AnMBR microbial community represented by *Bacteroidetes*, *Proteobacteria*, *Firmicutes,* and *Chloroflexi* phyla is unique and not influenced by the influent wastewater microbial community. The AnMBR microbial community structure not only enables proactive ecological management for efficient

bioreactor operation but also informs the potential microbial interactions with the soil microbiota for beneficial land/crop application. The third objective aims to evaluate the ammonia sorbed clinoptilolite and anaerobically treated biosolids for cropland application and plant nutrient bioavailability. Soil incubation studies showed that the ammonia sorbed clinoptilolite exhibited slow nitrogen diffusion compared to conventional fertilizers such as urea and ammonium sulfate. However, biosolids obtained after anaerobic digestion of wastewater showed negligible nutrient release, likely due to slow mineralization of organic nitrogen over the duration of this study. In view of these results, additional greenhouse pot experiments were conducted with maize crop to evaluate plant nitrogen uptake with ammonia sorbed clinoptilolite as a supplement to urea application and possibly to reduce the urea application rate. Treatments included 100% urea, 90% urea+10% ammonia sorbed clinoptilolite mixture, 80% urea+20% ammonia sorbed clinoptilolite mixture, and 100% ammonia sorbed clinoptilolite. The treatments were compared for plant nitrogen uptake, total dry biomass, and leaf chlorophyll content. The results on plant dry biomass and leaf chlorophyll content showed no statistically significant difference between the different treatments, suggesting that the ammonia sorbed clinoptilolite can be used as a nitrogen supplement, effectively reducing nitrogen losses from urea.

The fourth objective of this dissertation aims to demonstrate sustainable recovery of phosphorus as high-quality calcium phosphate from anaerobic membrane bioreactor treated swine permeate for targeted use as fertilizer or raw material for the fertilizer industry. Phosphorus removal efficiencies from treated swine permeate were evaluated by adding various calcium/phosphorus molar ratios ranging from 1/1 to 12/1. Results showed that removal efficiencies were inconsistent in duplicate trials at the same calcium doses (maximum P removal 93 % in Trial 1 and <20 % removal in Trial 2). The variability in P removal was due to the high

bicarbonate alkalinity of the swine permeate, which buffered the system and thereby prevented it from reaching alkaline pH conditions ideal for P removal. Total alkalinity and initial solution pH had the greatest impact on P removal and caused unintended precipitation of non-specific calcium minerals (Calcite). The carbonate alkalinity from the permeate was removed using process modifications that included acid addition and aeration for stripping the CO_2. Carbonate removal resulted in 97% P removal with increased total P content (11.8% P) in the final product and its better solubility. Additional COD removal (~18%) was also observed during the flocculation process.

Finally, sequential recovery of phosphorus as struvite ($MgNH_4PO_4.6H_2O$) and calcium phosphate in the pH altered CO_2 stripped swine permeate was also investigated. The results of the preliminary test run conducted at pH 9.5, showed a P removal efficiency of 56.4% after Magnesium (Mg) addition at a Mg/P molar ratio of 2/1, followed by 40.9% P removal after Calcium (Ca) addition (Ca/P molar ratio of 4/1) resulting in a combined P removal efficiency of 97.3 %. Phase identification of the solid precipitate collected after Mg addition showed the presence of struvite mineral. Similar experiments performed at a pH of 8.5 showed a maximum combined P removal of 61%, with 15% P removal after Mg addition and 46.2 % P removal after Ca addition. These results showed that P can be effectively recovered from the modified swine permeate as tailor-made products such as struvite and calcium phosphates sequentially. Overall, the results of this dissertation demonstrate that AnMBRs can be a sustainable nutrient recovery platform enabling tailored recovery of nutrient products with commercial value. Additionally, the ammonia captured clinoptilolite can be used as a soil amendment to supplement conventional fertilizers and avoid their over application.

Tailored recovery of nutrients from the anaerobic membrane bioreactor (AnMBR) resource
recovery platform and their subsequent beneficial reuse

by

Arvind Damodara Kannan

B.Tech., Anna University, 2012
M.Tech., Anna University, 2014
M.S., Manhattan College, 2017

A DISSERTATION

submitted in partial fulfillment of the requirements for the degree

DOCTOR OF PHILOSOPHY

Department of Civil Engineering
Carl R. Ice College of Engineering

KANSAS STATE UNIVERSITY
Manhattan, Kansas

2022

Approved by:

Major Professor
Dr. Prathap Parameswaran

Copyright

Abstract

Agriculture runoff, animal farming wastewater, and processed livestock wastes contain high concentrations of nutrients and organic matter. There is a great potential to recover the nitrogen and phosphorus from agriculture wastewater as stabilized sludge biosolids or value-added Recovered Nutrient Products (RNPs) in the form of ammonia nitrogen and/or phosphorus (P) mineral precipitates, using suitable treatment technology. This research aims to demonstrate tailored recovery of valuable macronutrients like Nitrogen and Phosphorus from anaerobic environmental biotechnology platforms such as Anaerobic Membrane Bioreactors (AnMBR) treating swine wastewater from confined animal feeding operations (CAFOs) for targeted reuse as fertilizer products. The first objective of this study was the recovery of ammonium (NH_4^+) from real swine wastewater and simulated AnMBR treated swine permeate using natural clinoptilolite. Batch experimental results showed a maximum adsorption capacity of 14 mg N/g clinoptilolite from synthetic swine permeate. Column experiments revealed that the breakthrough times for the real swine and synthetic swine wastewaters to be similar indicating that the wastewater matrix did not really have an effect on ammonia adsorption. Ion release profiles showed sodium to be the main counter ion for ammonium capture. The presence of potassium ion had the greatest impact on ammonia adsorption and the selectivity series was summarized to be Potassium (K^+) > Calcium (Ca^{2+}) > Sodium (Na^+) > Magnesium (Mg^{2+}).

The second objective was to identify the core microbial community in Anaerobic sludge for beneficial soil application as stabilized biosolids. Results revealed that the core of the AnMBR microbial community represented by *Bacteroidetes*, *Proteobacteria*, *Firmicutes,* and *Chloroflexi* phyla is unique and not influenced by the influent wastewater microbial community. The AnMBR microbial community structure not only enables proactive ecological management for efficient

bioreactor operation but also informs the potential microbial interactions with the soil microbiota for beneficial land/crop application. The third objective aims to evaluate the ammonia sorbed clinoptilolite and anaerobically treated biosolids for cropland application and plant nutrient bioavailability. Soil incubation studies showed that the ammonia sorbed clinoptilolite exhibited slow nitrogen diffusion compared to conventional fertilizers such as urea and ammonium sulfate. However, biosolids obtained after anaerobic digestion of wastewater showed negligible nutrient release, likely due to slow mineralization of organic nitrogen over the duration of this study. In view of these results, additional greenhouse pot experiments were conducted with maize crop to evaluate plant nitrogen uptake with ammonia sorbed clinoptilolite as a supplement to urea application and possibly to reduce the urea application rate. Treatments included 100% urea, 90% urea+10% ammonia sorbed clinoptilolite mixture, 80% urea+20% ammonia sorbed clinoptilolite mixture, and 100% ammonia sorbed clinoptilolite. The treatments were compared for plant nitrogen uptake, total dry biomass, and leaf chlorophyll content. The results on plant dry biomass and leaf chlorophyll content showed no statistically significant difference between the different treatments, suggesting that the ammonia sorbed clinoptilolite can be used as a nitrogen supplement, effectively reducing nitrogen losses from urea.

The fourth objective of this dissertation aims to demonstrate sustainable recovery of phosphorus as high-quality calcium phosphate from anaerobic membrane bioreactor treated swine permeate for targeted use as fertilizer or raw material for the fertilizer industry. Phosphorus removal efficiencies from treated swine permeate were evaluated by adding various calcium/phosphorus molar ratios ranging from 1/1 to 12/1. Results showed that removal efficiencies were inconsistent in duplicate trials at the same calcium doses (maximum P removal 93 % in Trial 1 and <20 % removal in Trial 2). The variability in P removal was due to the high

bicarbonate alkalinity of the swine permeate, which buffered the system and thereby prevented it from reaching alkaline pH conditions ideal for P removal. Total alkalinity and initial solution pH had the greatest impact on P removal and caused unintended precipitation of non-specific calcium minerals (Calcite). The carbonate alkalinity from the permeate was removed using process modifications that included acid addition and aeration for stripping the CO_2. Carbonate removal resulted in 97% P removal with increased total P content (11.8% P) in the final product and its better solubility. Additional COD removal (~18%) was also observed during the flocculation process.

Finally, sequential recovery of phosphorus as struvite ($MgNH_4PO_4.6H_2O$) and calcium phosphate in the pH altered CO_2 stripped swine permeate was also investigated. The results of the preliminary test run conducted at pH 9.5, showed a P removal efficiency of 56.4% after Magnesium (Mg) addition at a Mg/P molar ratio of 2/1, followed by 40.9% P removal after Calcium (Ca) addition (Ca/P molar ratio of 4/1) resulting in a combined P removal efficiency of 97.3 %. Phase identification of the solid precipitate collected after Mg addition showed the presence of struvite mineral. Similar experiments performed at a pH of 8.5 showed a maximum combined P removal of 61%, with 15% P removal after Mg addition and 46.2 % P removal after Ca addition. These results showed that P can be effectively recovered from the modified swine permeate as tailor-made products such as struvite and calcium phosphates sequentially. Overall, the results of this dissertation demonstrate that AnMBRs can be a sustainable nutrient recovery platform enabling tailored recovery of nutrient products with commercial value. Additionally, the ammonia captured clinoptilolite can be used as a soil amendment to supplement conventional fertilizers and avoid their over application.

Table of Contents

List of Figures

List of Tables

Acknowledgements

I am grateful to my advisor, Dr. Prathap Parameswaran, for the opportunity to pursue my doctoral study under his guidance. I owe him a huge debt of gratitude for his patience and encouragement as I went through the different phases of my PhD journey.

Additionally, I want to thank my committee members Dr. Jeongdae Im, Dr. Matthew Kirk, and Dr. Ganga Hettiarachchi, for their guidance, thoughtful comments and ideas.

I would like to acknowledge all the present and past undergraduate members of our research group, Amy Kowalczewski, Elizabeth Motter, Caitlin Swope, and Jack Dillavou, for dedicatedly helping with my research in the lab. I would also like to thank the graduate students Chris Chiu, Evan Heronemus, Priyasha Fernando, and Emily Randig for all the fun and support in the office. I specially want to thank my lab mate and former PhD colleague Dr. Kahao Lim for helping me in all aspects of my research. I would also like to thank Dr. Ruwandi Kumarasinghe and Kasuni Gamage for all their help during my experiments in the soil chemistry lab.

Chapter 1 - Background and Literature Review

1.1 Need for nutrient recovery

The increasing global food production driven by the rapidly growing human population has accelerated the demand for nutrient fertilizers. Nutrients such as nitrogen (N) and phosphorus (P) are critical for the plant growth and livestock operations and to ensure continuous food supply (Sengupta et al., 2015). While mineral fertilizers are essential for agriculture and food production, not all the applied nutrients are utilized by plants and a large proportion of such nutrients are wasted or lost to the environment (Tilman et al., 2002). Such fertilizer nutrient losses increase agricultural cost, waste energy, and pollute the environment, thereby affecting the sustainability of modern agriculture (Chen et al., 2018). In addition, there is an increasing amount of nutrient-rich wastewaters generated from diverse sources including municipal, agricultural and industrial wastewaters such as swine, poultry, dairy, wool scours, abattoirs, human urine, sewage, tanneries, etc. (Kumar & Pal, 2015; Saliu & Oladoja, 2021). If discharged untreated, nutrient rich wastewaters can pose adverse public health risks and environmental impacts including harmful freshwater algal blooms, exposure to harmful pathogens, heavy metals, and negative effects to surface water and groundwater quality (Sampat et al., 2018). Therefore, there is a need to move from the current linear approach in nutrient utilization to a more sustainable circular economy model. In the circular economy, the nutrients or energy move between different elements in an ecosystem changing their form and use without being wasted (Deutz, 2020). The nutrients can be recovered from wastewater or animal waste, for example, and used in agricultural production, helping to reduce dependency on unsustainable nitrogen and phosphorus fertilizer production methods.

Although N is the most abundant element in the earth's atmosphere, its availability as a synthetic ammonia (urea) fertilizer is currently reliant upon the Haber Bosch process (Mulder, 2003). Haber Bosch process is an energy intensive ammonia generation (~10 kWh/kg N) process consuming large amounts of fossil fuels for energy and resulting in significant quantities of greenhouse gas emissions (Maurer et al., 2003; Razon, 2014). Similarly, phosphorus, a non-renewable resource is an essential macronutrient supporting all life forms and extensively used as a fertilizer (Azam et al., 2019). The main source of P for societal use is from the mining of phosphate rock. Such mineral phosphate rock reserves are predominantly located in just a handful of countries, increasing supply chain dependency and impact on global food security (Cordell & Neset, 2014; Blackwell et al., 2019; Golroudbary et al., 2019). While mineral fertilizers are essential for agriculture and food production, not all the applied nutrients are utilized by plants and a large proportion is wasted or lost to the environment (Tilman et al., 2002). Such fertilizer nutrient losses increase agricultural costs, waste energy, negatively impact global climate, and pollute the environment, thereby affecting the sustainability of modern agriculture (Chen et al., 2018).

On the other hand, there is great potential to recover N, P, and other value-added products from wastewater through appropriate resource recovery technologies. The choice of the resource recovery platform is dictated by the concentrations of nutrients (N and P) and organic carbon in the wastewaters, which could vary widely depending on the type or source of wastewater (Feng et al., 2009).

In the case of livestock (such as swine) farming in confined animal feeding operations, animals are fed a nutrient rich diet (including cereals etc.) which are often not fully assimilated by the animals. This low efficiency of cereal uptake results in nutrient accumulation in animal wastes

and can lead to negative environmental impacts (Martinez et al., 2009). Additionally, livestock waste is a major source of pathogens, odor, pollution and greenhouse gas emissions, contributing to around 40% of global methane (Sorathiya et al., 2014).

Overall, agriculture runoff, swine wastewater, and processed livestock wastes contain high concentrations of nutrients and organic matter. Apart from nutrients, livestock waste also offer great potential for waste-to-energy applications such as biogas production or other carbon valorization routes such as the carboxylate platform, which can allow agricultural farmers to reduce their reliance on fossil fuels and generate energy and revenue from their farm-based products (Muller et al., 2007; Agler et al., 2011; Seiple et al., 2017). Thus, for economic and environmental reasons, it makes sense to adopt sustainable waste management practices while maintaining the profitability of farming operations through circular economy.
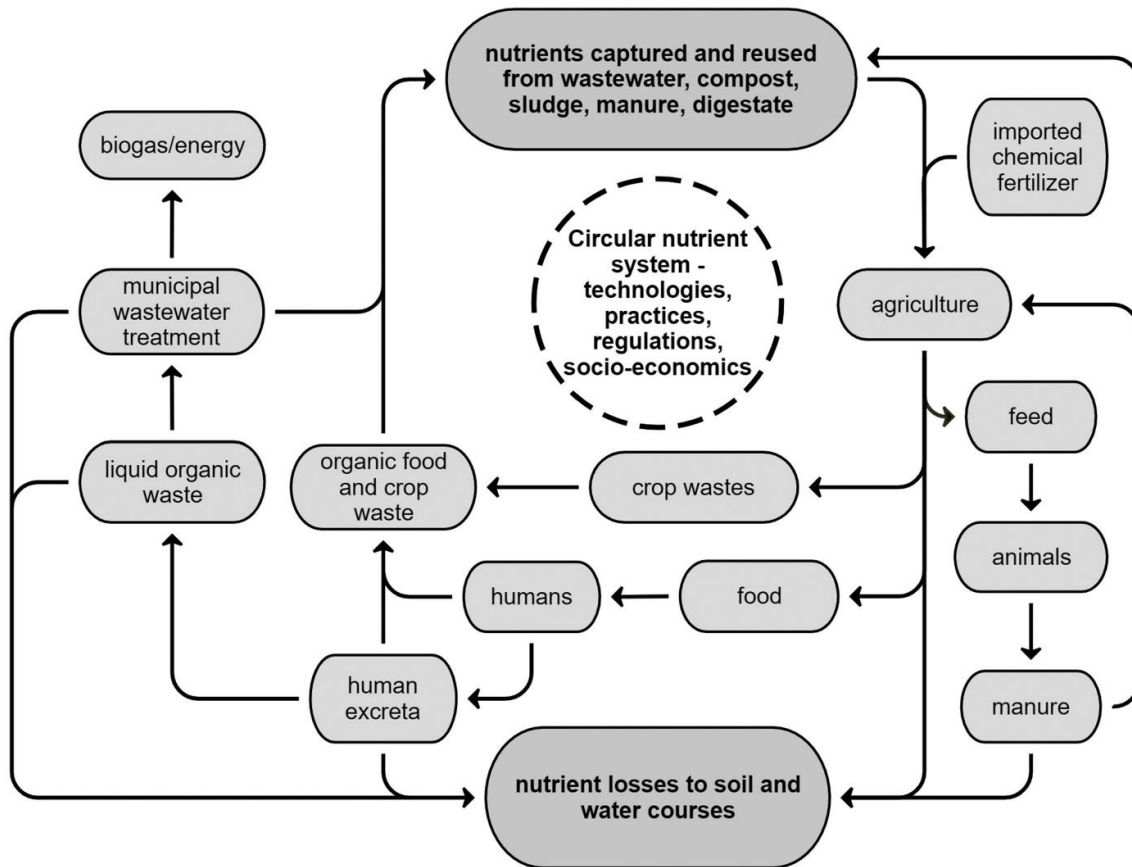
Figure 1.1 Overview of the constituent components of the agriculture and wastewater sectors that comprise the circular nutrient system (Rosemarin et al., 2020). Note: Reprinted from "Rosemarin, A., Macura, B., Carolus, J., Barquet, K., Ek, F., Järnberg, L., Lorick, D., Johannesdottir, S., Pedersen, S. M., Koskiaho, J., Haddaway, N. R., & Okruszko, T. (2020). Circular nutrient solutions for agriculture and wastewater – a review of technologies and practices. *Current Opinion in Environmental Sustainability*, *45*, 78-91. © 2020 Elsevier Inc. All rights reserved.

1.2 Anaerobic treatment processes

Anaerobic processes are predominant treatment platforms for treating livestock wastes which can produce gaseous (biogas) fuel by degrading organic matter (Cantrell et al., 2008). A community of anaerobic microorganisms are responsible for the breakdown of organic matter which occur in three separate stages namely: hydrolysis, fermentation (acidogenesis and acetogenesis), and methanogenesis Metcalf et al., 1991). Several intermediate products generated

during different stages of digestion are eventually metabolized to methane (CH_4) which can be used for energy generation (Chen et al., 2002). During anaerobic treatment, the nutrients present in the wastewater remain untreated in their reduced form and require post digestion nutrient treatment (Ma et al., 2018). The residual solid products from anaerobic processes are nutrient-rich with potential for reuse as soil fertilizer (Van Lier et al., 2008).

However, anaerobic processes suffer from several drawbacks limiting their widespread implementation as a standalone technology. Anaerobic bacteria are slow growers, highly sensitive to changes in pH; operating anaerobic processes at low temperatures are challenging, and the system requires a sufficient amount of alkalinity within the reactor (Stuart, 2006). Furthermore, anaerobic processes and cogeneration units allow only part of the energy consumed (20-30%) to be recovered and their economic viability depends on exploiting other benefits of the process such as nutrient capture and recovery for subsequent sale as inorganic fertilizers. Equally important to note is that the final effluent water quality from these conventional anaerobic platforms do not directly meet discharge or reuse standards and necessitate further treatment prior to end-use. Thus, it is necessary to change the paradigm of wastewater treatment to evolve toward a more sustainable scenario with the goal of turning wastewater into an endless source of energy and nutrients while progressively shifting from removal to recovery-based processes.

1.3 Anaerobic membrane bioreactors

One such emerging wastewater technology that facilitates treatment of high strength wastewater and enables subsequent recovery of nutrients like N and P as valuable fertilizer products along with water for indirect potable reuse is the Anaerobic Membrane Bioreactor (AnMBR). AnMBRs combine anaerobic treatment process and physical separation using

membranes resulting in high treatment efficiency and reuse quality permeate (Smith et al., 2012; Evans et al., 2019; Lim et al., 2019). AnMBRs can effectively degrade the organic pollutants within the bioreactor to produce methane gas while the membranes, either as side stream or submerged configuration, ensure retention of all suspended biomass to produce high quality nutrient rich permeate. Thus, it is possible to recover the nutrients from the permeate in a concentrated, purer, and tailored form through various nutrient recovery techniques.

1.3.1 Nutrient recovery from AnMBR systems

Literature on nutrient recovery from AnMBRs is lacking as the focus of most studies has largely been on the biological treatment of organic pollutants for energy positive treatment and addressing the issue of membrane fouling (Liao et al., 2006; Kim et al., 2011). Limited studies addressing nutrient management from treated AnMBR suggest direct land application of the permeate for soil fertigation (Prieto et al., 2013; Pretel et al., 2015). However, land application of permeate does not allow for tailored application of ammonia and phosphorus. Additionally, the presence of high sulfide concentrations in the permeate also need to be addressed (Damodara Kannan et al., 2020). For instance, coagulation based nutrient removal requires additional chemical dosing to remove the sulfides along with the phosphorus (Evans et al., 2018; Lim et al., 2019).

1.4 Nutrient recovery techniques

Several nutrient removal techniques exist including biological nitrogen removal which destroys organic nitrogen and converts to nitrogen gas. However, biological nitrogen removal processes will severely reduce the cost and energy benefits created from AnMBRs due to the energy requirement of continuous air supply for nitrification and the addition of external carbon as electron donor for denitrification (Deng et al., 2014). This section primarily summarizes

processes which are currently used for or have the potential for recovery of nutrients as valuable products rather than achieving mere nutrient removal.

1.4.1 Chemical precipitation

Chemical precipitation as Struvite ($Mg.NH_4.PO_4. 6H_2O$) mineral is a well-established technology for simultaneous orthophosphate and ammonia recovery from wastewaters (Jordaan et al., 2010; Huang et al., 2011). Chemical precipitation involves addition of Magnesium (Mg) salts as MgO, $MgCl_2$ and $Mg(OH)_2$ to induce precipitate formation with ammonium (NH_4^+) and phosphate (PO_4^{3-}) (Stolzenburg et al., 2015). This is because Mg is considered the limiting ion for struvite precipitation in wastewater systems and thus requires additional source of Mg. Struvite exhibits slow-release fertilizer properties and is considered a valuable nutrient product (Britton et al., 2007). Several factors affect struvite formation such as pH, solubility, temperature, phosphate supersaturation, and presence of foreign ions (Azam et al., 2019). Of these, pH and presence of foreign ions are very important. Optimum pH of struvite precipitation is reported to be between 8.5-10 (Jaffer et al., 2002; Nelson et al., 2003; Çelen et al., 2007). Although at higher pH, the availability of PO_4^{3-} increases, ammonia undergoes volatilization and is unavailable for struvite precipitation reaction. Thus, operating at an optimum pH condition is needed to maximize P and N recovery as struvite.

Table 1.1 Summary of different commercial P recovery technologies. Information obtained from Barak (2017); de Boer et al. (2018); Egle et al. (2016); Ghosh et al. (2019)

Technology	Type of reactor	Removal efficiency (%)	Final product	Product P content (wt % P_2O_5)
Ostara Pearl	Fluidized bed reactor	85	Struvite	28
Multiform	Fluidized bed reactor	80-90	Struvite	-
DHV crystalactor	Fluidized bed reactor	70-80	Calcium phosphate	25.9
Phosnix	Fluidized bed reactor	90	Struvite	30.5
Airprex	Stirred	90	Struvite	19.8-22.9
PHOSPAQ	Stirred	85	Struvite	-
NuReSys	Stirred	85	Struvite	26.5-27.8
ANPHOS	Stirred	80-90	Struvite	14.7
PHOXNAN	-	50	magnesium ammonium phosphate (MAP)	26.8
Calprex	Fluidized bed reactor	50%	Calcium phosphate (Brushite)	29.8

Additionally, the presence of competing ions such as potassium and calcium also affect struvite precipitation. Potassium ions interfere to form K-struvite ($K.NH_4.PO_4. 6H_2O$), an analogue of magnesium struvite (Shih & Yan, 2016), while calcium forms calcium-based P minerals. Overall, it is estimated that if precipitation of soluble P as struvite can recover 10 – 50% of influent P depending on the treatment process (Kehrein et al., 2020).

Another widely used technique for P removal is coagulation and flocculation by the addition of ferric chloride ($FeCl_3$), ferrous sulphate ($FeSO_4$), lime ($Ca (OH)_2$), calcium chloride ($CaCl_2$), and alum ($KAl_2.12H_2O$). However, coagulation results in huge amount of sludge generation and it is difficult to separate the phosphorus from the formed precipitate (Yargeau, 2012). Although coagulation is effective from a nutrient removal perspective, it still has limitations as a recovery process. Within the context of AnMBR permeate, studies have reported P removal using chemical coagulation would require large chemical doses to effectively remove both P as well as the sulfides present in the anaerobic permeate. The chemical precipitation of phosphorus as a high-quality calcium phosphate product is discussed in Chapter 6 of this dissertation. In Chapter 7, the sequential recovery of both struvite and calcium phosphate was examined.

1.4.2 Ammonia stripping

Ammonia stripping involves the conversion of aqueous ammonium from the waste stream to ammonia gas by raising the pH.The ammonia gas can then be recovered using an acidic solution (usually sulfuric or nitric acid). The resulting nutrient products, ammonium sulfate ($(NH_4)_2SO_4$ and ammonium nitrate (NH_4NO_3), are valuable fertilizers and can replace conventional fertilizers manufactured using fossil fuels (Bonmatí & Flotats, 2003; Lei et al., 2007; Wu & Modin, 2013). While the resulting end products from ammonia stripping are of high

quality, the major drawback of ammonia stripping is the high energy required for air stripping the ammonia as well as the cost of chemicals to increase pH and acid to trap the volatile ammonia gas are some of the challenges of air stripping (Kuntke et al., 2012).

1.4.3 Ammonia adsorption or ion exchange

Ion exchange and adsorption-based processes are widely researched for ammonia capture. Zeolites are the most common adsorbents used for ammonia adsorption due to their high cation exchange capacity and greater affinity for NH_4^+, low cost, and simple operation and ability to withstand shock loadings (Koon; Huang et al., 2010; Perera et al., 2019). The porous tetrahedral structure of natural zeolites made up of aluminum (Al^{3+}), silicon (Si^{4+}), and oxygen (O) have exchangeable cations such as Na^+, K^+, Ca^{2+}, and Mg^{2+} (Sengupta et al., 2015). The ammonium ions in solutions are captured on the zeolite in exchange for these surface cations. Modifications to zeolite surface are known to improve its ammonia removal capacity (Watanabe et al., 2005). For this reason, several studies have modified natural zeolites with sodium chloride solution as exchange capacity is known to increase with increasing content of low valence homoionic sodium (Booker et al., 1996; Milan et al., 1997; Weatherley & Miladinovic, 2004). However, such chemical modifications incur to the cost of operation. The ammonium adsorption capacity of zeolites has been reported to be in the range of 2.7 – 30.6 mg/g (Wang & Peng, 2010). The presence of co-existing cations in the permeate can also affect ammonia sorption capacity.

While zeolites have been extensively studied for ammonia removal from various waste streams, very few studies have been performed with AnMBR permeate (Deng et al., 2014; Mullen et al., 2019). For instance, Deng et al. (2014) studied ammonium removal from AnMBR treated municipal wastewater permeate using different brands of commercially available natural

zeolites and observed maximum removal of 12 mg N/g clinoptilolite. While adsorption is highly

effective, the regeneration of adsorbent requires chemicals such as sodium hydroxide (NaOH)

and brine (NaCl) (Zhang et al., 2017). Alternatively, saturated zeolites can also be used as soil

amendments for slow release of nutrients in soil (Bansiwal et al., 2006; Li et al., 2013). Chapter

3 of this dissertation discusses the use of clinoptilolite for ammonia sorption from swine

wastewater permeate.

1.4.4 Electrochemical nutrient recovery

A comparatively recent development in wastewater treatment is the use of

electrochemical processes for nutrient recovery. There are electrochemical processes developed

for both separate and co-capture of N and P. Electrodialysis is a membrane based

electrochemical process where ammonia is concentrated from waste streams in the presence of

an electric field and using ion exchange membranes (Ippersiel et al., 2012). In a study on

ammonia recovery from swine waste using ED, a concentration of up to18g/L of ammonium-N

was reached within the system (Mondor et al., 2008). ED is proposed as a pretreatment system

for ammonia stripping, but its implementation is currently limited by the high energy

consumption of around 3.25-3.60 kWh/kg NH_4-N (Mondor et al., 2008; Ippersiel et al., 2012).

Several other electrochemical techniques are available for nutrient recovery including

electrocoagulation (İrdemez, Demircioğlu, Yıldız, et al., 2006; Vasudevan et al., 2008; Gharibi et

al., 2010; Chen et al., 2014; Elyasi et al., 2015), microbial electrochemical cells (Min et al.,

2005; Tao et al., 2015), and electrochemical precipitation of struvite (Cusick & Logan, 2012;

Zang et al., 2012).

Overall, the nutrient recovery technologies discussed above are suitable for wastewater

streams with high relative concentrations of N and P such as swine waste. However, it is

important to ensure the recovered resources meet the requirements of the end-users and further applications.

1.5 Beneficial reuse of recovered nutrient products

Recovered nutrients from wastewaters are projected as potential substitute of synthetic fertilizers. The fertilizer utility of recovered nutrient products have been reported by researchers at both pot and field scale (Ganrot et al., 2007; Yetilmezsoy & Sapci-Zengin, 2009; Ryu & Lee, 2016; Szymańska et al., 2019). Plant uptake studies by Ryu and Lee (2016) showed that lettuce growth with swine waste derived struvite yielded better produce compared to that grown with commercial fertilizer. Contrarily, application of urine derived struvite addition resulted in lower yield of wheat compared to commercial N:P:K fertilizer (14:4:21) (Ganrot et al., 2007). Low plant uptake was attributed to the high pH condition of soil. Nutrient availability in soil is impacted by soil pH which is optimum for plant uptake within pH 6.5-7.5. Furthermore, it is reported that pH has the most effect on P availability in soil than N. Phosphorus gets adsorbed or precipitated with iron or aluminum in acidic soil and with magnesium or calcium in alkaline soil (Saliu & Oladoja, 2021). Other wastewater derived products such as calcium phosphate (Vogel et al., 2017), nutrient loaded biochar and clinoptilolite (Kizito et al., 2019; Kocatürk-Schumacher et al., 2019) have also been evaluated for plant uptake studies. In the case of nutrient loaded clinoptilolite from digestate, the authors observed higher plant biomass uptake of N compared to untreated clinoptilolite as control (Kocatürk-Schumacher et al., 2019). Chapter 4 of this thesis evaluates the fertilizer applicability of ammonia saturated clinoptilolite. Apart from performing plant uptake studies, nutrient release and plant availability potential of recovered nutrient products can also be studied based on soil incubation studies without the use of plants (Pierzynski & Hettiarachchi, 2018; Weeks Jr & Hettiarachchi, 2020). One such study evaluating

the phosphorus release rate and nutrient availability from recovered nutrient products (RNPs) from AnMBR permeate treating municipal wastewater was performed by Heronemus et al. (2021). The study showed that the RNPs derived from the AnMBR permeate is not suitable for application as fertilizer but rather act as P sink in the soil. The suitability of RNPs as fertilizers could be affected by the presence of organic micropollutants and heavy metals in wastewaters and hence their presence should be eliminated (Ronteltap et al., 2007). Additionally, data on product purity, quality, composition, and effectiveness compared to synthetic industrial fertilizers is needed to make recovered products marketable (Kogler et al., 2021).

The quality of the recovered nutrient product is often compromised by the quality of the waste stream from which it is derived, reducing its effectiveness compared to commercial fertilizers. In this regard, AnMBRs offer the advantage of solid-liquid separation, producing a nutrient-rich permeate free of particulates, colloidal interferences, and other suspended contaminants, enabling recovery of high-quality nutrient products. Obtaining such high-quality nutrient products can offset some of the economic limitations hampering the large-scale adaptation of AnMBR technology. Overall, the AnMBR integrated nutrient recovery system can greatly improve the economic and life cycle benefits by producing tailored high quality N and P products, thus closing the loop of nutrient circularity to achieve a circular economy.

Chapter 2 - Research Objectives

The main goals of the proposed research are to demonstrate tailored nutrient capture from anaerobically treated membrane bioreactor permeate as value added products through sustainable techniques and evaluate the reuse potential of such waste derived nutrient products with an aim to close the loop on nutrient based circular economy.

The following objectives are proposed to achieve the above-mentioned goals:

1. Evaluate targeted ammonium recovery from synthetic AnMBR swine permeate, real swine wastewater, using naturally occurring clinoptilolite.

    a. Perform bench experiments to gain mechanistic understanding of ammonia adsorption onto clinoptilolite from swine wastewater.

    b. Intimately couple experimental data to adsorption models to enable extrapolation of clinoptilolite adsorption performance for a variety of ammonia capture scenarios from swine permeate, real swine wastewater and potentially other comparable wastewater types.

    c. Demonstrate sustainable regeneration of spent clinoptilolite for maximizing reuse potential of exhausted clinoptilolite.

2. Identifying the key microbial consortia present in the AnMBR sludge and clinoptilolite applied soils.

    a. Use high throughput Illumina Miseq based sequencing technique to confirm trends in microbial community changes.

3. Evaluate the fertilizer utility and bioavailability of ammonia saturated clinoptilolite and anaerobically digested wastewater derived biosolids in soil incubation experiments and greenhouse based crop uptake studies.

    a. Perform soil incubation studies to evaluate ammonia nutrient diffusion in soil amended with saturated clinoptilolite.

    b. Investigate bioavailability of ammonia from saturated clinoptilolite through plant uptake studies in a greenhouse.

    c. Understand the impact of different nitrogen treatments on soil microbiota and potential changes in microbial community using a DNA based high throughput technique.

4. Recover phosphorus as high quality calcium phosphate fertilizer product with enhanced P content from swine permeate.

    a. Identify factors that hinder phosphorus precipitation using calcium coagulants and improve product P content and overall quality.

5. Sequentially recover phosphorus as struvite and calcium phosphate minerals in the same process train as a two-stage process.

2.1 Dissertation overview

Note: There is some repetition of information as the chapters were written in the format of manuscripts for publication in peer-reviewed journals.

- **Chapter 3 has been published in the Journal of Water Process Engineering**
  Kannan, A. D., & Parameswaran, P. (2021). Ammonia adsorption and recovery from swine wastewater permeate using naturally occurring clinoptilolite. *Journal of Water Process Engineering*, *43*, 102234.

- **Chapter 4 has been published in Bioresource Technology Journal**
  Kannan, A. D., Evans, P., & Parameswaran, P. (2020). Long-term microbial community dynamics in a pilot-scale gas sparged anaerobic membrane bioreactor treating municipal wastewater under seasonal variations. *Bioresource technology*, *310*, 123425.

- **Chapter 6 has been published in Chemical Engineering Journal**
  Damodara Kannan, A., Dillavou, J., H.H. Gamage, K., Randig, E., M. Hettiarachchi, G., & Parameswaran, P. (2023, 2023/02/01/). Recovery of high-quality calcium phosphate fertilizer products from anaerobic membrane bioreactor treated swine wastewater. *Chemical Engineering Journal, 453*, 139539.
  https://doi.org/https://doi.org/10.1016/j.cej.2022.139539

Chapter 3 - Ammonia adsorption and recovery from swine wastewater permeate using naturally occurring clinoptilolite

This chapter has been published in the *Journal of Water Process Engineering*. The citation is as follows:

Kannan, A. D., & Parameswaran, P. (2021). Ammonia adsorption and recovery from swine wastewater permeate using naturally occurring clinoptilolite. *Journal of Water Process Engineering*, *43*, 102234.

3.1 Introduction

The focus of this study is to gain mechanistic understanding of untreated natural clinoptilolite based ammonia capture from real swine wastewater and simulated Anaerobic Membrane Bioreactor (AnMBR) treated swine permeate through extensive experimental and modeling analysis. Ion exchange using low-cost zeolite materials such as clinoptilolite has been extensively used in various types of wastewater for ammonia and heavy metal removal (Wang & Peng, 2010; Belova, 2019; Kotoulas et al., 2019; Genethliou et al., 2021). Clinoptilolite, an abundant natural zeolite, is a microporous crystalline aluminosilicate material having high surface area with a three-dimensional framework composed of exchangeable cations (Margeta et al., 2013). Apart from ion-exchange, clinoptilolite can also capture ammonia by molecular adsorption mechanism (Guo, 2016).

The use of clinoptilolite for ammonia recovery from AnMBR treated swine permeate can be advantageous for capturing ammonium in a highly concentrated form devoid of suspended particles, thereby preventing clogging in the clinoptilolite column (Deng et al., 2014). Subsequently, the ammonia sorbed clinoptilolite can be used as a slow-release fertilizer (Li, Wee, et al., 2013) or regenerated using brine (NaCl) solution, Sodium hypochlorite (NaOCl) (Zhang et al., 2017), by air stripping at alkaline pH (Deng et al., 2016), by biological regeneration through nitrification (Martins et al., 2017), or for transportation to offsite locations

for energy generation (Evans et al., 2018). Brine solution has been used as a regenerant for ammonia saturated clinoptilolite column integrated to a pilot scale AnMBR treating municipal wastewater (Evans et al., 2018). The sequestered ammonia can further be electrolyzed to produce hydrogen gas which can be captured for energy generation (Guy & Page, 2019).

The ammonia recovery capacity is affected by presence of commonly occurring cations in wastewater such as Potassium (K^+), Calcium (Ca^{2+}), Magnesium (Mg^{2+}), and Sodium (Na^+) and depends on the selectivity of the clinoptilolite towards these different ions. K^+, having a similar ionic size and monovalent charge as ammonium, has been reported to effectively compete with ammonium (Hedström & Rastas Amofah, 2008). The selectivity of ammonia relative to other cations are reported disparately in the literature (Farkaš et al., 2005; Lei et al., 2008; Wang & Peng, 2010). This is attributed to various factors including the presence of co-existing ions, variable initial NH_4-N concentration, pH, temperature, composition and chemical modification of clinoptilolite that are known to impact the adsorption capacity of clinoptilolite (Kurama et al., 2002; Huang et al., 2010a; Li et al., 2019).

Although clinoptilolite has been extensively studied for ammonia adsorption, only a few studies have focused on clinoptilolite-based ammonia recovery from swine wastewater (Milan, Sánchez, et al., 1997; Huang et al., 2014; Huang et al., 2015; Guo, 2016; Montégut et al., 2016; Amini et al., 2017). Furthermore, there are no known studies on targeted ammonia recovery from AnMBR treated swine permeate using natural clinoptilolite which has obvious benefits as discussed earlier. In this context, this is the first comprehensive study to evaluate clinoptilolite based ammonia recovery from simulated synthetic AnMBR swine permeate using batch experiments combined with appropriate modeling analysis and detailed surface elemental characterization by scanning electron microscopy-energy dispersive spectroscopy (SEM-EDS).

Additionally, to evaluate the applicability and scale up potential, replicable dynamic column experiments with side-by-side breakthrough curve comparisons for both synthetic swine permeate and real swine wastewater were performed with detailed temporal characterization of ion release profile from the columns. The breakthrough curves were intimately coupled with fixed bed modeling analysis, thereby enabling extrapolation of clinoptilolite adsorption performance for a variety of ammonia capture scenarios from swine permeate, real swine wastewater and potentially other comparable wastewater types. Experiments on the effects of co-existing competing ions on ammonia recovery and sorbed clinoptilolite regenerability evaluations with NaCl were also performed.

3.2. Materials and Methods

3.2.1 Clinoptilolite characteristics

Clinoptilolite media (Zeobest®) used in this study to remove ammonia was purchased from Northern Filter Media Inc., Iowa, USA. The chemical composition of the clinoptilolite media was provided by the vendor and is shown in Table A1. The total cation exchange capacity determined for ammonium-N was reported to be between 1.2 to 1.8 meq/g clinoptilolite, as per the manufacturer's specifications. For all experiments in this study, the clinoptilolite media was used as received without any pretreatment or rinsing with DI water.

3.2.2 Synthetic swine permeate composition

Synthetic swine effluent simulating treated permeate from an anaerobic membrane bioreactor (AnMBR) system was prepared in reference to , and the wastewater composition from the swine waste lagoon located at the Kansas State University animal farm, Manhattan, Kansas, USA. In addition, the following assumptions were made: 1) 90% Chemical Oxygen Demand (COD) removal can be achieved within the AnMBR system treating an influent total

COD of 10800 mg/L resulting in an effluent COD of 1080 mg/L, based on the system's previous

performance (Lim et al., 2019); 2) No nutrient removal occurs within the bioreactor and hence,

the concentrations of NH_4^+-N, P and other cations in the effluent will remain the same as the

influent. The composition of the prepared solution is shown in Table 3.1.

Table 3.1 Composition of simulated synthetic swine permeate and real swine wastewater (from two sampling events corresponding to each column run) used in this study. The synthetic permeate has very little to no suspended solids, while the real swine wastewater was filtered to obtain the liquid fraction alone. All values for real swine wastewater (except COD) are reported as average of duplicate analysis.

	Simulated synthetic swine permeate	Real swine wastewater run 1	Real swine wastewater run 2
pH	8	8.5	8.34
Borate buffer (mM)	50	N.A.	N.A.
Total ammonia -N (mg/L, as N)	400	108	81
COD soluble (mg/L)	1080	560	543
Propionic acid (mg COD/L)	233	N.D.	N.D.
Acetic acid (mg COD/L)	157	N.D.	N.D.
Lactic acid (mg COD/L)	321	N.D.	N.D.
Butyric acid (mg COD/L)	13	N.D.	N.D.
Ethanol (mg COD/L)	355	N.D.	N.D.
Potassium, K^+ (mg/L)	342	423	383
Magnesium, Mg^{2+} (mg/L)	21	56	61
Calcium, Ca^{2+} (mg/L)	39	65	61
Iron, Fe^{3+}	0.9	N.A.	N.A.
Total phosphorus as P (mg/L as P)	105	N.A.	N.A.
Ortho Phosphate (mg/L as P)	N.A.	17	46
Sulfate (mg/L as S)	N.A.	29	17
Nitrate (mg/L as N)	N.A.	1.4	1.4

N.D. – Non detectable

N.A. – Not applicable/not analyzed

3.2.3 Batch equilibrium studies

Batch equilibrium experiments were performed by varying the initial ammonium concentrations from 0 to 800 mg/L (0, 50, 100, 200, 400, 600, 800 mg/L NH_4^+-N) in 100 mL of deionized water with 10 g/L clinoptilolite. The experiments were carried out in conical glass flasks placed on an orbital shaker under constant rotation at 200 rpm under room temperature (20 °C). The pH of the experimental solutions was adjusted to mimic real swine wastewater pH of 8 by adding 0.1 N NaOH or 0.1 N HCl. Initial and final sample aliquots were collected at time, t = 0 and 24 hours, respectively, and analyzed for NH_4^+-N. Additionally, equilibrium studies with synthetic swine permeate at varying initial ammonium concentrations were also performed to compare the removal capacity with that from the ammonium chloride solution. The isotherm experiment was performed in duplicate and average values were used to plot the data which were fitted to Freundlich (Freundlich, 1906) and Langmuir (Langmuir, 1916) isotherm models.

3.2.4 Particle characterization using Scanning electron microscopy (SEM)-Energy Dispersive X-Ray Spectroscopy (EDS)

Surface high-resolution imaging to determine the surface morphology and elemental composition of the clinoptilolite particles from the batch experiment with synthetic swine wastewater before and after ammonia capture was done using an FEINova NanoSEM 450 scanning electron microscope (SEM) with an Oxford X-Max 20mm^2 integrated EDAX silicon-drift detector located at the Electron Nanoscopy Instrumentation Facility, University of Nebraska, Lincoln, USA. The working distance and accelerating voltage were set to around 5mm and 20kV, respectively.

Prior to the SEM analysis, the synthetic swine permeate treated clinoptilolite particles were allowed to dry in a desiccator to remove all the moisture and the dried clinoptilolite was used for surface imaging.

3.2.5 Interference of competing ions on ammonia adsorption

The impact of co-occurring competitive cations such as K^+, Mg^{2+}, Ca^{2+}, and Na^+ on ammonia capture was investigated using the respective binary solutions with ammonia (the maximum expected swine wastewater concentration of 400mg/L NH_4^+-N) and each correspondingly different competing ion of choice, added at an initial concentration of 28 meq/L (corresponding to 400mg/L NH_4-N) to10g/L clinoptilolite in 100 mL DI water. In addition, the effect of simultaneous competition from multiple competing ions in the same working solution was evaluated by adding each of the different ions (K^+, Mg^{2+}, Ca^{2+}, and Na^+) along with NH_4^+-N at an equal concentration of 28 meq/L, respectively. All the experimental solutions were placed in an orbital shaker at 200 rpm. Aliquot samples were collected after 24 hours and filtered through 0.2-micron syringe filters to analyze the concentrations of ammonia and the corresponding competing ion(s). The experiment was performed in duplicate and average values are reported in this study.

3.2.6 Effect of contact time and kinetics of ammonia recovery

The effect of contact time to reach equilibrium was studied for an initial concentration of 400mg/L NH_4-N in NH_4Cl solution. Samples were collected periodically for 840 minutes, a duration long enough to achieve equilibrium based on preliminary contact time experiments. These samples were filtered through 0.2-micron syringe filters and analyzed for ammonium concentration. Subsequently, kinetic models such as Pseudo-first order (PFO) (Lagergren, 1898) and pseudo second order (PSO) (Ho & McKay, 1999) were evaluated to understand the kinetics

of ammonia removal using clinoptilolite. Further, to understand the mechanism of ammonia capture, intra-particle diffusion model (Weber & Morris, 1963) was also investigated on the kinetic data. The kinetic experiment was performed in duplicate and average ammonia concentration was used to plot the graph and modeling analysis.

3.2.7 Column studies on synthetic swine permeate

Fixed bed column adsorption studies were performed with a glass column having a diameter of 2.5 cm, column height of 15 cm and a packed bed height of 10 cm. Breakthrough curves to understand the ammonia capture pattern was performed by feeding the synthetic swine permeate (composition shown in Table 3.1) into the column in upflow mode using a Masterflex peristaltic pump at 1mL/min. The breakthrough data from the experiments were fitted to Thomas model (Thomas, 1944) and compared to the model predicted curves to predict the maximum adsorbate removal capacity as well as understand the dynamic behavior of the ammonia capture in the packed-bed column. The breakthrough data were also fitted to the Yoon Nelson model (Yoon & Nelson, 1984) to predict the 50% column breakthrough time. Each column run was repeated twice.

3.2.8 Application on actual swine wastewater

To evaluate the potential use of clinoptilolite as a pre-treatment system, untreated actual swine wastewater collected from the swine waste lagoon at the Kansas State University animal farm was treated in a clinoptilolite packed bed column having the same dimension as used in the previous column experiment at flow rate of 1 ml/min. All column experiments were performed at an environmentally relevant temperature of 25 °C. Prior to column feeding, the collected swine wastewater was centrifuged for 10 minutes in an Eppendorf centrifuge 5920 R (Hauppauge, New York, USA) at 10,000 rpm (rotations per minute). The supernatant was then filtered through a

1.6 µm glass fiber filter paper. The composition of the actual filtered swine wastewater was characterized and is also shown in Table 3.1. Additionally, synthetic swine wastewater simulating the average composition of the collected real swine wastewater was also prepared and treated in the column to compare the breakthrough behavior of the two different types of wastewater. Each column experiment was repeated twice.

3.2.9 Regeneration of spent clinoptilolite

The recoverability of ammonia and reusability of spent clinoptilolite was evaluated in a batch experiment involving four successive adsorption and desorption cycles. Each adsorption cycle involved adding 1 g of clinoptilolite in 100 mL of each of the two synthetic swine permeate solutions having different initial ammonia concentrations of 400 mg/L NH_4-N or 100 mg/L NH_4-N, respectively, and placed on an orbital shaker for 24 hours at 300 rpm. At the end of each adsorption cycle, the spent clinoptilolite was filtered out from the swine permeate solutions using 1.6 µm glass fiber filter and added to 100 mL solutions of 0.5 M NaCl to desorb the captured ammonia and regenerate the spent clinoptilolite. All experiments were performed in duplicates. Initial and final sample aliquots were collected and analyzed for ammonia concentrations to determine the amount of ammonia adsorbed or desorbed.

3.2.10 Analytical methods

The concentration of ammonia in the batch isotherm experiments and desorption study was analyzed with HACH® TNT 832 high range ammonia kit using a HACH DR3900 (Loveland, CO, USA) spectrophotometer. In all other experiments, concentration of ions including Na^+, K^+, Ca^{2+}, Mg^{2+}, NH_4^+, SO_4^{2-}, and NO_3^- were measured using Dionex ICS-5000+ Ion Chromatography System. PO_4^{3-} was also analyzed using the Dionex ICS-5000+ Ion Chromatography System with a few exceptions when HACH® TNT 846 Phosphorus Reactive

(Ortho) kit was used. Deionized water (18.2 MΩ-cm resistivity) was used to make stock solutions, for preparing dilutions and all chemical analyses. Chemical oxygen demand (COD) was analyzed with HACH® kits (TNT 825). pH was monitored using Fisherbrand™ accumet™ AB150 pH Benchtop Meters.

3.3 Batch Equilibrium and continuous column experiments

3.3.1 Batch equilibrium experiments with clinoptilolite and NH4-N only

Batch isotherm experiments were performed using varying initial ammonium concentrations. The ammonium recovery is calculated using equation3.1:

$$q_e = \frac{(C_o - C_e) V}{M} \quad (3.1)$$

where, q_e is the amount of adsorbate uptake per gram clinoptilolite at equilibrium (mg/g); C_o = initial concentration of ammonium in solution (mg/L as N); C_e = equilibrium concentration of ammonium in solution (mg/L as N); V= volume of working solution (L); M = mass of clinoptilolite used (g).

The results of the equilibrium experiment are shown in Figure 3.1. The ammonium capture/recovery capacity increased with increasing initial ammonium concentration and reached a maximum of 18.2 mg/g (1.3 meq/g) for an initial concentration of 600 mg/L NH4-N. The removal capacity observed in the present study is similar to 1.3 meq/g reported by Montégut et al. (2016) for an initial concentration of 0.43M ammonium chloride solution and comparable to 1.11 meq/g as per the data plotted in the article by Jorgensen and Weatherley (2003). Overall, ammonia capture capacity reported in the present study is within the range summarized by Wang and Peng (2010). However, it is to be noted that any comparison of ammonia removal capacity

of zeolites should be done for normalized initial ammonium concentration in solution (Millar et al., 2016).

The ammonia recovery from synthetic swine permeate was evaluated with initial concentrations of 50, 100, 200, 300, 400, 500, and 600 mg/L NH_4-N, respectively. The results summarized in Appendix Figure A.1 reveal lower adsorption capacities in the permeate than in NH_4Cl solution, although a similar trend of increasing ammonium uptake with increasing initial concentration was observed. The lower ammonium capture compared to NH_4Cl solution is attributed to the presence of ions such as Ca^{2+}, K^+, or Mg^{2+} in the simulated synthetic swine AnMBR permeate that compete with the ammonia adsorption sites (Deng et al., 2014).

The ammonia exchange data from the NH_4Cl solution were modelled using the Langmuir and Freundlich isotherm models to characterize the distribution of ammonium ions adsorbed on the clinoptilolite and remaining in solution. The Langmuir isotherm in its nonlinear original form is represented by equation 3.2:

$$q_e = \frac{q_{max}*K_L*Ce}{1+KL*Ce} \quad (3.2)$$

where q_{max} (mg. g^{-1}) is the maximum adsorption capacity of clinoptilolite, K_L (L/mg) is Langmuir constant, q_e is the amount of adsorbate uptake per gram clinoptilolite at equilibrium (mg/g), Ce = Equilibrium concentration of ammonium in solution (mg/L).

The Freundlich equation represented by equation 3.3 is applied to multilayer adsorption with heterogeneous adsorption sites (Freundlich, 1906).

$$q_e = K_F C_e^{1/n} \quad (3.3)$$

where q_e is the equilibrium ammonia uptake per gram clinoptilolite (mg/g), C_e is equilibrium concentration of ammonium in solution (mg/L), K_F ((mg/g) (L/mg)$^{1/n}$) and n are the Freundlich isotherm and empirical constants, respectively.

Non-linear regression analysis using the Levenberg Marquadt algorithm was performed to fit the experimental data to the isotherm models in OriginPro 2020b software (OriginLab Corporation).
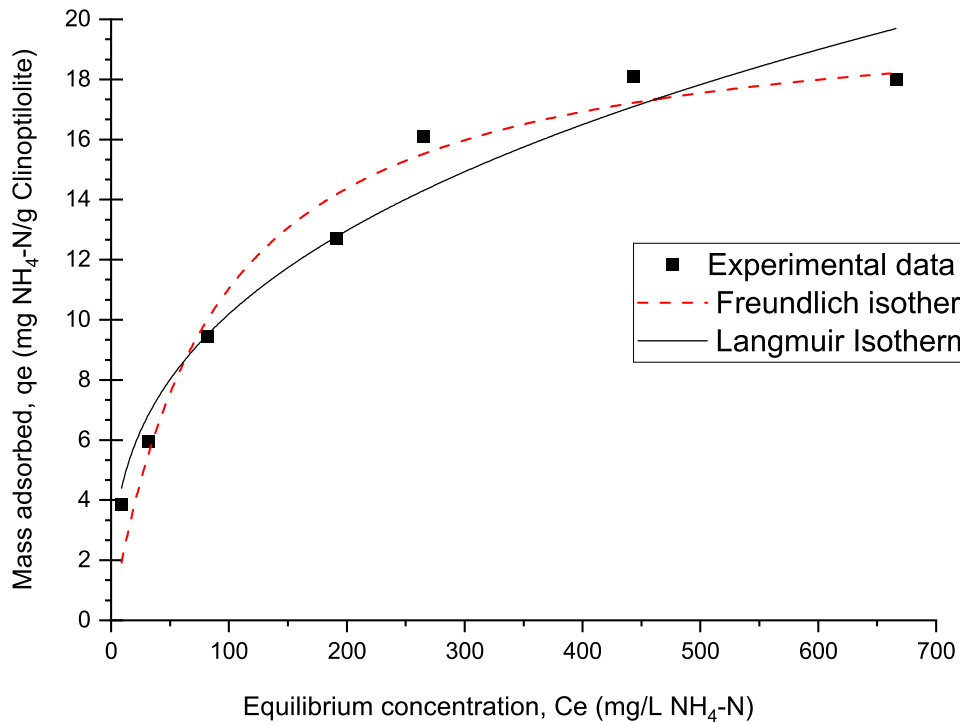
Figure 3.1 Ammonia adsorption isotherm curves for an equilibrium concentration range of 8.9 - 666 mg/L NH$_4$-N, determined through batch experiments. These experiments establish the adsorption isotherm in NH$_4$Cl solution only (The reported experimental data is the average of duplicate runs). The model fits were obtained by performing nonlinear regression analysis.

The result of the isotherm model fit is shown in Figure 3.1 and the calculated model parameters are summarized in Table 3.2. The calculated Langmuir maximum ammonium adsorption capacity (q_m) of clinoptilolite was 20.5773 mg/g with a Langmuir constant (K_L) of 0.01154 (L/mg). The Freundlich constant K_F and n were estimated to be 2.05928 ((mg/g)

$(L/mg)^{1/n}$) and 2.8742, respectively. The estimated isotherm parameters in this study are comparable to a similar natural clinoptilolite-based ammonia removal isotherm experiment performed by Sarioglu (2005) at 20 °C with a Langmuir $q_{max} = 23.70$ mg/g and Freundlich $K_F = 2.23$, $1/n = 0.38$ (n= 2.632).

Table 3.2 Langmuir and Freundlich isotherm parameters. The model parameters were obtained by performing nonlinear regression analysis.

Langmuir			Freundlich		
q_m (mg/g)	K_L (L/mg)	R^2	n	K_F ((mg/g) (L/mg)$^{1/n}$)	R^2
20.5773	0.01158	0.9625	2.8742	2.05928	0.9588

Based on the R^2 values and the curve fit, it can be seen that both Langmuir ($R^2 = 0.9625$) and Freundlich ($R^2 = 0.9588$) models represented the isotherm data quite well, with Langmuir displaying a slightly better fit and higher R^2 value. Discussion on which isotherm model better describes ammonia removal by clinoptilolite has been varied with some studies finding better results with the Langmuir isotherm (Malekian et al., 2011; Mazloomi & Jalali, 2016; Stocker et al., 2019), and others with the Freundlich isotherm (Sarioglu, 2005; Widiastuti et al., 2011). This suggests that ammonia sorption by clinoptilolite can fit well with different isotherm models, and the better fit with the Langmuir isotherm model in this study may not be used to draw conclusions on the type of ammonia capture mechanism. However, such isotherm models are still useful for empirical representation of the experimental data and the resulting model parameters will enable comparison of adsorption characteristics with other adsorbents (Kithome et al., 1999).

3.3.2 Kinetics of ammonia adsorption

The kinetics of ammonia adsorption was studied using the pseudo first order and pseudo second order models. The nonlinear pseudo first order kinetic rate order proposed by Lagergren (1898) is represented by equation 3.4

$$q_t = q_e \left(1 - e^{k_1 t}\right) \quad (3.4)$$

where q_t, q_e, and k_1 are the amount of ammonia captured per gram clinoptilolite (mg/g) at time t

(min), and amount of ammonia captured at equilibrium (mg/g), and the PFO rate constant

(min^{-1}), respectively.

The nonlinear form of pseudo second order model is represented by equation.3.5

$$q_t = \frac{(q_e)^2 k_2 t}{1 + q_e k_2 t} \quad (3.5)$$

where q_t, q_e, and k_2 are the amount of ammonia captured per gram clinoptilolite (mg/g) at time t

(min), and amount of ammonia captured at equilibrium (mg/g), and the PSO rate constant (g.mg^{-1}.min^{-1}), respectively.

The kinetic experiment data were fitted to both the models by nonlinear regression curve

fitting using the Levenberg-Marquardt algorithm. Figure 3.2A presents the nonlinear regression

curve fitting plots of both models along with the experimental ammonia uptake data and the

estimated model parameters are summarized in Table 3.3. Based on the R^2 value, pseudo second

order ($R^2 = 0.98$) seems a better fit than pseudo first order ($R^2 = 0.93$) and the PSO model

calculated q_e (15.8 mg/g) was also very close to the experimental equilibrium uptake of 15.77

mg/g. The better fit with pseudo second order kinetic model suggests that ammonia capture by

clinoptilolite is likely governed by chemisorption or ion-exchange mechanism and dependent on

both the adsorbent (clinoptilolite) and the adsorbate (ammonia). (Halim et al., 2010; Shaban et

al., 2017; Taddeo et al., 2017).

The pseudo first order and pseudo second order models do not give any information on

the ammonia diffusion mechanism. Therefore, to gain insight into the diffusion mechanisms of

ammonia adsorption and determine the rate controlling steps, the experimental data were applied to the intra-particle diffusion model described by Weber and Morris (1963) (equation. 3.6).

$$q_t = k\, t^{0.5} + C \qquad (3.6)$$

where q_t (mg/g) is the ammonia uptake at time t (min), and k (mg.g^{-1}.min $^{-0.5}$) is the intraparticle diffusion rate constant, and C is the intercept of the slope of the curve which is also indicative of the boundary layer thickness. The model assumes intraparticle diffusion to be rate controlling if the line from the plot of q_t versus $t^{0.5}$ intercepts the origin.
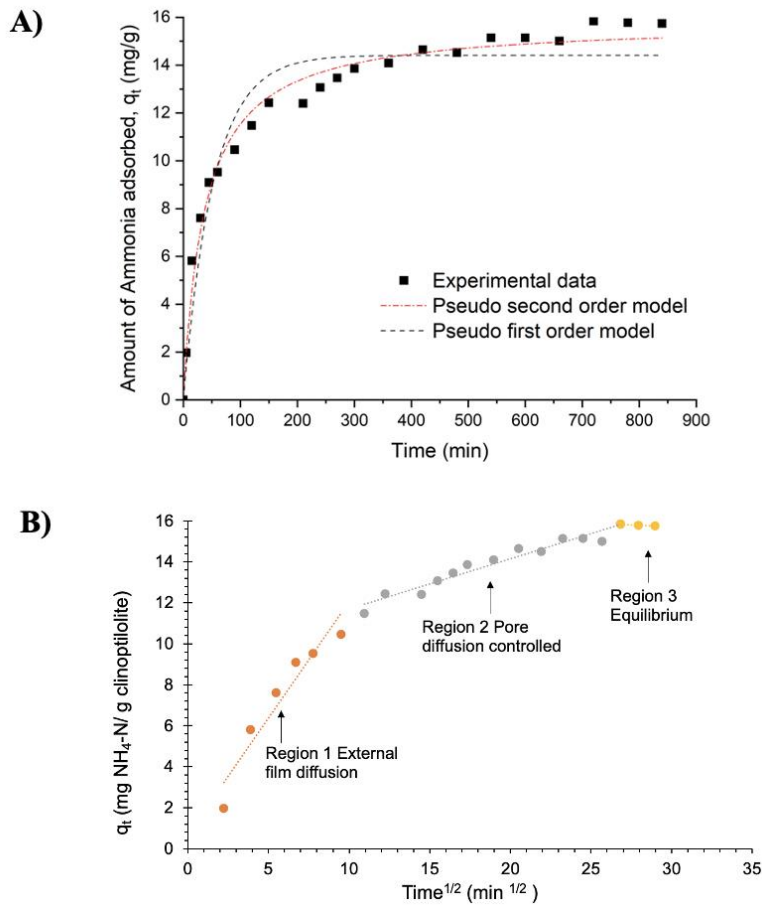
Figure 3.2 Ammonia adsorption kinetics from NH$_4$Cl solution (initial concentration = 400 mg/L NH$_4$-N) using A) Non-linear pseudo first order and pseudo second order analysis; B) Intraparticle diffusion kinetic analysis. Data from duplicate experimental runs. The analysis shows multi-linearity of plotted data depicting external film diffusion (Region 1 data points in orange color), pore diffusion (Region 2 – data points in grey color) and equilibrium stage (Region 3 - data points in yellow color)

Figure 3.2B shows three linear regions of ammonia uptake. Region 1 with a steeper slope represents the external film diffusion-controlled adsorption and the Region 2 likely being pore diffusion controlled followed by the equilibrium stage in Region 3. The results reveal that ammonium adsorption occurs as a combination of both external film diffusion and pore diffusion, the former with a steeper slope occurs very fast and the latter is the slower rate controlling process. This was further investigated by determining the film diffusion (D_f) and particle diffusion (D_p) coefficients to understand the contribution of each diffusion mechanism using equations 3.7 and 3.8, respectively.

$$\text{Film diffusion model} \quad ln\left(1 - \left(\frac{q_t}{q_e}\right)\right) = -k_f t \quad\quad (3.7)$$

$$\text{Particle diffusion model} \quad ln\left(1 - \left(\frac{q_t}{q_e}\right)^2\right) = -2k_p t \quad\quad (3.8)$$

where q_t and q_e are the amount of ammonia uptake per gram clinoptilolite (mg/g) at time t (min), k_f is the film diffusion rate constant represented by $k_f = D_f C/C_z hr$ and k_p is the particle diffusion rate constant represented by $k_p = D_p \pi^2/r^2$. C and C_z (mg/kg) are the concentration of ammonia in solution and on the zeolite, respectively; r is the average particle radius (0.0001 m) of clinoptilolite used in the present study, h is the thickness of film around the clinoptilolite particle (10^{-5} m for poorly stirred solution) (Moussavi et al., 2011; Guaya et al., 2016). D_f and D_p are the film and particle diffusion coefficients (m^2/s), respectively.

The calculated values of D_f and D_p are summarized in Table 3.3. The value of film diffusion coefficient D_f was greater than the particle diffusion coefficient D_p which further confirmed particle diffusion to be the rate limiting step. A similar conclusion was reached by Lin et al. (2013) for natural clinoptilolite based ammonia removal at an initial concentration of 1000 mg N/L.

Table 3.3 Kinetic parameters of ammonia adsorption from NH$_4$Cl solution by natural clinoptilolite (initial concentration = 400 mg/L NH$_4$-N, pH = 8

Model		Parameters	
Pseudo first order		q$_e$ calculated (mg/g)	14.41
		k$_1$ (min^{-1})	0.019
		R^2	0.93
Pseudo second order		q$_e$ calculated (mg/g)	15.8
		k$_2$ (g.mg^{-1}.min^{-1})	0.0017
		R^2	0.98
Intra particle diffusion model	Region 1	k (mg.min$^{-0.5}$.g^{-1})	1.13
		R^2	0.91
	Region 2	k (mg.min$^{-0.5}$.g^{-1})	0.246
		R^2	0.95
Fim diffusion model		D$_f$ (m^2/s)	3.85×10^{-10}
		R^2	0.95
Particle diffusion model		D$_p$ (m^2/s)	2.18×10^{-12}
		R^2	0.98

3.3.3 Scanning electron microscopy and surface elemental composition of clinoptilolite

Scanning electron microscopy analysis was performed to compare the surface morphology of the clinoptilolite particle before and after contact with synthetic swine permeate. The scanning electron micrographs of the untreated clinoptilolite particle (Figure 3.3A) and synthetic swine permeate contacted particle (Figure 3.3B) showed the particle surface as rough and irregular. Additionally, the untreated raw natural clinoptilolite particle surface appeared to be covered with fine particles on the surface unlike the synthetic swine permeate treated micrograph which appeared more refined likely due to the absence of fine particles. This refined appearance

of the treated clinoptilolite could possibly be due to the rinsing effect of permeate treatment on the particles which were under constant agitation during the batch experiments.

The representative EDS spectrum for both raw and treated clinoptilolite samples is shown in Figure 3.3C and Figure 3.3D, respectively. The raw clinoptilolite spectrum had peaks corresponding to Calcium, Sodium, Oxygen, Silica, Aluminum, Iron, and Potassium. The presence of the above-mentioned ions is similar to the elemental composition from the XRF data for raw clinoptilolite provided by the manufacturer (Table A1). The EDS based surface elemental composition of both synthetic swine permeate treated and raw clinoptilolite is represented as atomic percentage and weight percentage in Table 3.4. The sodium percentage contribution in the raw clinoptilolite reduced from 1.73 % to 0.41 weight % in the treated sample indicating loss of sodium ion from the particle. This is indicative of sodium likely being a counter ion for ion exchange of ammonia on the clinoptilolite surface. A similar pattern of decrease in sodium and potassium from natural clinoptilolite after adsorption in NH_4Cl solution was observed by Lin et al. (2013). Furthermore, the treated clinoptilolite also witnessed a decrease in Potassium (K) and Iron (Fe) percentages which may have been also been involved in the ion exchange process.
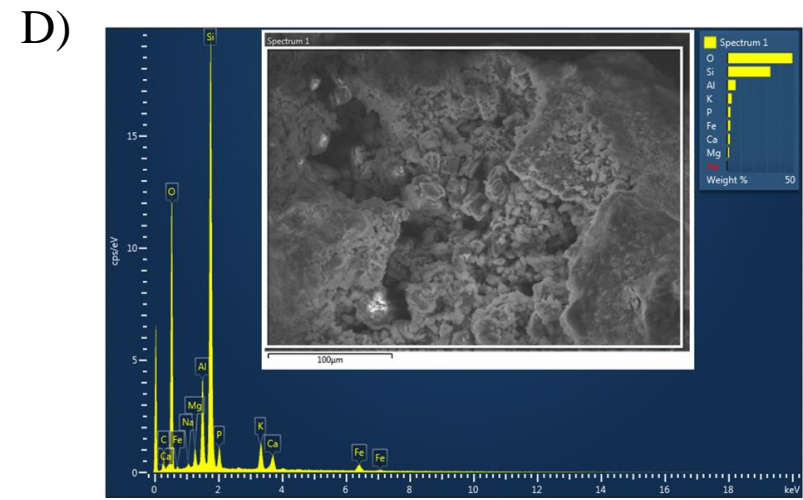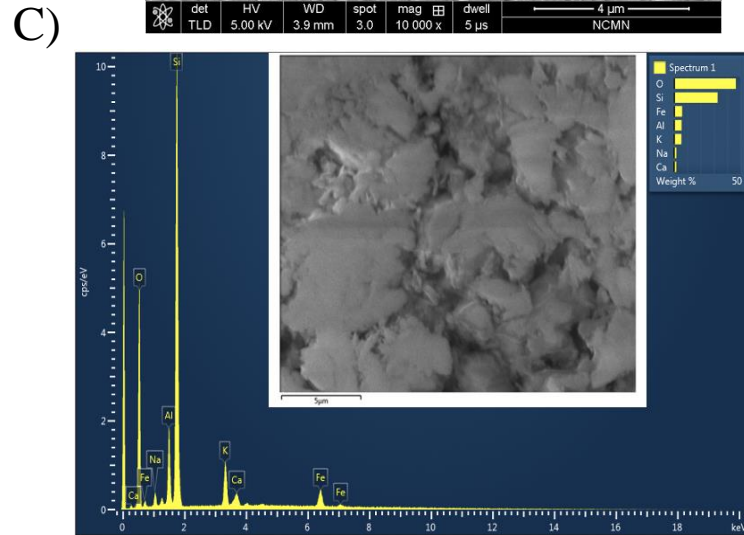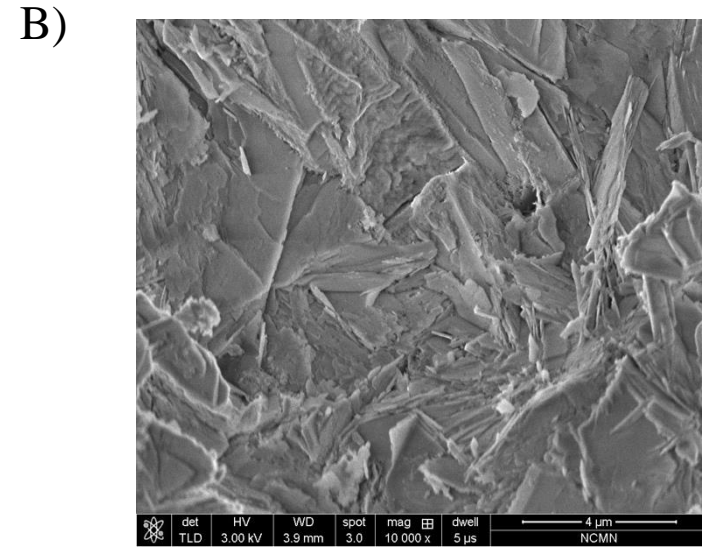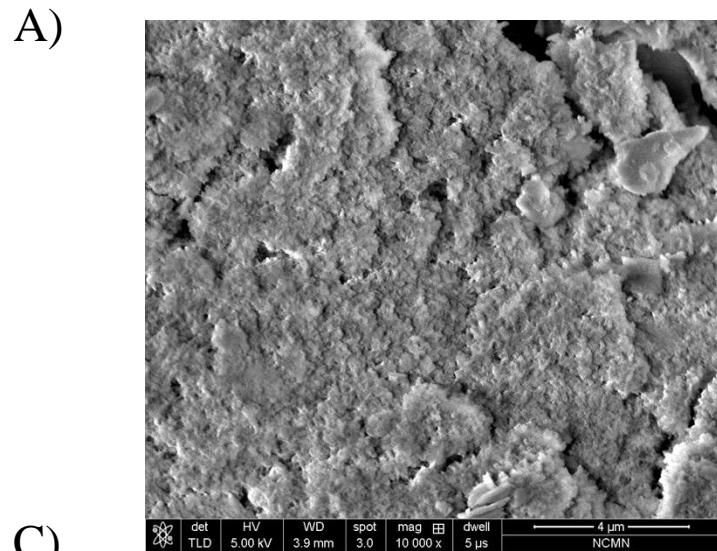
Figure 3.3 Scanning electron micrographs of A) raw untreated clinoptilolite particle, B) Synthetic swine treated permeate; EDS spectrum of C) untreated natural clinoptilolite particle and D) synthetic swine permeate (400 mg/L NH4+-N) treated clinoptilolite particle obtained using SEM-EDS analysis.

Interestingly, Mg and Phosphorus (P) were detected in the treated particle but their absence from the raw natural clinoptilolite indicate that they likely originated from the synthetic swine permeate. The presence of P indicated that apart from ion-exchange mechanism of ammonia capture, there is also the possibility of precipitation of phosphate-based minerals that are formed when phosphate reacts with ammonia, magnesium or calcium. The detection of P in the present study is consistent with the EDS result from a previous study that reported the formation of phosphate-based precipitates (calcium phosphate and struvite) and that the zeolite could provide nucleation sites for precipitate formation (Amini et al., 2017). Further investigation with XRD or other relevant surface characterization can confirm this possibility.

Table 3.4 Surface elemental composition of raw and synthetic swine wastewater treated clinoptilolite determined using EDS. The red colored elements in the synthetic swine permeate treated clinoptilolite column represent the ones with about 2X decrease in the weight % compared to the raw clinoptilolite, likely due to desorption, while the blue colored elements witnessed more than 2X increase in the weight% compared to the raw particles, likely due to precipitation on the particle surface.

Raw clinoptilolite			Synthetic swine wastewater treated clinoptilolite		
Spectrum 1	Weight %	Atomic %	Spectrum 1	Weight %	Atomic %
O	46.57	62.53	O	49.1	63.97
Na	1.73	1.62	Na	0.41	0.37
Al	5.62	4.48	Mg	1.51	1.3
Si	32.87	25.14	Al	6.35	4.91
K	5.49	3.02	Si	32.44	24.07
Ca	1.65	0.89	P	2.47	1.66
Fe	6.07	2.33	K	3.37	1.8
Total	100	100	Ca	2.03	1.06
			Fe	2.32	0.87
			Total	100	100

3.3.4 Column adsorption study with synthetic swine permeate

The breakthrough curves of two synthetic swine permeate replicate runs are shown in

Figure 3.4 A and 3.4B respectively. The breakthrough curve of each run appeared S-shaped, and

the breakpoint ($C/C_0 = 0.1$) occurred around 10.5 hours in both replicates. The column reached

exhaustion ($C/C_0 = 0.9$) after 28 hours in run 1 and 30 hours in run 2.
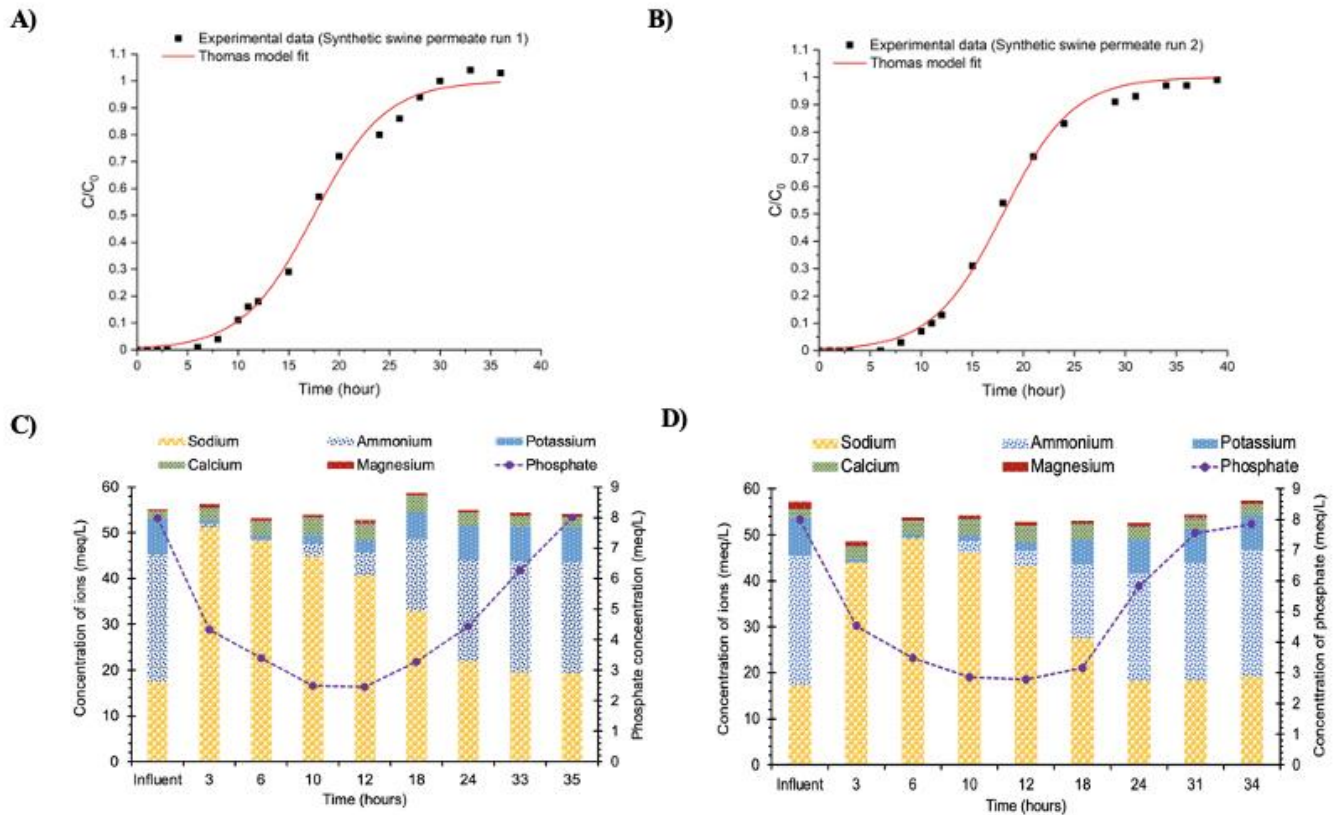
Figure 3.4 Clinoptilolite based column breakthrough curves for treatment of A) synthetic swine permeate run 1, B) synthetic swine permeate run 2; Ion release/capture profiles for C) synthetic swine permeate run 1; D) Synthetic swine permeate run 2. Both the runs were performed with an NH_4-N concentration of 400mg/L N.

The adsorption capacity of the clinoptilolite bed at breakthrough and exhaustion were calculated

using equation 3.9

$$q_t = \frac{C_0 Q \int_0^t \left(1 - \frac{C}{C_O}\right) dt}{M} \qquad (3.9)$$

where, q_t (mg/g) is the adsorption capacity at time t, C_0 is the initial influent ammonium concentration (mg/L), C is the effluent ammonium concentration (mg/L) at time t (hour), M is the mass clinoptilolite in the column (44.5 grams), Q (L/hour) is the flow rate of synthetic swine permeate fed into the column.

At breakthrough point, the adsorption capacity of the column was found to be 5.55 mg/g and 5.63 mg/g for run 1 and 2, respectively. The total ammonia capture capacity of the column calculated at $C/C_0=1$ was 10.15 mg/g for run1 and 9.68 mg/g for run 2. These values were slightly lower than 11.2 mg/g from the batch study (Figure A.1) at similar initial concentration (400 mg/L NH_4-N) in the synthetic swine permeate. The lower adsorption capacity of the column may be due to the column bed not reaching equilibrium due to shorter contact time than the batch experiment (Nguyen et al., 2015).

The ion exchange mechanism within the column was investigated by analyzing the temporal ion release or capture profile of different cations in samples collected from the column outlet. The release profiles for each column are presented in Figure 3.4C and 3.4D, respectively. Results indicate that sodium ions were abundantly released from the column during the initial phase of operation while witnessing simultaneous capture of ammonium and potassium ions from the solution. Approximately 33.8 meq/L of Na^+ was released in the third hour sample of the first column run while all the ammonium (27.8 meq/L) in the feed water was captured in the column by that time. The release trend showed that Na^+ ions were sharply released during the first three hours before its concentration in the effluent gradually decreased with continuous operation of the column. In addition, 7.1 meq/L of K^+ was captured in the column as per the sample collected in the third hour. The release of sodium during the initial duration indicated that the sodium ions were displaced in exchange for ammonia and potassium capture. The equivalent amount of sodium

released compared to the equivalents of ammonium and potassium captured indicated that sodium was the main counter ion for ammonia capture during this initial phase.

Apart from sodium, calcium and potassium ions were also observed to increase with the duration of operation. After the column reached breakthrough ($C/C_0 = 0.1$), the concentration of Na^+ started to gradually decrease while the ammonium and potassium started to increase in the outlet samples. These findings are further supported by the SEM-EDX data (Table 3.4) shown earlier, which confirmed the decrease in Na and to a lesser extent, K, from the synthetic swine permeate treated clinoptilolite particles (Figures 3.3C and 3.3D). The reversal in adsorption pattern for potassium after reaching breakthrough was also reported by Karadag, Akkaya, et al. (2008) who studied ammonia removal from leachate wastewater in a clinoptilolite bed column.

The affinity of clinoptilolite for potassium is known to be greater than ammonium (Jama & Yücel, 1989; Sarioglu, 2005). However, in the present study, potassium eluted from the column prior to ammonium which may have been due to the ammonium equivalents being far greater than potassium in the feed and thereby possibly outcompeting potassium on the clinoptilolite surface. Overall, ion release profile of each column run showed replicable trends of ion elution and needs further deeper investigation to understand the ammonia adsorption behavior in the presence of competing ions.

3.3.5 Breakthrough curve modeling

The experimental data-based breakthrough curve from each run was applied to the Thomas model and Yoon-Nelson model. Thomas model represented by equation 3.10 is used to estimate the maximum ammonia adsorption capacity and adsorption rate on the column (Thomas, 1944).

$$\frac{C_t}{C_0} = \frac{1}{1+\exp\left(\frac{k_{Th}q_e\text{M}}{\text{Q}} - k_{th}C_0\text{t}\right)} \quad (3.10)$$

where C_t (mg/L) and C_0 (mg/L) are the concentration of ammonia in the effluent at time t (hour) and the concentration of ammonia in the influent feed, respectively. The flow time t (hour) in the expression is calculated as a ratio of effluent volume (L) at time t and flow rate, Q (L/hour). k_{Th} is the model rate constant (L.hour^{-1}.mg^{-1}), q_e is the amount of ammonia adsorbed at equilibrium per gram clinoptilolite (mg/g), and M is the mass of clinoptilolite used in the column (g).

The Yoon Nelson model represented by equation 3.11 is useful in predicting the time required to reach 50% adsorbate saturation in the column

$$\frac{C_t}{C_0} = \frac{1}{1+\exp{(K_{YN}\tau - K_{YN}t)}} \qquad (3.11)$$

Where K_{YN} (hour^{-1}) is the Yoon-Nelson rate constant and τ is the time required to reach 50% adsorbate saturation in the column (hour).

It is to be noted that both the Yoon-Nelson and Thomas models are mathematically equivalent and can be expressed as a logistic function (equation 3.12) (Chu, 2020). Since both the models are mathematically similar, it cannot be compared based on the R^2 value fitting but can be used simultaneously to determine the different derived parameters from each model (Chu, 2020).

$$\frac{C_t}{C_0} = \frac{1}{1+\exp{(a-bt)}} \qquad (3.12)$$

The model parameters were estimated using non-linear regression analysis as it gives a better fit than linear regression (Han et al., 2007), using the Levenberg-Marquadt algorithm in OriginPro software.

Since both the Thomas and Yoon-Nelson models are mathematically equivalent, the model predicted breakthrough curves had similar fit qualities and shape. For this reason, only the Thomas model predicted breakthrough curves are shown in Figure 3.4A and Figure 3.4B while the predicted parameters for both the models are summarized in Table 3.5. The Thomas model

predicted maximum ammonia uptake capacity of 9.8 mg/g and 9.54 mg/g for each of the column run was very close to the experimentally determined column capacity of 10.15 mg/g for run1 and 9.68 mg/g for run 2. Additionally, the time required to reach 50% ammonia breakthrough predicted by the Yoon-Nelson model was also in close agreement with the experimental data. For instance, 50% ammonia breakthrough time for synthetic permeate Run 1 (Fig 3.4A) was achieved close to 18 hours and the model predicted it to be at 17.49 hours (Table 3.5). Overall, Thomas model and Yoon Nelson models fit well with the experimental data and can be used to predict ammonia capture from synthetic swine permeate in fixed bed clinoptilolite columns.

Table 3.5 Thomas and Yoon Nelson model parameters of ammonia breakthrough data from column treatment of synthetic swine permeate

Model		Synthetic Swine permeate run1	Synthetic Swine permeate run 2
Thomas model	q_e calculated (mg/g)	9.81	9.54
	k_{Th} (L.hour^{-1}.mg^{-1})	7.28×10^{-4}	7.05×10^{-4}
	R^2	0.99	0.99
Yoon-Nelson model	τ (hour)	17.49	18
	k_{YN} (hour^{-1})	0.282	0.291
	R^2	0.99	0.99

3.3.6 Ammonia capture from real swine wastewater – column studies

Additional column experiments to study ammonia capture from real swine wastewater were performed in duplicate. According to the results of the breakthrough curve shown in Figure 3.5, breakpoint ($C/C_0 = 0.1$) of ammonia occurred at around 18 hours for both replicate runs. The column exhaustion ($C/C_0 = 0.9$) happened faster for the first run of real swine waste ($C_0 = 104$ mg/L) after 35 hours while taking 44 hours for the second run of real swine waste ($C_0 = 78$ mg/L). This difference of bed exhaustion time between the two swine wastewater runs could be attributed

to the slightly higher ammonium concentration in run 1 than run 2 leading to a faster saturation of

column

(Karadag, Tok, et al., 2008).
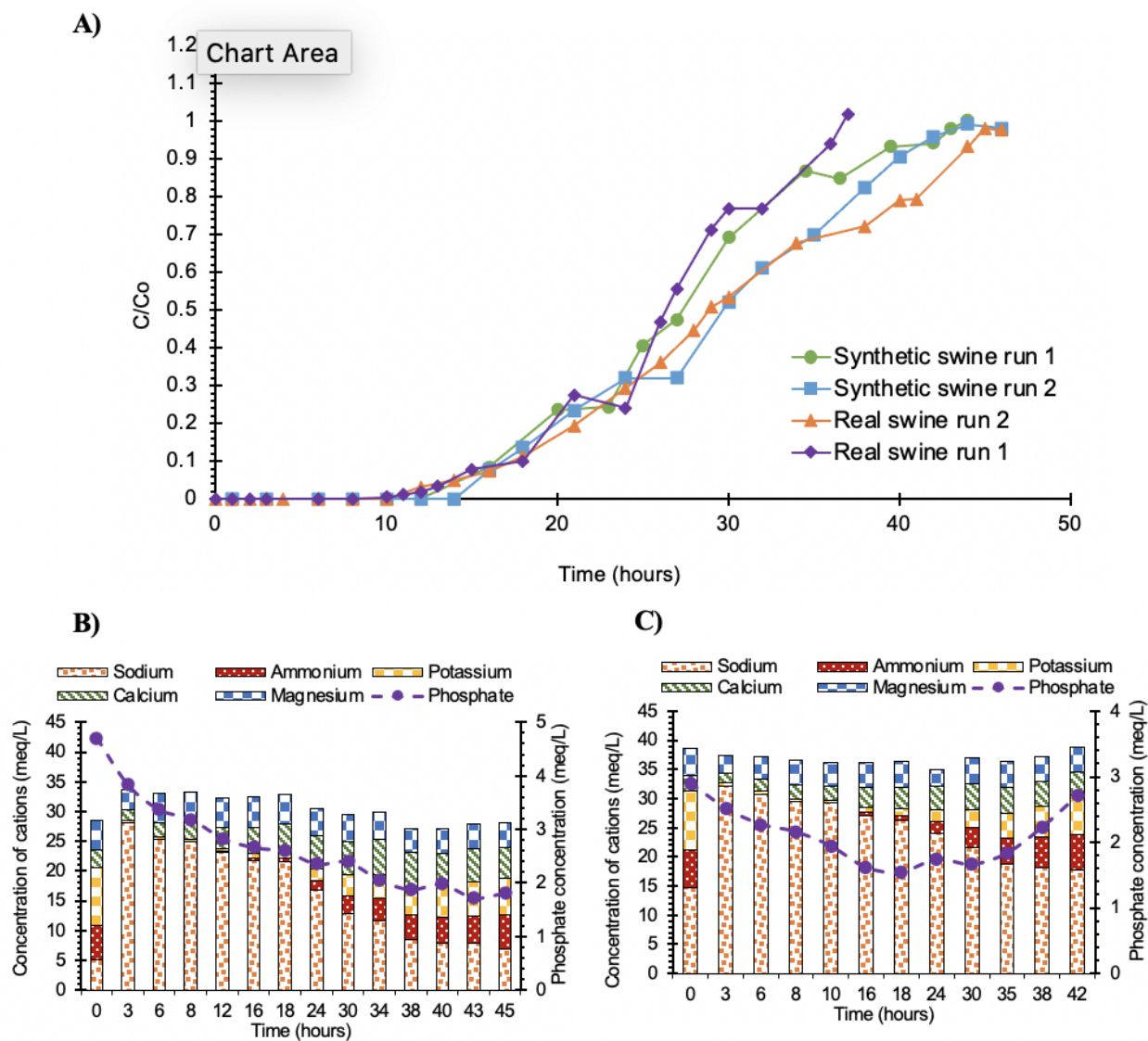
Figure 3.5. A) Clinoptilolite based column breakthrough curves for treatment of real swine wastewaters; Ion release/capture profile for B) real swine wastewater run 2, C) Synthetic swine wastewater. The NH_4-N concentrations in the real swine wastewater and synthetic swine wastewater were 79 mg/L NH_4-N and 94 mg/L NH_4-N, respectively. Concentration of cations at t = 0 hour in Figure 5B and 5C depicts influent feed composition. The breakpoint times ($C/C_0 = 0.1$) for these runs were fairly similar, likely indicating that the real wastewater matrix did not influence this behavior.

Comparing the breakthrough curves of the simulated swine wastewater with those from the real swine runs (Figure 3.5), it was seen that there is not much difference in the breakpoint times of the two samples, which bodes well for extending the mechanistic understanding from the synthetic swine permeate to the real swine wastewater. Fig 3.5 also demonstrated that ammonia recovery on clinoptilolite was not adversely impacted by the real wastewater matrix. The ion release profile of the two different samples shown in Fig 3.5 B and C showed similar trends of ion capture and release as the synthetic permeate runs, which is one of the first side by side comparisons for ammonia sorption from synthetic and real swine wastewater on clinoptilolite.

3.3.7 Simultaneous phosphorus removal from swine waste

In all the column studies, there was a decline in phosphate (PO_4^{3-}) concentration while treating both the synthetic swine permeate and real swine wastewater. For both the simulated swine permeate column runs (Figure 3.4 C and 3.4D), the concentration of phosphate gradually declined from 8 meq/L in the feed to 2.7 meq/L. A similar pattern of phosphate removal was observed in the real swine wastewater run 2 (Figure 5B) during which the PO_4^{3-} concentration declined from 4.7 meq/L in the feed to as low as 1.8 meq/L. This was further confirmed by using synthetic swine wastewater with similar composition to the real swine wastewater (Figure 3.5C), as the PO_4^{3-} concentration decreased from 2.9 meq/L in the feed to 1.5 meq/L in the column effluent after 18 hours. These results further confirm the detection of phosphorus in the EDS results for clinoptilolite particles treated with the synthetic swine permeate which could be due to the formation of phosphate-based precipitates. Previous studies (Huang et al., 2014; Lin et al., 2014; Amini et al., 2017; Wan et al., 2017; Mitrogiannis et al., 2020) have reported removal of phosphorus on zeolites although natural clinoptilolite does not have any anion exchange

capacity. The removal mechanism postulated is that cations (Ca^{2+} and Mg^{2+}) released from the surface of the zeolite during NH_4^+ capture bind to phosphate to form calcium phosphate, hydroxyapatite and struvite precipitates (Hedström & Rastas Amofah, 2008; Huang et al., 2014; Wan et al., 2017). In the present study, the localized precipitation on the clinoptilolite surface did not decrease the overall ammonia capture efficiency indicating that precipitation did not cause pore clogging nor consequently decrease the ion exchange capacity. Apart from binding with the cations released from the zeolite, phosphate could also possibly participate in precipitation reactions with the cations present in the wastewater. Overall, clinoptilolite can effectively remove ammonia from swine wastewater with simultaneous recovery of phosphorus. Additionally, the sorbed clinoptilolite can be directly applied as a soil amendment enabling slow release of nutrients in the soil.

3.3.8 Effect of competing ions on ammonia sorption

The ammonium selectivity with respect to each of the tested competing ions was assessed by comparing the adsorption capacity of ammonium in the different solutions and is shown in Figure 3.6. It was observed that ammonium adsorption was lowest at 7.22 mg/g in the presence of potassium followed by calcium (14.4 mg/g), sodium (15.4 mg/g) and magnesium (16 mg/g). In the solution containing the same equivalent concentration of all the ions, the ammonia adsorption was lowest at 4.7 mg/g, which is likely due to the high equivalent concentration of all ions exerting a greater competition for the adsorption sites on the clinoptilolite, than in any of the binary solution mixtures. Based on the observed results, the order of selectivity of different cations with respect to ammonia recovery was found to be $K^+ > Ca^{2+} > Na^+ > Mg^{2+}$. This is in agreement with previous studies which have also reported a similar selectivity of $K^+ > Ca^{2+} > Na^+$ (Ćurković et al., 1997; Farkaš et al., 2005). However, there is variability in the selectivity

preference of calcium, sodium and potassium ions in the literature. Some studies have reported

greater affinity for sodium over potassium and calcium (Lei et al., 2008; Huang et al., 2010),

while others have reported an order of preference of $Ca^{2+} > Mg^{2+} > K^+ > Na^+$ (Huang et al.,

2014). This variability in preference could be attributed to the properties and composition of the

zeolite used and the conditions that they are used in. In summary, the present study investigated

the effect of different cations that are most commonly encountered in wastewater and are

anticipated to have the greatest impact on ammonia recovery; it is recommended to study the

effects of various other cations and anions including Fe^{3+}, Cl^-, CO_3^{2-}, and SO_4^{2-} to develop a

deeper understanding and further optimize real world applicability of clinoptilolite for swine

wastewater ammonia capture.
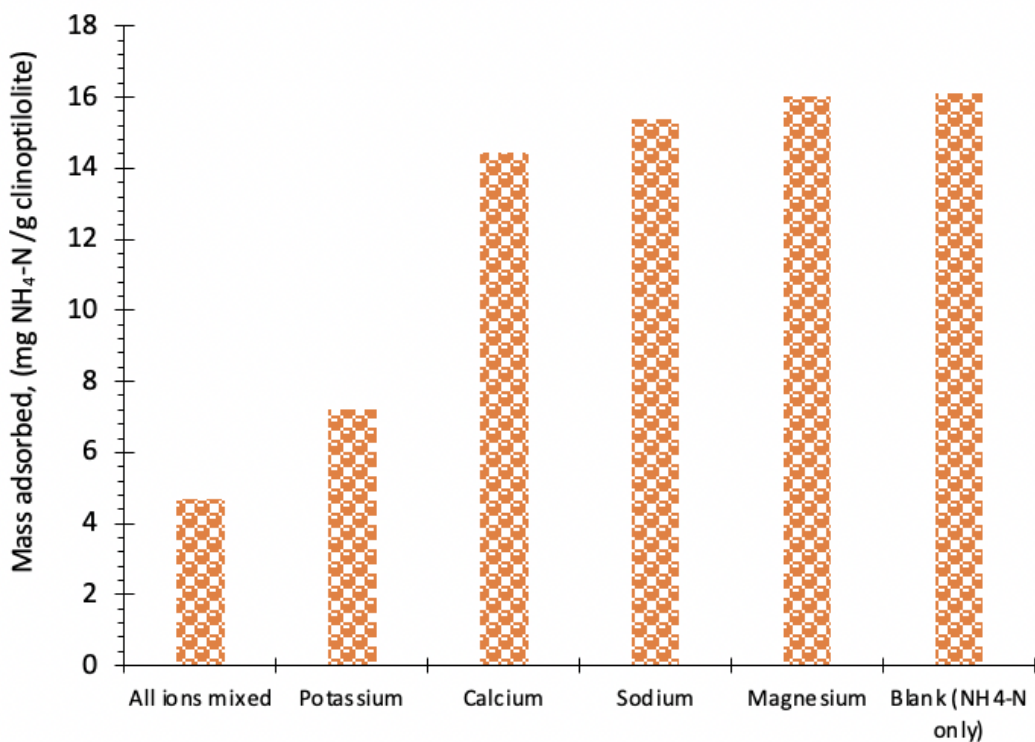
Figure 3.6. Effect of interference of competing cations on ammonia capture using clinoptilolite at same equivalent concentrations. The data shown here are from individual batch experiments with the respective ionic mixtures. The interference from potassium was the most pronounced in the

binary mixture, while the interferences from other ions were further exacerbated when all ions were mixed.

3.3.9 Clinoptilolite regeneration using brine solution

The results of the regeneration efficiency of the spent clinoptilolite are shown in Figure 3.7. The amount of ammonia desorbed, and desorption efficiency are calculated by equation13 and equation 14, respectively.

$$q_d = \frac{C_d V}{M} \quad (3.13)$$

$$Desorption\ efficieny\ (\%) = \frac{q_d}{q_e} * 100 \quad (3.14)$$

where q_d (mg/g) and q_e (mg/g) are the amount of ammonia desorbed and amount of ammonia adsorbed, respectively. C_d is the concentration of ammonia released from the clinoptilolite in the regenerant solution (mg/L), V is the volume of regenerant used (L), and M is the mass of clinoptilolite (g).

The adsorption capacity at 400 mg/L NH_4-N in synthetic swine permeate gradually declined from 11.6 mg/g (Cycle 1) → 7.5 mg/g (Cycle 4). In the desorption experiments, ammonia desorption capacity was 8.3 mg/g (Cycle 1) → 7.57 mg/g (Cycle 2) → 7.8 mg/g (Cycle 3) → 6.64 mg (Cycle 4) indicating that although the 0.5 M NaCl brine solution could not completely desorb all the ammonium ions from the clinoptilolite, it was consistently able to maintain a desorption efficiency greater than 69% from clinoptilolite treated with 400 mg/L NH_4-N. The variability in the adsorption and desorption capacities is attributed to accumulation of ammonium along with other cations (K^+, Mg^{2+} or Ca^{2+}) present in the synthetic swine permeate on the clinoptilolite (Huang, Yang, et al., 2015).

The ammonia adsorption capacity in 100 mg/L NH_4-N simulated swine permeate solution was in the range of 2.97 to 4.6 mg/g and desorption efficiency was consistently above 78% for

the four cycles. Overall, the regeneration results indicate that NaCl as a regenerant can be applied in an AnMBR treatment system to maximize NH_4^+ recovery while minimizing volatilization losses. Furthermore, the brine solution needed for this purpose can be sustainably recovered from the swine wastewater itself with microbial reverse-electrodialysis cells (MREC) (Kim & Logan, 2011).
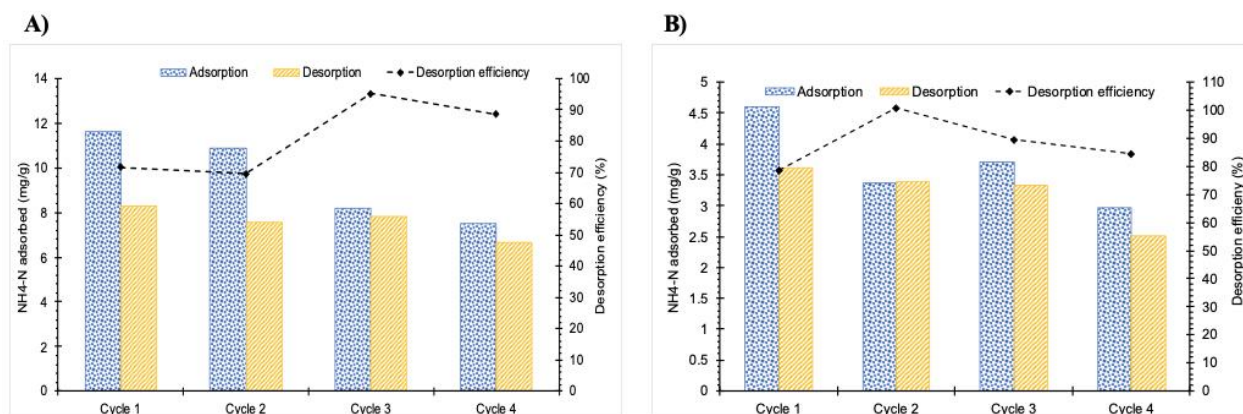
Figure 3.7 Regeneration cycles of adsorption in synthetic swine permeate and desorption in 0.5 M NaCl for initial ammonium concentrations of A) 400 mg/L NH_4-N and B) 100 mg/L NH_4-N, respectively, in synthetic swine permeate. No appreciable loss in desorption efficiency was observed.

3.4 Summary

The results of this study represent a comprehensive and reliable demonstration of the potential of clinoptilolite as an effective adsorbent for sustainably capturing and recovering ammonia from both synthetic swine permeate and real swine wastewater. Maximum ammonia recovery was found to be 18.2 mg/g in NH_4Cl solution. The kinetic experimental data fitted better with Pseudo Second Order model and intraparticle pore diffusion was determined to be the rate limiting process for ammonia adsorption by clinoptilolite.

EDS results revealed changes in surface elemental composition on the synthetic swine treated clinoptilolite particles with increases in phosphorus and magnesium and reduction in sodium weight percentages.

Replicate column studies showed successful capture of ammonia from the swine wastewater with simultaneous phosphate based mineral precipitation. Ion release profiles revealed that Na^+ and Ca^{2+} were the main counterions for ammonia capture, which further support the earlier observations from SEM-EDS analyses of the swine permeate treated clinoptilolite particles. Ammonia capture is affected by the presence of competing ions (especially K^+) and the selectivity of different cations with respect to ammonia exchange was found to be $K^+ > Ca^{2+} > Na^+ > Mg^{2+}$. Regeneration of spent clinoptilolite with NaCl consistently achieved desorption efficiency greater than 69% over 4 cycles which showed that brine solution can be an effective way to recover ammonia in the liquid form while reusing the clinoptilolite. Further studies on the reuse potential of recovered ammonia saturated clinoptilolite as a soil fertilizer is proposed in Chapter 4.

Chapter 4 - Microbial Community Dynamics within a Pilot Scale AnMBR

This chapter has been published in *Bioresource Technology Journal.* The citation is as follows:

Kannan, A. D., Evans, P., & Parameswaran, P. (2020). Long-term microbial community dynamics in a pilot-scale gas sparged anaerobic membrane bioreactor treating municipal wastewater under seasonal variations. *Bioresource technology*, *310*, 123425.

A pilot scale gas sparged AnMBR system treating municipal wastewater under ambient conditions was operated at Fort Riley, Kansas, USA. The microbial community development in the anaerobic sludge and its temporal evolution in response to varying operational or environmental parameters including ambient temperature fluctuations, the impact of microbial groups in influent wastewater, as well as competing sinks such as sulfate reduction was evaluated in the pilot scale gas sparged AnMBR. Additionally, bacterial genera performing key functional roles were identified based on relative bacterial abundances determined from the 16s rRNA gene-based Illumina Miseq high throughput sequencing analysis. The techniques and tools described in this chapter are further used to understand the impacts of applying biosolids derived from anaerobic sludges on the soil microbial community in Chapter 5.

4.1 Microbial Community Analysis Materials and Methods

4.1.1 Sampling and DNA Extractions

Following inoculation of the reactor using seed sludge collected from the Topeka WWTP mesophilic anaerobic digester, representative bioreactor samples were collected from the middle sampling port of the reactor at various times during the operational period (Days 0, 157, 203, 222, 229, 243, 257, 262, 271, 384, 416, 445, and 472). Additionally, influent feed samples were collected for DNA extractions during the later phase of operation (Days 384, 416, 432, 445, 458, and 472) to understand the impact of the influent feed on the reactor microbial community. The

sampling points were grouped into three stages of reactor operation: Stage 1 (Day 0 to 157), Stage 2 (Days 203 to 272), and Stage 3 (Days 384 to 472).

4.1.2 DNA Extraction from AnMBR Bulk Sludge

50 mL bioreactor samples were collected for each sampling point and centrifuged in an Eppendorf centrifuge 5920 R (Hauppauge, New York, USA) at 21000 RCF (relative centrifugal force) to concentrate the biomass. The supernatant was discarded, and the settled biomass pellets were either immediately used for DNA extraction (samples collected after Day 384) or stored in a freezer at -20 °C (samples collected before Day 384). The biomass pellets (after thawing frozen pellets) were subsequently weighed out for DNA extraction. The extractions were carried out using E.Z.N.A ® Water DNA kit (Omega bio-tek, Norcross, Georgia, USA) as per the manufacturer's protocol. Further, an optimization process to compare the extraction efficiency and quality of DNA using different weights of the freeze thawed pellets versus immediately extracted samples was also performed. Data summarized in the Table 4.1 shows some limitations for the stored samples as the freshly extracted samples resulted in higher DNA concentrations for similar weights of biomass pellets, although the storage method did not have an impact on the DNA quality (260/280 absorbance ratio).

Table 4.1 Summary of extracted dna concentrations from freeze thawed biomass pellets and freshly extracted samples

Day	Concentration (ng/µl)	260/280 ratio	Source
0	88.58	1.87	Bioreactor
157	59.84	1.87	Bioreactor
203	132.8	1.87	Bioreactor
222	99.72	1.84	Bioreactor
229	113.15	1.84	Bioreactor
243	78.65	1.84	Bioreactor
257	83.4	1.85	Bioreactor
262	75.6	1.8	Bioreactor
271	126.6	1.85	Bioreactor
384	23.75	1.59	Influent
384	288.04	1.88	Bioreactor
416	57.26	1.71	Influent
416	631.22	1.92	Bioreactor
445	339.36	1.91	Influent
445	278.46	1.91	Bioreactor
472	306.83	1.88	Bioreactor
472	257.96	1.9	Influent

4.1.3 High Throughput Sequencing and Data Processing

To determine the structure of the Bacterial and Archaeal community in the AnMBR, DNA was sequenced at MR DNA (www.mrdnalab.com, Shallowater, TX, USA) on an Illumina MiSeq (Illumina, USA) platform. 16S rRNA universal prokaryotic primers 519F and 806R (Wuchter et al., 2013), with barcode on the forward primer, were used to amplify the V4 hyper-variable region of this highly conserved gene (Takai & Horikoshi, 2000). The reads were paired end sequenced with DNA fragments consisting of 2×300 bp reads using an Illumina MiSeq with the MiSeq Reagent Kit v3. MR DNA provided sequencing data in pr.FASTA and pr.QUAL files containing joined reads which were further combined into FASTQ files using the "Combine FASTA and

QUAL" tool on Galaxy. The FASTQ files were uploaded to the Beocat Research Cluster at Kansas State University for subsequent analysis. Reads were sorted by sample ID into separate FASTQ files using grep. The sorted sequence files were imported into QIIME2 (Bolyen et al., 2019) and denoised with qiime deblur denoise-16S to obtain representative sequences. After denoising, the sequences were clustered into OTUs in QIIME2 based on 99% similarity threshold (Edgar, 2018). Phylogenetic analysis of representative sequences was performed using qiime phylogeny fast tree and qiime phylogeny midpoint-root.

Representative sequences were classified in QIIME 2 with a Naive Bayes classifier trained with the Greengenes 13_8 99_otu_taxonomy and 519F/806R reference sequences from Greengenes 13_8 99% OTUs. The qiime taxa barplot function was used to visualize the resulting taxonomy and results were exported from QIIME2View as a .csv file for further processing in Microsoft Excel.

4.1.4 Statistical Analysis

The taxonomic table containing the sequence reads at different taxonomical levels in each sample was used to calculate the relative bacterial abundances and relative archaeal abundances separately in Microsoft Excel (Version 16.30). Both bacterial and archaeal relative abundances at different taxonomic levels were determined by normalizing against the total number of bacterial sequences and archaeal sequences, per sample, respectively. Taxonomically unassigned reads were excluded from the relative abundance calculations and only taxa representing ≥1% relative abundance in at least one of the sampling points were reported in this study. The impact of influent wastewater microbial composition on AnMBR microbial community was investigated with beta diversity analysis performed using QIIME2 based on weighted unifrac metric, visualized as Principal Coordinate Analysis (PCOA) plots and neighbor joining dendrograms.

The resulting emperor plot output of PCOA was viewed on QIIME2View
(https://view.qiime2.org) and the dendrogram was visualized using iTOL (Letunic & Bork,
2019). Canonical correspondence analysis (CCA) and Pearson's correlation analysis was carried
out to correlate the phylum level *Bacteria* and genus level *Archaea* with environmental and
operational variables [pH, temperature, organic loading rate (OLR), Bioreactor volatile solids
(VS)]. Sequence reads of *Bacteria* and *Archaea* greater than 1% relative abundance in different
samples were input to XLSTAT software to construct CCA biplots and determine the Pearson's
correlation coefficients. Pearson's correlation was also performed with potential syntrophic
genera in the microbial community.

4.1.5 Sample characterization

Biogas generation from the bioreactor exhaust, hollow-fiber gas transfer membrane
(vacuum pump discharge), and combined gas exhaust was quantified using a variable gas flow
meter (Alicat Scientific). An online gas flow sensor was used to measure the methane content of
the biogas (Nova Analytical Systems Inc). Total chemical oxygen demand (TCOD) was analyzed
with HACH® kits using a HACH DR5900 (Loveland, CO, USA) spectrophotometer.

BOD$_5$, Total solids (TS), Total suspended solids (TSS), fixed and volatile solids were
analyzed following methods 5210B, 2540B, 2540D, and 2540E, respectively of the Standard
Methods for the Examination of Water and Wastewater, 22nd Edition. Sulfide and sulfate
concentrations were measured using standard HACH methods (HACH methods 8051 and 8131,
respectively) and measured on a HACH (Loveland, CO, USA) DR3900 spectrophotometer.
Sulfide measurements were done immediately after sampling in order to minimize the oxidation
or escape of sulfides in the sample. Additional sulfate measurements were made using an ion
chromatograph (ICS1000, Thermo Fisher, Waltham, Massachusetts, USA). Organic loading rate

(OLR) was calculated based on the influent wastewater COD values, reactor volume, and the influent flowrate measured by an online flow meter. All chemical analyses were done using Milli-Q water.

4.2 Overall microbial community diversity in pilot-scale AnMBR

4.2.1 Distribution of predominant bacterial communities

The distribution of bacterial communities in the AnMBR sludge are shown in Figure 4.1. The AnMBR was dominated by a core group of bacterial phyla comprised of *Bacteroidetes*, *Proteobacteria*, *Firmicutes,* and *Chloroflexi* throughout the operational period (Figure 4.1A). This is consistent with previous studies on microbial communities in mesophilic anaerobic systems and psycrophilic AnMBRs (Regueiro et al., 2012; Smith et al., 2013). *Proteobacteria and Bacteroidetes* together consistently constituted > 50 % of average relative bacterial abundance in each of the three stages of reactor operation. *Bacteroidetes* are known to metabolize proteins and carbohydrates to produce volatile fatty acids (propionate and acetate) (Seo et al., 2019). *Firmicutes* are volatile fatty acid degrading syntrophic bacteria that produce hydrogen (Riviere et al., 2009) increasing up to 24.2% on day 257. The relative bacterial abundance of *Chloroflexi* decreased with the reactor operation and temperature decrease. The functional role of *Chloroflexi* are still unclear, but studies have identified their probable role in the anaerobic degradation of glucose and other complex organic substances (Ariesyady et al., 2007). Phyla such as *Synergistetes, Spirochaetes*, and *Verrucomicrobia* together constituted only a low fraction of the bacterial phyla in the first two stages but increased up to 22.5% of the total bacterial abundance during stage 3 of operation. *Actinobacteria* and *Tenericutes* were present as a minor fraction in the seed sludge but eventually diminished during the later stages of reactor operation.

53
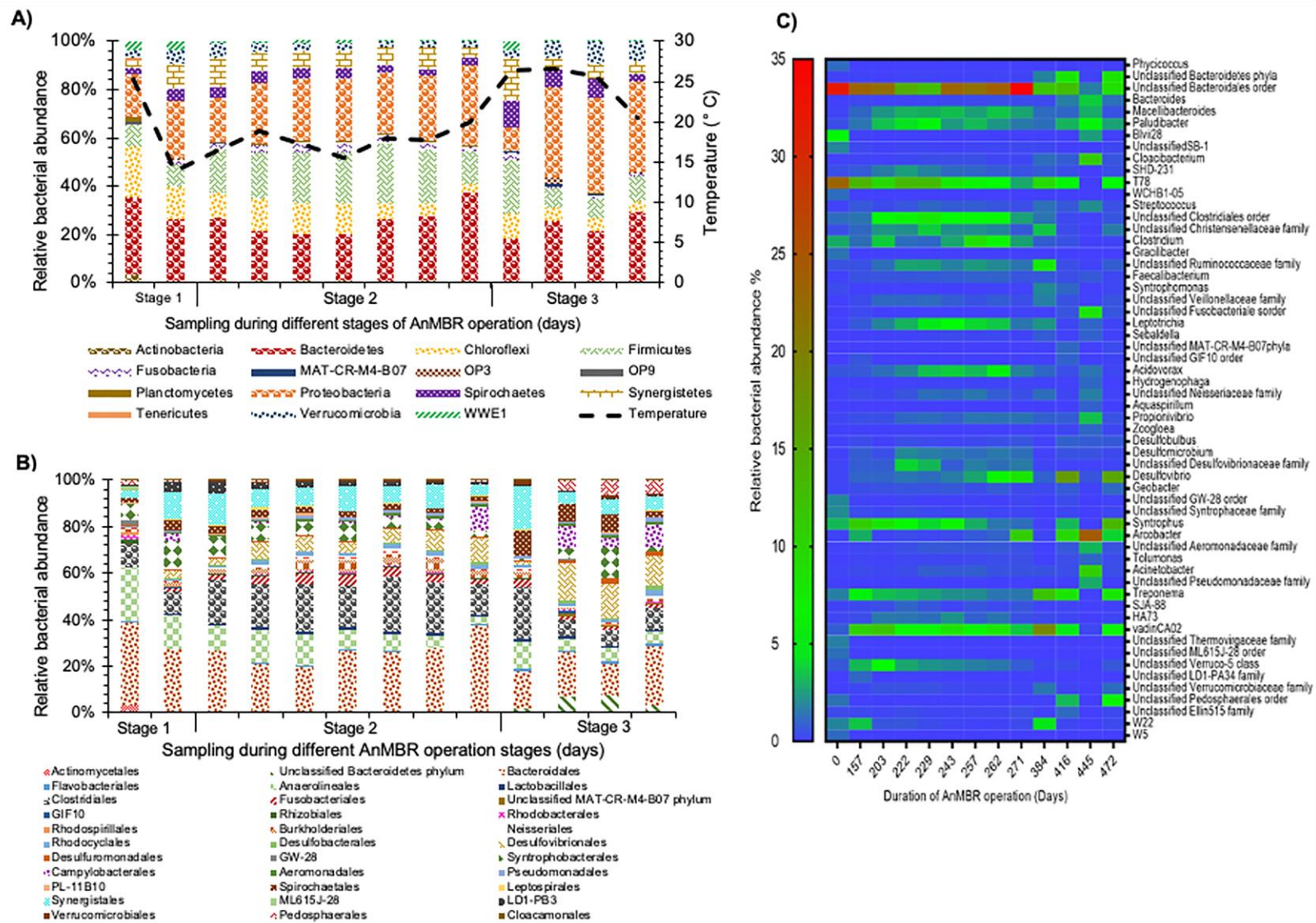
Figure 4.1 A) Distribution of bacterial phyla with ≥1% relative bacterial abundance in bioreactor sludge samples; B) Distribution of order level bacteria with ≥1% relative bacterial abundance in bioreactor sludge samples; C) heat map showing distribution of genus level bacteria with ≥1% relative bacterial abundances.

54

The order level bacterial community showed ample diversity and was well represented by members of the predominant phyla (Figure 4.1B). *Bacteroidales*, a member of the *Bacteroidetes* phylum were very stable (13.63% - 37.15%) and were always present in the community and their relative abundance did not diminish with time of operation in the reactor. *Clostridiales* (affiliated to *Firmicutes* phylum) increased with reactor operation increasing from 9.7% (Stage 1) → 19.1 % (Stage 2) and were a significant part of the bioreactor, although its abundance decreased and levelled off during the final stage (11.6 %) of reactor operation.

4.2.2 Distribution of predominant archaeal communities

High-throughput sequencing revealed that the relative abundance of *Euryarchaeota* consisting of the methanogenic *Archaea* in the AnMBR system was consistently below 2.5% of the overall microbial community profile (Figure 4.2A). This is similar to previously reported archaeal abundance values in AnMBR studies (Smith et al., 2015; Zamorano-López et al., 2019). The inoculum was initially predominant with unclassified *WSA2* genera belonging to the *Methanobacteriales* order and were completely out competed over the course of AnMBR operation. Although *WSA2* is classified as a family of *Methanobacteriales* order, it is considered a class-level monophyletic lineage within Euryarchaeota distinct from the *Methanobacteriales*, and likely perform methylated thiol reduction to drive methanogenesis (Chouari et al., 2005; Riviere et al., 2009; Wilkins et al., 2015; Nobu et al., 2016). The genus *Methanosaeta* (also known as *Methanothrix*) belonging to the *Methanosaetacea* family was a minor fraction (4.73 % relative archaeal abundance) in the inoculum on Day 0 of the AnMBR operation (Figure 4.2B). However, it continued to increase and was at a significant level for most of the reactor operation reaching up to 82.23 % and 76.93 % during Stages 2 and 3, respectively, indicating that temperature did not have a big impact on its metabolic abilities. *Methanosaeta* are

acetoclastic methanogens capable of forming methane from acetate cleavage and is the dominant acetoclastic methanogen under low acetate concentrations (van Haandel et al., 2014). The increase in *Methanosaeta* abundance indicated a shift from methyl group reducing methanogenesis by unclassified *WSA2* genera to acetoclastic methanogenesis.

The bioreactor witnessed a slow and progressive increase in *Methanospirillum,* reaching appreciable relative archaeal abundance levels between day 262 (5.45%) and day 416 (15%) of reactor operation. *Methanospirillum* are psychrotolerant hydrogenotrophic methanogens that produce methane from H_2 and CO_2 or from formate (Oren, 2014). *VadinCA11*, an archaeal genus whose metabolic functions are unclear and has been previously found in other anaerobic systems (Buhlmann et al., 2019), also surged in abundance around days 445 (34.84%) and 472 (20.16%) as shown in Figure 4.2B. Hydrogenotrophic methanogens such as *Methanobrevibacter* and *Methanobacterium* were consistently present in the reactor, with *Methanobrevibacter* abundance exceeding *Methanosaeta* around day 262 of reactor operation. The genus *Methanobacterium*, generates methane from CO_2 and H_2 or formaldehyde (H_2CO). Based on the microbial community profile, there was a competition between acetoclastic methanogenesis and hydrogenotrophic methanogenesis with acetoclastic methanogenesis dominating for the most part. In the present study, the surge in abundance of hydrogenotrophic methanogens (*Methanobrevibacter* and *Methanobacterium*) around days 257 (39.2 %) and 262 (76.3 %) could likely be attributed to the preceding low temperatures in the bioreactor which would have increased the availability of dissolved hydrogen in the reactor. Overall, the taxonomic profile of archaeal community demonstrated synergistic occurrence of different methanogenesis pathways including acetoclastic,

hydrogenotrophic and possibly methylotrophic indicating methanogenic adaptation to ambient temperature AnMBR operation.
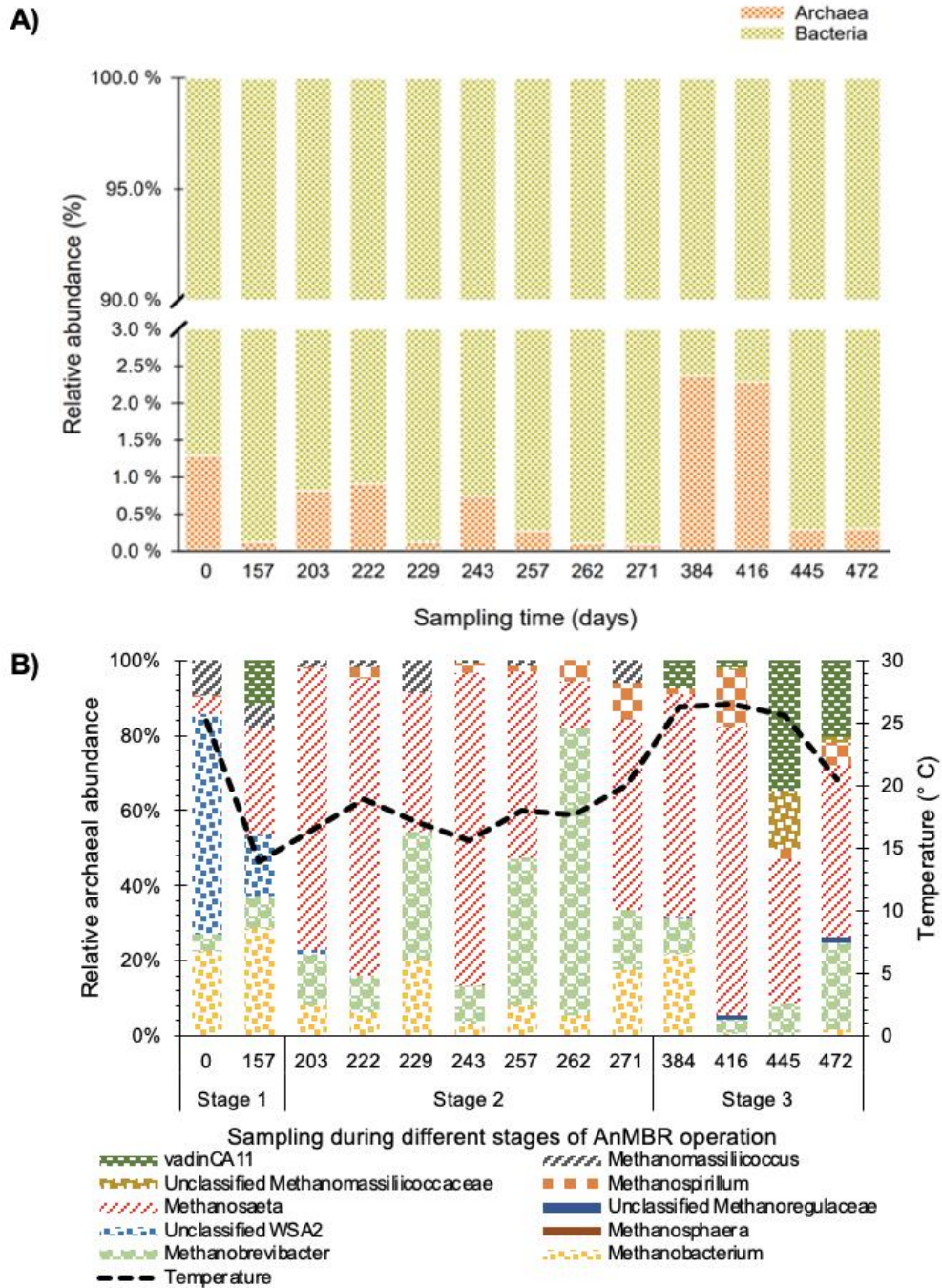
Figure 4.2 Distribution of A) total relative abundance of archaea and bacteria in bioreactor samples; B) archaea with ≥ 1% relative archaeal abundance at genus level in the bioreactor sludge samples.

4.2.3 Role of syntrophic interactions leading to methanogenesis

Syntrophic oxidation-reduction reactions involving syntrophic bacteria and methanogens play an important role in methane generation in anaerobic systems. High-throughput sequencing data of the AnMBR samples revealed presence of several syntrophic bacterial orders including *Synergistales*, *Anaerolineales*, *Clostridiales,* and *Syntrophobacterales* (Figure 4.1B). *Synergistales* are syntrophic fermentative bacteria in the *Synergistetes* phylum that have the ability to degrade amino acids into volatile fatty acids and contribute to acidogenesis and acetogenesis via syntrophic relationships with methanogens (Ferguson et al., 2016). The genus *VadinCA02* within *Synergistales* was present as a major constituent in AnMBR and their relative abundance reached up to 21% on Day 384. *Bacteria* assigned to *vadinCA02* and the genus *HA73* (also belonging to *Synergistales*) are likely to degrade peptone and amino acids into acetate (Yamashita et al., 2016; Yin et al., 2017).

Syntrophobacterales represented by the genus *Syntrophus* was consistently present in the reactor and was not a trivial community (relative bacterial abundance 3.6% at Day 0 and 14.4% at Day 452). *Syntrophus* can degrade butyrate, benzoate, and other fatty acids through synergistic interaction with hydrogenotrophic methanogens (Jackson et al., 1999). The bacterial order *Anaerolineales* were a bigger portion of the community during the initial start-up phase of reactor operation but gradually declined in abundance with time (decreased from 26% at Day 0 → 6.4% Day 472) as shown in Figure 4.1B. The *Clostridiales* order (belonging to *Clostridia* class) was represented by the syntrophy promoting genus *Clostridium* and the known syntrophic genus, *Syntrophomonas* (Narihiro et al., 2015). *Clostridium* was steadily present for most of the reactor operation, but its relative bacterial abundance declined during the later stages of reactor operation (reduced to 0.18% on Day 472). *Syntrophomonas (Syntrophomonadaceae* family*)*

grow in obligate syntrophy with hydrogenotrophic methanogens and SRBs to oxidize butyrate into acetate and H_2 (Sousa et al., 2009). In this study, Syntrophomonas was present in low abundance (0.44% on Day 0 → 2.37% (Day 384) → 0.3% (Day 472)) but their presence was positively correlated with hydrogenotrophic *Methanobacterium* (Pearson correlation coefficient r = 0.731, p = 0.005) and *Methanobrevibacter* (Pearson correlation coefficient r = 0.729, p = 0.005) indicating that the genus may have contributed to hydrogen production in the reactor. Interestingly, *Syntrophomonas* also showed strong positive correlation with acetoclastic *Methanosaeta* which could be possibly be due to interspecies acetate transfer which has been postulated as the basis for Direct interspecies electron transfer (DIET).

The genus *T78* (member of *Anaerolinieae* family) metabolize alcohols and carbohydrates through syntrophic interactions (Praveckova et al., 2016). Although present in high relative abundance during the initial reactor operation phase (23.5% at Day 0), *T78* steadily declined to reach 5.8% at Day 472 but were still one of the dominant genera in the biomass suspension. The genus *Treponema* was present throughout the AnMBR operation and their relative bacterial abundance spiked during the final stage of AnMBR operation (11.94% on day 384 and 7.91% on Day 472) (Figure 4.1C). *Treponema* consists of likely homoacetogenic strains that produce acetate from H_2 and CO_2 which could work in synergy with acetoclastic methanogens to produce methane (Zhang et al., 2009). Interestingly, the surge in *Treponema* during the later AnMBR operation stages corresponded to a parallel surge in acetoclastic *Methanosaeta* (Figure 4.2B), likely confirming a coordinated synergy between the homoacetogen and acetoclastic methanogen. The synergy was further confirmed based on the statistically significant positive correlation between the two genera (Pearson's correlation coefficient, r= 0.677 and p= 0.011).

Additionally, genus *Geobacter,* whose relative abundance reached up to 1.4 %, may have also been involved in syntrophic interactions with or without DIET (Rotaru et al., 2014).

4.2.4 Impact of Influent municipal wastewater on AnMBR microbial community dynamics

The dendrogram comparing the samples from the influent and suspended sludge, shown in Figure 4.3A, revealed that the influent feedwater samples grouped distinctly separate from the bioreactor samples, indicating that it did not impact the microbial dynamics in the reactor. Based on the PCoA plot (Figure 4.3B), the sample clusters had a maximum variation in 39.01 % (Axis 1) and 25.26 % (Axis 2) with separate clustering of the influent group and the bioreactor group samples. The variation of clustering patterns indicates significant differences in community structure in samples from the two sources with the bioreactor samples clustering separately, away from the influent wastewater. Similar difference in clustering pattern between the influent and bulk sludge samples was observed in a study on granular activated carbon fluidized AnMBR and it was concluded that the influent wastewater had little impact on the sludge microbial community (Evans et al., 2018). Although samples from the bioreactor and influent wastewater grouped distinctly, the spatial variation in clustering pattern of microbial communities in samples within each group could possibly be due to the effect of temperature.
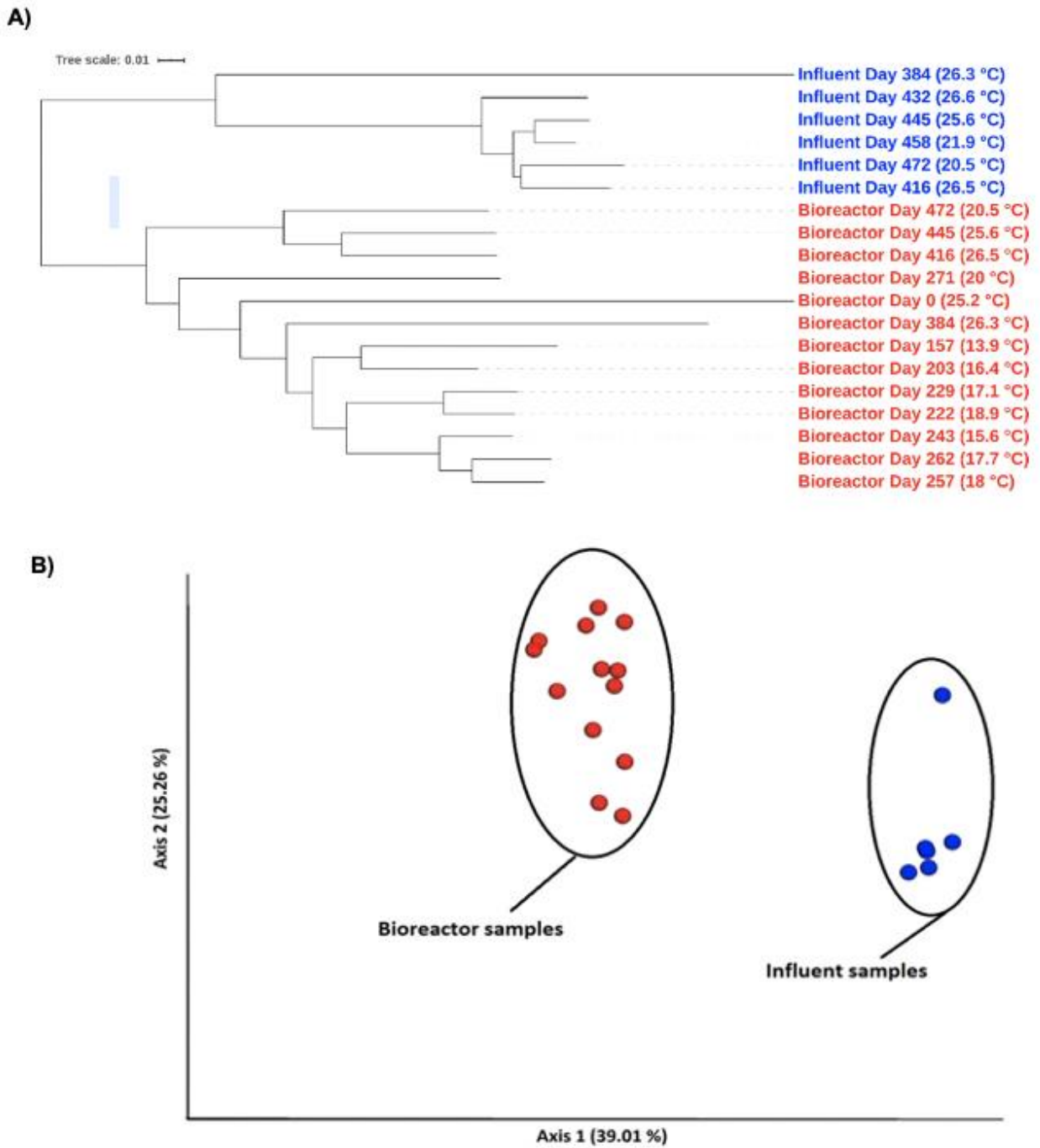
Figure 4.3 A) Weighted Unifrac dissimilarity cluster analysis dendrogram of microbial populations in the influent and bioreactor sludge using neighbor joining method.; B) Principal coordinates analysis (PCoA) plot showing clustering of bioreactor samples and influent samples as determined by Weighted Unifrac analysis.

The microbial differences in the observed sample clustering were further investigated with taxonomic analysis of the influent (Appendix Figure B.1), which revealed that *Bacteroidetes*, *Firmicutes*, *Fusobacteria*, and *Proteobacteria* together representing > 98 % relative bacterial abundance in all the influent samples. The predominant phyla level distribution of *Bacteria* reported in this study is consistent with previously reported studies on influent wastewater microbial composition (McLellan et al., 2010; Lee et al., 2015), although their relative abundances were not similar. Comparison of key bacterial orders (≥1% bacterial relative abundance) revealed sixteen overlapping bacterial orders in samples from the two sources. Of these orders, *Campylobacterales* (range 6.4% - 25.5%), *Flavobacteriales* (range 3.2% - 15.4%) and *Bacteroidales* (range 3.1% - 18.7%) were the main candidates in the influent (Appendix Figure B.2) and may be considered as generalists that can possibly survive in both sewerage drains and activated sludges (Lee et al., 2015). Within the bioreactor, *Campylobacterales* may likely have originated from the influent as its abundance remained small throughout the AnMBR operation. However, they progressively increased after 257 days of reactor operation which could likely be a transient surge within the AnMBR possibly due to their dominant abundance in the influent. Furthermore, the genus *Arcobacter* (belonging to *Campylobacterales* order), a potential enteric human pathogen (Vandenberg et al., 2004), was present in the reactor at low abundances (<1.5%) but spiked towards the final stages as shown in Appendix Figure B.3 (10.5% at Day 445) of reactor operation. *Arcobacter* is reported to grow under both aerobic and anaerobic conditions, and often found in raw sewage (Fisher et al., 2014).

The archaeal abundance in the influent samples was negligible as shown in Appendix Figure B.4; *Methanobacteriales* and *Methanomassilliicoccales* were the only identified orders and therefore are unlikely to have influenced the bioreactor archaeal community. Overall, the

core microbial population within the AnMBR reactor and the inherent shifts in the community dynamics is unlikely to be attributed to the influent wastewater microbial signature. The influence of influent wastewater could be limited to a mere transient surge in minor microbial genera for a few days but no influence on the core AnMBR bacterial or archaeal community composition.

4.2.5 Proliferation of Sulfate Reducing Bacteria (SRB)

Sulfate reducing bacteria proliferated with the duration of the AnMBR operation, although their relative abundance in the seed sludge was below 1% on Day 0. *Desulfovibrio* genus (*Desulfovibrionaceae* family) was the dominant SRB with relative abundance increasing from 0.2% (Day 0) → 3.1 % (Day 257) → 15.4 % (Day 472). *Desulfovibrio* utilizes sulfate as a terminal electron acceptor while oxidizing H_2, formate, ethanol, and lactate (Devereux et al., 1990). The genus *Desulfomicrobium*, which utilizes H_2 as an electron donor and acetate as carbon source was consistently present in the reactor, but their abundance decreased after Day 384 from 0.1% (Day 0) → 1.6% (Day 257) → 0.4% (Day 472). The proliferation of SRB in the bioreactor can be correlated with the increase in bioreactor sulfide, represented in Figure 4.4, which shows a reduction in sulfate concentrations and concomitant biological production of sulfide in the permeate. In addition, the sulfide concentration in the influent feed wastewater was always below detection indicating the role of SRB as the most likely factor for the sulfide generation, further evidenced from the high throughput sequencing data. Overall, the increasing abundance of SRB with an increasing production of sulfide (as hydrogen sulfide) causes concern because of the potential of microbially induced sulfide corrosion that could degrade the inner metallic parts of the AnMBR system. Additionally, certain SRB genera including *Desulfovibrio* are capable of shifting from being sulfidogenic to syntrophic VFA fermenters under sulfate

limiting conditions (Plugge et al., 2011). Therefore, the metabolic flexibility of SRB could add to the microbial community redundancy in the AnMBR system.
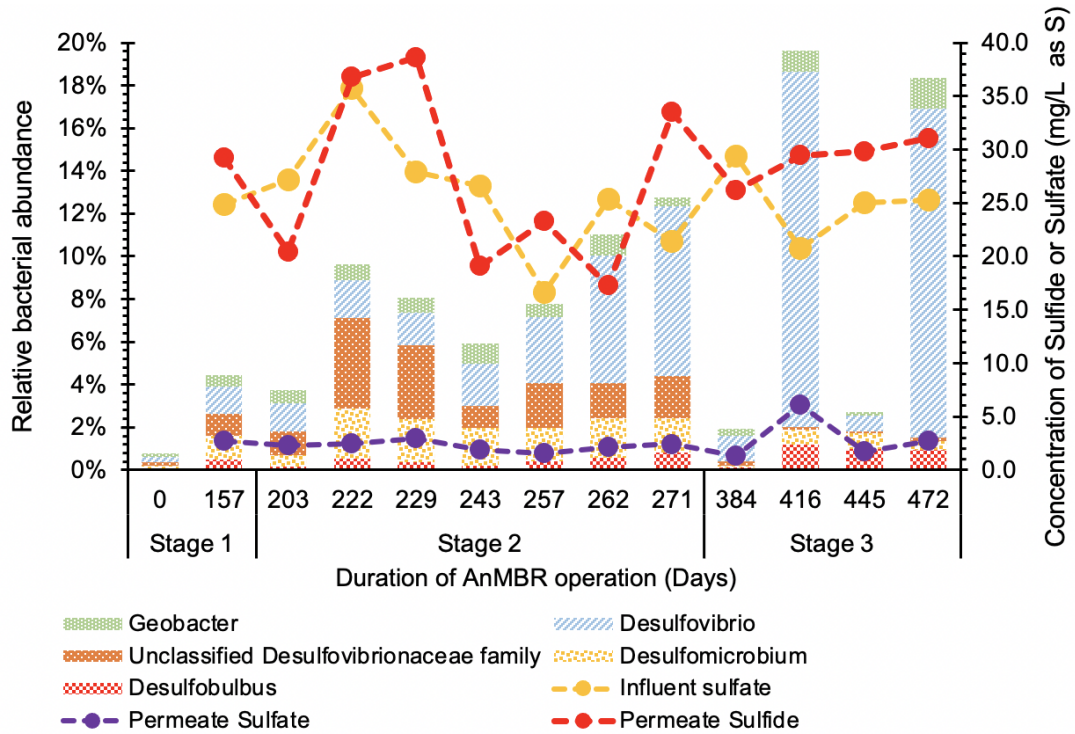
Figure 4.4. Key sulfate reducing bacteria (SRB) genera at ≥1 % relative bacterial abundance in the bioreactor sample over the long term AnMBR operation under ambient operational conditions. Gradual proliferation of selected key SRB ((*Desulfovibrio, Desulfobulbus* and *Geobacter*) while other SRB (*Desulfomicrobium*, unclassified *Desulfovibrionales*) gradually declined in relative abundance.

4.2.6 Influence of environmental and operational variables on microbial population

In the 2-dimensional canonical correspondence analysis biplots (Figure 4.5), the environmental and operational variables are represented as vector lines. The length of the lines indicates the significance of the environmental and operational variables on respective bacterial phyla and archaeal genera within the bioreactor. The cosine angle between the vector variables lines indicates their correlation with the environmental variables. The phyla level bacterial CCA biplot (Figure 4.5A) had 49.02% variation along the first axis (F1) and 34.26 % variation along the second axis (F2) and together represented 83.28% variation of relative bacterial abundances

of the phyla. Bioreactor VS was shown to have the most significant correlation on the relative abundances of phyla. Bacterial phyla with minor relative abundance such as *Actinobacteria and Planctomycetes* positively correlated with bioreactor VS while *Spirochaetes* correlated negatively. Synergistetes correlated positively with OLR. At the genus level of *Archaea* (Figure 4.5B), *Methanobrevibacter* and M*ethanomassiliicoccus* showed a positive correlation with pH, while *VadinCA11* and *Methanospirillium* showed positive correlation with OLR. Temperature was negatively correlated with *Methanobrevibacter* which possibly explains their surge in abundance in response to low temperature conditions. Additionally, *Methanosaeta* was also found to be negatively correlated to temperature. However, due to it being positioned closer to the origin, it may not have been strongly impacted by the different operational parameters including temperature and was therefore seen to be present throughout the duration of AnMBR operation.

To confirm the trends in correlation between environmental variables and the taxa as well as to analyze correlations between different taxa, Pearson's correlation analysis was also performed. The Pearson's correlation analysis revealed that the Bioreactor volatile solids strongly correlated with *Actinobacteria* (r=0.826, p<0.003). Although the Pearson's correlation results did not exactly match with all the CCA correlation trends, it established crucial correlations between environmental variables and sample taxa. Interestingly, the core bacterial phyla *Bacteroidetes, Firmicutes, Chloroflexi, and Proteobacteria* clustered close to the origin in the CCA plot, indicating that they are not really affected by environmental variables. This could be indicative of the resilience of the core microbial community to the environmental variables

including temperature along with the likely presence of psychrotolerant mesophilic bacteria originating from the seed sludge.
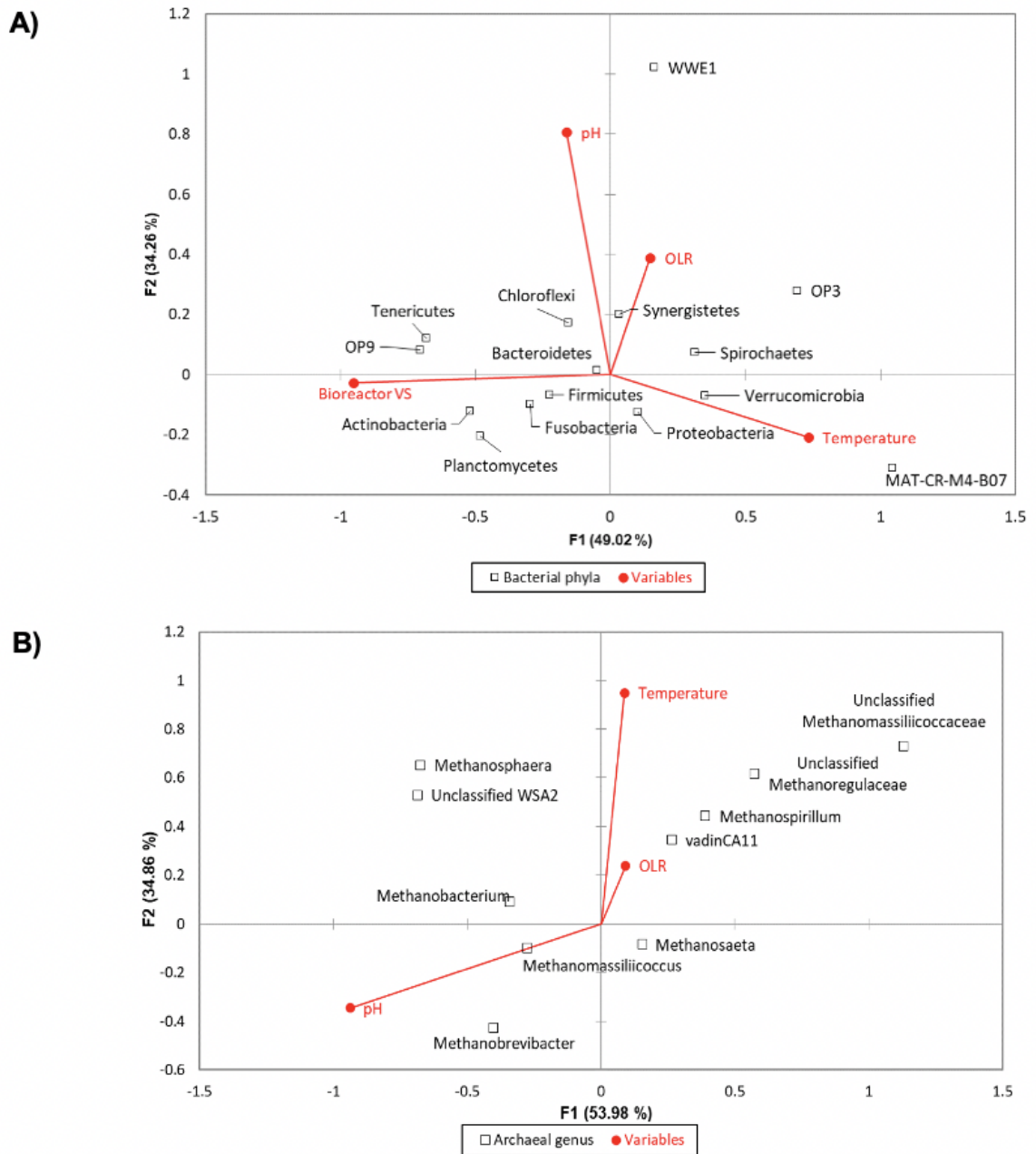
Figure 4.5. Canonical correspondence analysis (CCA) plot to investigate the relationship between relative abundance of AnMBR microbial communities and key operational parameters (pH, temperature, OLR, and bioreactor VS) for a) bacteria at phylum level, and b) archaea at genus level.

4.2.7 Identification of key microbial communities

Bacterial genera at ≥ 1% of average relative bacterial abundance in at least one of the three stages were identified as the key members of the AnMBR system. The core microbiome of the AnMBR system was represented by the phyla *Bacteroidetes, Proteobacateria, Chloroflexi, Firmicutes, Fusobacteria, Spirochaetes, and Synergistetes* and their associated genera as shown in Table 4.2. The *Bacteroidetes* phylum was mainly represented by the unclassified genera belonging to the *Bacteroidales* order. Overall, a core microbial community and its likely role in the AnMBR system has been identified. However, the limitations of amplicon gene based microbial community analysis may need to be addressed to understand the functional roles of microbes and not just based on their relative abundance.

Table 4.2. Bacterial genera representing core and transient microbiome of the AnMBR system

Phylum	Order/Family	Associated Genus	Average relative bacterial abundance (%)			Probable Role	References
			Stage 1	Stage 2	Stage 3		
Bacteroidetes	*Favobacteriales*	*Cloacibacterium*	0.16%	0.35%	3.60%	Hydrolysis of starch	Allen et al. (2006)
Bacteroidetes	*Porphyromonadaceae*	*Macellibacteroides*	0.83%	3.26%	1.69%	Glucose fermentation to lactate, acetate, butyrate and isobutyrate	Jabari et al. (2012)
Bacteroidetes	*Porphyromonadaceae*	*Paludibacter*	1.15%	3.40%	3.19%	Glucose fermentation to propionate	Ueki et al. (2006)
Bacteroidetes	Unclassified *Bacteroidales* order	-	27.49%	21.78%	8.80%	-	-
Proteobacteria	*Rhodocyclaceae*	*Propionivibrio*	0.42%	1.42%	1.63%	Fermentation	Brune et al. (2002)
Proteobacteria	*Desulfomicrobiaceae*	*Desulfomicrobium*	0.59%	1.68%	0.49%	Sulfate reduction	Dias et al. (2008)
Proteobacteria	*Desulfovibrionaceae*	Unclassified *Desulfovibrionaceae* family	0.62%	2.22%	0.14%	Sulfate reduction	Suzuki et al. (2010)
Proteobacteria	*Desulfovibrionaceae*	*Desulfovibrio*	0.75%	3.37%	8.50%	Sulfate reduction	Devereux et al. (1990)
Proteobacteria	*Syntrophaceae*	*Syntrophus*	7.21%	4.41%	4.23%	Syntroph butryrate VFA degradation	Jackson et al. (1999)
Proteobacteria	*Campylobacteraceae*	*Arcobacter*	1.70%	2.05%	9.47%	Acetate oxidation	Supaphol et al. (2011)
Chloroflexi	*Anaerolinaceae*	*T78*	18.43%	8.28%	4.89%	Metabolize alcohols and carbohydrates (Semi-syntroph)	Praveckova et al. (2016)
Firmicutes	Unclassified *Christensenellaceae* family	Unclassified *Christensenellaceae* family	0.99%	2.50%	1.59%	Glucose fermentation (Acidogenesis)	Morotomi et al. (2012)
Firmicutes	Unclassified *Clostridiales* order	-	1.64%	5.54%	0.74%	Likely fermenters	Jo et al. (2015)
Firmicutes	*Clostridiaceae*	*Clostridium*	2.47%	3.95%	0.50%	Glucose fermenters, biohydrogen production	Zhang et al. (2006)
Firmicutes	Unclassified *Ruminococcaceae*	Unclassified *Ruminococcaceae*	0.64%	2.38%	2.27%	Fermentation	Parameswaran et al. (2010)
Firmicutes	*Syntrophomonadaceae*	*Syntrophomonas*	0.24%	0.05%	1.02%	Syntrophic oxidation of Butyrate to acetate and H_2	McInerney et al. (1981); Sousa et al. (2009)
Firmicutes	*Streptococcacea*	*Streptococcus*	0.48%	0.87%	1.43%	Glucose fermentation; Capable of extracellular electron transfer via DIET	De Soet et al. (2000); Lei et al. (2016)
Fusobacteria	Unlcassified *Fusobacteriales* order	-	0.19%	0.06%	2.43%	Hydrolysis/acidogenesis	Miura et al. (2015)
Fusobacteria	*Leptotrichiaceae*	*Leptotrichia*	0.50%	3.59%	1.12%	Fermentation	Zhou and Li (2015)
Spirochaetes	*Spirochaetaceae*	*Treponema*	3.44%	2.68%	6.99%	Homoacetogen	Zhang et al. (2009)
Synergistetes	*Dethiosulfovibrionaceae*	*HA73*	0.41%	1.64%	0.23%	Protein degradation to produce acetate	Yamashita et al. (2016); Yin et al. (2017)
Synergistetes	*Synergistacea*	*VadinCA02*	5.78%	7.13%	7.42%	Protein degradation to produce acetate	Yamashita et al. (2016)

4.3 Summary

The findings of this study indicate that the bacterial microbial community are resilient to the environmental variables of temperature, OLR, and maybe pH. Syntrophic relationships are evidenced throughout the period of AnMBR operation with the presence of members belonging to the *Synergistales*, *Anaerolineales*, *Clostridiales,* and *Syntrophobacterales* bacterial orders. Acetoclastic methanogenesis was observed to be the predominant pathway and is resilient to ambient temperature operation. The mechanisms of methane production at low temperature still needs more investigation. The core of the AnMBR microbial community represented by *Bacteroidetes*, *Proteobacteria*, *Firmicutes,* and *Chloroflexi* phyla is distinctly unique and developed within the bioreactor and not influenced by the influent wastewater microbial community. Proliferation of SRB with long term operation and as a response to the influent sulfate concentrations might necessitate sound microbial community management or reactor modifications in the long term to enable high microbial efficiency.

Chapter 5 - Ammonia sorbed clinoptilolite from swine permeate as an alternative fertilizer product to conventional urea fertilizers using greenhouse studies and soil incubation tests

5.1 Introduction

Excessive fertilizer application in irrigated agricultural soils and the associated nitrogen (N) losses continue to be a major source of environmental pollution affecting both surface and groundwater quality as well as human health. Despite the hope that excessive fertilizer application increases the phytoavailability of N, it is reported that plant uptake accounts for only 30-50% of applied N (Anas et al., 2020; Zhang et al., 2011; Naz & Sulaiman, 2016). The surplus N leads to losses through nitrate leaching, ammonia volatilization, emissions of nitric oxide (NO) and nitrous oxide (N_2O) (Zebarth et al., 2009). Such overapplication of N and the resulting losses cause unintended environmental damage including harmful freshwater algal blooms, global warming from greenhouse gas emissions, negative impacts on surface water and groundwater quality. In addition to the environmental costs due to nitrogen pollution, the economic costs and the greenhouse gas emissions footprint associated with producing ammonia on a commercial scale using the Haber-Bosch process and urea synthesis processes make it unsustainable. Contrarily, the recovery of nutrients including nitrogen and phosphorus from wastewater offers significant environmental benefit and reusing the recovered nutrient products as fertilizers could offset fertilizer costs thereby providing economic benefits. Currently, the most common nutrient products recovered from wastewater treatment facilities are treated wastewater biosolids and struvite ($Mg.NH_4.PO_4.6H_2O$), both of which are marketed for subsequent land application. However, biosolids and struvite present some challenges when it comes to land application. Biosolids application can alter soil P status, uncertainty in phytoavailability of nutrients, potential accumulation of heavy metals in soil, and plant uptake (Antille et al., 2017). In

addition, struvite and biosolids comprise both nitrogen and phosphorus together, making it difficult to meet plant nutrient requirements for one without exceeding the application rate of the other. Moreover, the wastewater industry mainly focusses on recovery of phosphorus and not on nitrogen. Therefore, there is a need for tailored nutrient recovery processes that can result in nitrogen products that can release N slowly and minimize losses.

Proper estimation of N losses along with maintaining a balance between N fertilizer supply and crop N demand remains crucial for understanding the nitrogen dynamics and minimizing nutrient pollution. One strategy to address nutrient losses from soil is the use of appropriate N sinks in soil such as zeolites which can also act as slow-release fertilizers (He et al., 2002, Dong et al., 2020). The application of clinoptilolite, a natural zeolite to soil is known to increase the soil cation exchange capacity, retard ammonium or nitrate leaching, and retain moisture content (Perrin et al., 1998). Additionally, clinoptilolite exhibits greater affinity for cations including ammonium, potassium ions and is known to simultaneously remove phosphate along with ammonia adsorption from wastewater based on the results presented in Chapter 3 (Kannan & Parameswaran, 2021) and other published studies (Lin et al., 2014, Guaya et al., 2020). These properties of clinoptilolite make it an attractive ion exchange material in wastewater treatment and as a soil amendment.

Some previous studies have focused on the use of untreated clinoptilolite or other natural zeolites as soil amendments for controlling N losses in soil (He et al., 2002; Haruna Ahmed et al., 2008; Ippolito et al., 2011; Jakkula & Wani, 2018; Sun et al., 2019) while some others have focused on applying nutrient coated zeolites as slow-release fertilizers (Park et al., 2005; Bhardwaj et al., 2012; Souza et al., 2018; Dubey & Mailapalli, 2019; Mihok et al., 2020). However, there are very limited studies evaluating the fertilizer applicability of wastewater

derived ammonia saturated clinoptilolite. Furthermore, there are currently no known studies

evaluating the performance of AnMBR swine permeate based ammonia loaded clinoptilolite as a

slow nutrient release fertilizer and the present study will be one of the first attempts.

The aim of this study is to evaluate the slow nitrogen release potential of the ammonia

loaded clinoptilolite compared to conventional fertilizers (urea and ammonium sulfate) and

anaerobically treated biosolids by monitoring the N diffusion pattern in a Petri dish based soil

incubation setup. Additionally, the effect of ammonia loaded clinoptilolite on plant growth was

studied by conducting pot experiments with corn (*Zea mays*) in a greenhouse. Finally, potential

changes to the soil microbial community due to the application of the different N fertilizers in the

pot studies were also evaluated.

5.2 Materials and Methods

5.2.1 Soil collection

Surface soil was collected from Kansas State University's North Farm in Manhattan,

Kansas, USA. Soils, collected at a depth of 15-20 cm, were air dried, gently crushed and sieved

through a 2 mm sieve. After mixing for homogeneity, the soil was analyzed for pH (1:1,

soil:water slurry) using a Skalar SP50 Robotic Analyzer (Skalar Inc. Buford, GA 30518),

phosphorus, electrical conductivity (EC), soil texture, cation exchange capacity (CEC), organic

matter, inorganic nitrogen (NH_4 and NO_3), cations (potassium, calcium, magnesium, sodium,

zinc, iron, manganese, copper, aluminum), anions (sulfate, chloride), total nitrogen, and total

phosphorus at the Kansas State University Soil Testing Lab in Manhattan, Kansas, USA

following the recommended chemical soil test procedures for the north central region (Brown,

1998). The initial soil properties are summarized in Table 5.1. Maximum water holding capacity

was determined using the method from Jenkinson and Powlson (1976).

Table 5.1 Soil and biosolid characterization results

	Soil	AnMBR sludge
pH (1:1 soil:water)	7.4	6.8
Sulfur (mg/kg)	5.1	936.1
Sand (%)	20	67
Silt (%)	58	18
Clay (%)	22	15
Electrical conductivity (mS/cm)	0.47	3.75
Total N (%)	0.28	2.1
Ammonia NH_4-N (mg/kg)	4.4	634.7
Nitrate NO_3-N (mg/kg)	14	4
DTPA extractable Zn (mg/kg)	1.7	38.2
Total P (ppm)	524	7311
Mehlich 3 Phosphate (mg/kg)	77.6	468
Extractable Potassium, K (mg/kg)	475.1	242
Organic matter (%)	4.4	33.5
Sodium, Na (mg/kg)	5.83	146
Aluminum, Al (ppm)	0.35	0.67
Cation exchange capacity, cmol(+)/kg	24.4	16.1
Extractable Calcium, Ca (mg/kg)	2713	2159
DTPA extractable Copper, Cu (mg/kg)	0.73	2
Iron, Fe (mg/kg)	16.9	388
Magnesium, Mg (mg/kg)	186.4	190

Manganese, Mn (mg/kg)	15.1	41
Chlorine, Cl (mg/kg)	13.2	171
Lead, Pb (ppm)	NA	2.9
Arsenic, As (ppm)	NA	2.5
Cadmium, Cd (ppm)	NA	0.2
Chromium, Cr (ppm)	NA	3

5.2.2 Preparation of ammonia saturated clinoptilolite from AnMBR treated swine permeate

Ammonia sorbed clinoptilolite was prepared by treating swine permeate from a lab-scale anaerobic membrane bioreactor operated at Kansas State University, Manhattan, USA using natural clinoptilolite media (Zeobest®). Batch equilibrium studies were performed by adding 10 g/L of clinoptilolite to several 1 L beakers containing the swine permeate and placing on an orbital shaker for 24 hours to equilibrate. The ammonia adsorption capacity of the clinoptilolite at the end of the equilibrium experiment was found to be 12 mg NH_4-N/g clinoptilolite. The clinoptilolite sorbed with ammonia was evaluated as a nitrogen source in subsequent nutrient release experiments that included soil incubation and plant nitrogen uptake studies.

5.2.3 Biosolids from anaerobically treated wastewater

To evaluate nitrogen release from stabilized dewatered biosolids after anaerobic digestion, sample was collected from the Blue River Wastewater Treatment Plant in Kansas City, Missouri, USA. The collected sample was analyzed at the Kansas State University Soil testing lab. The biosolid properties are summarized in Table 5.1. The biosolid used for the incubation studies were assumed to undergo 40% mineralization Sullivan et al. (2018).

5.2.4 Incubation study experiment set up

Soil incubation experiments evaluating N diffusion from different treatments were performed in Petri dishes (87 mm diameter and 11 mm height). Treatments included urea [$(NH_2)_2CO$], ammonium sulfate [$(NH_4)_2SO_4$], ammonia-saturated clinoptilolite, anaerobically digested wastewater biosolids and no nitrogen control. All treatments were replicated five times. Petri dishes were packed to achieve bulk density of 1.2 g/m^3 using 10% maximum water holding capacity (MWHC) pre wetted soil. The packed Petri dishes were brought to 55% MWHC, covered, inverted and sealed with Parafilm and equilibrated in the dark for 24 hours at room temperature (25 °C). After equilibration, different nitrogen treatments targeting 10 mg-N per Petri dish were placed in a 12.5 mm diameter hole created exactly at the center of the Petri dish. To maintain uniformity and to account for the variability in mass and bulk density of different treatments placed in the hole, some voided holes were filled with a mixture of inert glass beads and sand after treatment placement to fill voids within the treatment hole. The Petri dishes were covered using a lid and sealed with parafilm. The soil packed Petri dishes were then placed within a larger Petri dish (150 mm diameter). The space between the two Petri dishes was packed with a 1.5 cm thick polyurethane sponge and filled with 15 mL of 2% boric acid to capture any ammonia released from the soil by volatilization. The sponges were previously cleaned and pretreated by soaking in 2% boric acid overnight and rinsing with 1N KCl to ensure residual ammonia is removed. The large Petri dish containing the smaller soil packed Petri dish and ammonia trap sponge was covered using a lid and sealed with parafilm to minimize moisture losses. All Petri dishes were then wrapped in aluminum foil and placed in a dark, temperature-controlled incubator at 25°C for two incubation periods of 1-week and 4-weeks, respectively.

5.2.4.1 Soil sectioning after incubation

At the end of each incubation period, the soil packed Petri dishes were marked and divided into three concentric sections starting from the center as shown in Figure 1 (section 1: 0-13.5 mm; Section 2: 13.5 – 25.5 mm, Section 3: 25.5 – 43.5 mm radius). Soil from each section was transferred to pre-weighed containers and mixed thoroughly. Next, 1 g of soil was collected from each section for wet extraction of ammonium (NH_4^+-N), nitrate (NO_3^-) and nitrite (NO_2^-) using a 2N KCl solution. The extractions were filtered through Whatman® Grade 42 ashless filter paper and used for chemical analyses. The remaining soil from each section was oven dried at 40 °C and used for pH analysis.
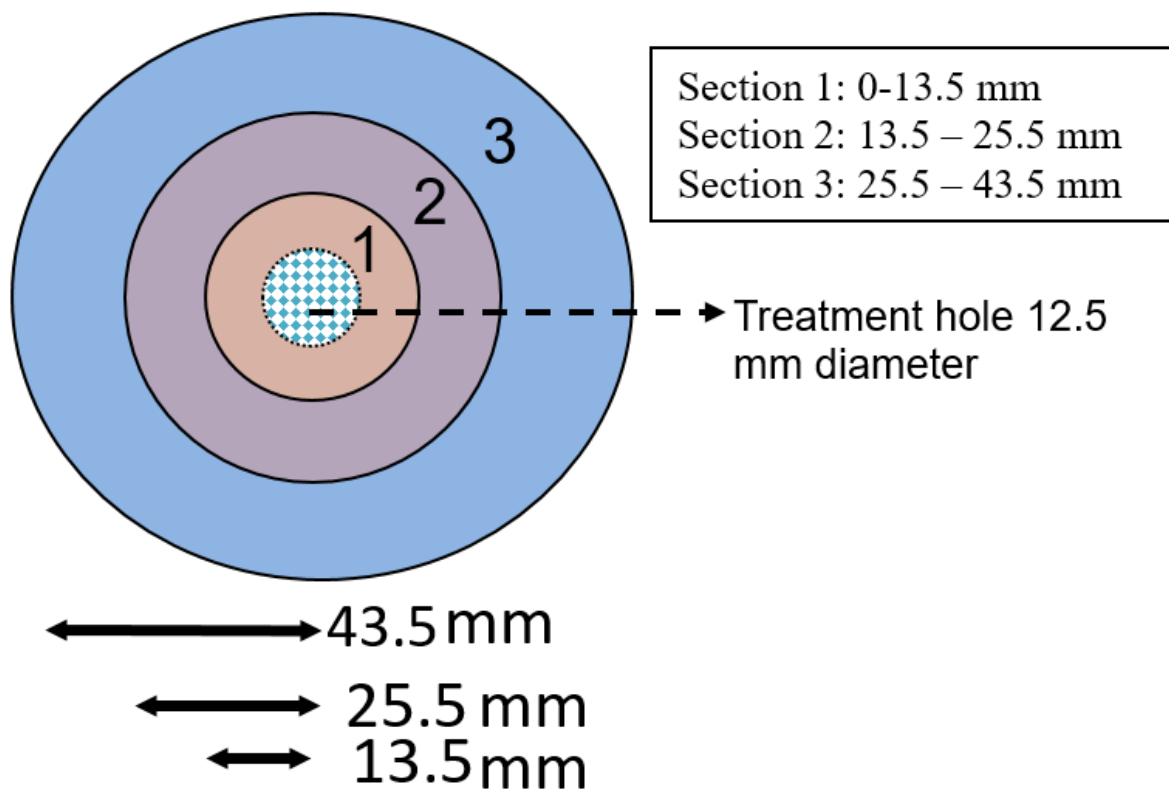
Figure 5.1 Illustrative representation of soil sections within the petri dish in the incubation study

5.2.4.2 Chemical analysis of soil samples from incubation study

The filtered soil solutions were analyzed for ammonia, nitrate, and nitrite. Ammonia was analyzed using HACH® TNT 832 ammonia test kits. Nitrate and nitrite were analyzed using the QuikChem® Method 12-107-04-1-J on the QuikChem® 8500 Series 2 FIA automated flow analyzer. Soil pH was measured in a 1:10 soil:Milli Q water extract (Watson, 1998) using a Fisherbrand™ accumet™ AB150 pH Benchtop Meter.

5.2.5 Plant nitrogen uptake studies

After the soil incubation experiments, pot experiments were performed with maize crop to evaluate plant nitrogen uptake with ammonia sorbed clinoptilolite as a supplement to urea application and possibly to reduce the urea application rate. The plant nitrogen uptake studies were conducted at Kansas State University's Throckmorton greenhouse complex. The experiment consisted of five treatments:

i.   T1 = 100% urea + 0% clinoptilolite

ii.   T2 = 90% urea + 10 % clinoptilolite

iii. T3 = 80% urea + 20% clinoptilolite

iv.   T4 = 0% urea + 100 % clinoptilolite

v.   T5 = Control with no added nitrogen

The treatments were incorporated into the same soil collected from K-State Agronomy North Farm, along with the basal dose of potassium and phosphorus, after the soil had been pre-wetted at 10% MWHC. The various nitrogen treatments and basal nutrients (potassium and phosphorus) were applied in half doses at a rate of 100:25:13 NPK kg/ha. After packing the soil in each pot, the soil moisture content was increased to 60% MWHC and equilibrated for 24 hours. Two corn seeds (Pioneer hybrid) were sown in each pot and later thinned out to 1 plant per pot after one

week. The greenhouse was maintained at temperatures of 23-25 °C and 16 h daylight and 8 h dark photoperiod. The duration of the experiment was 5 weeks from the day of sowing and on any given day, the soil moisture content in the pots was maintained at 60% MWHC of soil. Five weeks duration was chosen to evaluate the early N demand of the crop. All pots were rotated (within each block) each day to ensure even exposure to greenhouse conditions.

5.2.5.1 Processing of plant samples: Plant height, leaf area and above ground biomass

35 days after sowing, the plant height was measured with a ruler, and a 20 cm^2 piece of leaf was taken from the second leaf from the top. After sampling the leaf piece, the plants were dissected into leaves and stems and oven dried at 60°C until a constant weight was reached. The ratio of the total leaf dry biomass (g) and the cut leaf piece dry biomass (g/cm2) gives the leaf area of the plant. The sum of the dry biomass of the leaves and the dry biomass of the stem gives the above-ground biomass (g/plant). The dried biomass was finely ground and used for total nitrogen and total carbon analysis.

5.2.5.2 Chlorophyll estimation

The Chlorophyll content was determined according to Hu et al. (2013) with slight modification. One hundred mg of fresh leaf tissue was incubated overnight in 10 ml of acetone. The absorbance of the extract was measured using a spectrophotometer (Varian Cary 50 UV-Vis) at 645, 663 and 652 nm for chlorophyll 'a', chlorophyll 'b' and total chlorophyll respectively using acetone as blank. Total chlorophyll and its fractions are computed using the formula given by Arnon (1949).

$$Chlorophyll\ 'a'\ (mg/g) = \frac{12.7\ (A_{663}) - 2.69\ (A_{645})\ x\ V}{1000\ x\ W}$$

$$Chlorophyll\ 'b'\ (mg/g) = \frac{22.9\ (A_{645}) - 4.68\ (A_{663})\ x\ V}{1000\ x\ W}$$

$$Total\ Chlorophyll\ (mg/g) = \frac{A_{652}\ x\ V}{1000\ x\ 34.5\ x\ W}$$

V = Final volume of acetone extract; W = final weight in grams

In addition, a non-destructive chlorophyll estimation was performed using a portable, self-calibrating, non-destructive SPAD device at 3 weeks and 5 weeks of the growth period. The SPAD (Soil-Plant Analysis Development) chlorophyll meter (SPAD-502, Minolta Co., Japan) measures chlorophyll content as the ratio of radiation transmitted through a leaf at two wavelengths centered near 650 nm and 940 nm and converts them to digital signals and then to SPAD values (Minolta, 1989).

5.2.5.3 Chemical analysis

Dry plant biomass samples were analyzed for total nitrogen and total carbon at the Kansas State University soil testing lab using a LECO TruSpec CN Carbon/Nitrogen combustion analyzer (LECO Corporation, St.Joseph, MI, USA). Soil pH was measured in a 1:10 soil:Milli Q water extract (Watson, 1998).

5.2.6 Soil DNA extraction and sequencing

Soil DNA was extracted from soil samples collected from each pot at the end of 5 weeks using the EZNA® Soil DNA extraction kit (Omega Bio-tek). DNA sequencing to determine the microbial community of the soil was performed at MR DNA (Shallowater, TX, USA) using the Miseq platform (Illumina, USA). Primers (515f//806r) targeting the V4 region were used for the sequencing. The sequencing data files were processed in QIIME2 software (Bolyen et al., 2019). Taxonomically unassigned reads were excluded from the relative abundance estimation.

5.2.7 Statistical analysis

Statistical analysis of all data was done using IBM SPSS Statistics for Windows, Version 20.0 (SPSS Inc., USA). The green house experiment was laid in randomized completely block

design (RCBD) with treatments as main factor and replicates as blocking factor. The greenhouse data was analyzed using two-way ANOVA without interaction using univariate analysis in general linear model option available in SPSS. Tukey's Honestly Significant Difference (HSD) test was used to assess the significance of differences between pairs of group means. The incubation study was laid in completely randomized design (CRD) with two factors. The main factor was treatments and sub factor was sections. The incubation study data was analyzed using two-way ANOVA with interactions using univariate analysis in general linear model option available in SPSS. Tukey's post hoc test was used to compare the means. The significance was calculated at $p \leq 0.05$ for both the experiments.

5.3 Results and discussions

5.3.1 Soil incubation studies

Soil incubation studies were performed to understand the nitrogen diffusion and release in different treatments. The Petri dish setup for the incubation studies allowed to collect spactiotemporally resolved data. The results of the total inorganic nitrogen measured in each Petri dish at the end of the 1-week and 4-week incubation period are summarized in Figure 2A and Figure 2B, respectively. All treatments except the control received 10 mg N per Petri dish. The control had an initial background inorganic N mass of 1.4 mg N per Petri dish, which increased to 4.71 mg N after 1-week incubation and 5.16 mg N after 4-week incubation. The inorganic N increase in control samples was likely due to mineralization of organic N present in the soil. The sum of such mineralized N + added N is expected to exceed the added 10 mg N in the treatment samples. Expectedly, at the end of the one-week incubation period, total inorganic nitrogen was found to be 12.06 mg, 11.85 mg, and 11.8 mg in the ammonia-saturated clinoptilolite, ammonium sulfate, and urea treatments, respectively. However, the organic N

mineralization rate in the N- added treatment soil samples appeared to be slower than the control samples. This slower mineralization rate in treatment samples could be because the added N have had a slight negative impact on conversion of organic N in soil to inorganic N. In the case of biosolids, total inorganic nitrogen was found to be 7.07 mg. The amount of anaerobically digested biosolid added to each Petri dish was calculated based on the assumption that the biosolids would undergo 40% mineralization of organic nitrogen within the duration of a growing season. The lower than expected final inorganic N value in the biosolids added treatment is likely due to slow mineralization of organic N.

Organic nitrogen mineralization is reported to depend on the C/N ratio of the biosolids. Lower C/N ratio is expected to increase organic N mineralization (DELIN et al., 2012). In the present study, the C/N ratio for biosolids was found to be lower than 10, which is considered favorable for N mineralization. However, previous studies have reported that biomineralization of anaerobically processed biosolids is known to be slower than aerobically processed biosolids. In addition, studies have reported that the C/N ratio may not always be a good predictor of mineralization and other factors including organic carbon bioavailability and mineralization may affect N mineralization (Wang et al., 2003). This is plausible for anaerobic biosolids since the organic N and C could be so stable that they are not amenable to microbial mineralization.

The diffusion of N from different treatments was determined by estimating the amount of nitrogen in each section of the Petri dish. Diffusion from the point of treatment application was characterized by the increase in N concentration at the outer sections 2 and 3. At the end of 1-week incubation, it was observed that the inorganic N remained predominantly in section 1 (7.3 mg N) in the case of clinoptilolite, while the conventional fertilizers ammonium sulfate and urea showed significant diffusion to the outer sections. In the urea and ammonium sulphate dishes, the

nitrogen content was lower in section 1 than in sections 2 and 3, indicating that diffusion is faster in all treatments compared to clinoptilolite (Figure 5.2C). The fact that the nitrogen concentration remained high in the ammonia saturated clinoptilolite section 1 showed that the clinoptilolite released nitrogen slower than the conventional fertilizers. The results of the nitrogen distribution after the 4-week incubation summarized in Figure 5.2D showed that segment 3 had the highest amount of inorganic nitrogen for all treatments except clinoptilolite. Even the control had the highest inorganic N in section 3. The high amount of inorganic N in section 3 is likely due to the greater soil mass in section 3.

To clearly understand the distribution of different forms of the inorganic N, ammonia, nitrate and nitrite concentrations were determined in each section at the end of 1-week and 4-week incubation periods (Figure 5.3). Nitrite concentrations were below detection levels for all samples. Ammonium was the predominant form of inorganic N in all the treatments at the end of 1-week and was highest in section 1 for clinoptilolite at 867.7 mg N/kg soil (Figure 5.3A). Meanwhile, section 2 showed higher ammonia concentrations with ammonium sulfate and urea treatments, indicating that the nitrogen diffused more rapidly in these treatments. At the end of 4-week (Figure 5.3B), the ammonium concentration dropped considerably in all sections for all treatments except clinoptilolite showing that most of the ammonia had been converted to other forms of nitrogen, mainly nitrate, as seen in Figure 5.3D. The nitrate concentrations increased for all treatments at the end of week 4 compared to 1–week incubation (Figures 5.3C and 5.3D). The presence of ammonium (579 mg N/kg) in section 1 of the clinoptilolite treatment at the end of 4 weeks indicated that the ammonium ions are present in the internal pores of the clinoptilolite particles and requires an exchangeable counter ion from the soil to release the ammonium from the internal pores of the clinoptilolite to the surface (Perrin et al., 1998). The slow ammonium

82

release makes nitrification slower and minimizes nitrate leaching in clinoptilolite amended soil. This is evidence that the ammonia saturated clinoptilolite can be a sustainable source of N for plants in long term experiments compared to conventional fertilizers such as urea and ammonium sulphate, although long term incubation studies are needed to confirm the slow-release potential of the remaining ammonia from the clinoptilolite core.

Overall, the mass balance of the total inorganic N at 1- and 4-week inorganic N was well preserved, except for biosolids. The biosolids showed slow mineralization during the incubation periods and were therefore excluded from further greenhouse experiments. The N-diffusion patterns of ammonium sulphate and urea behaved similarly and therefore only urea was chosen as a treatment to represent the conventional fertilizer for the greenhouse experiments.
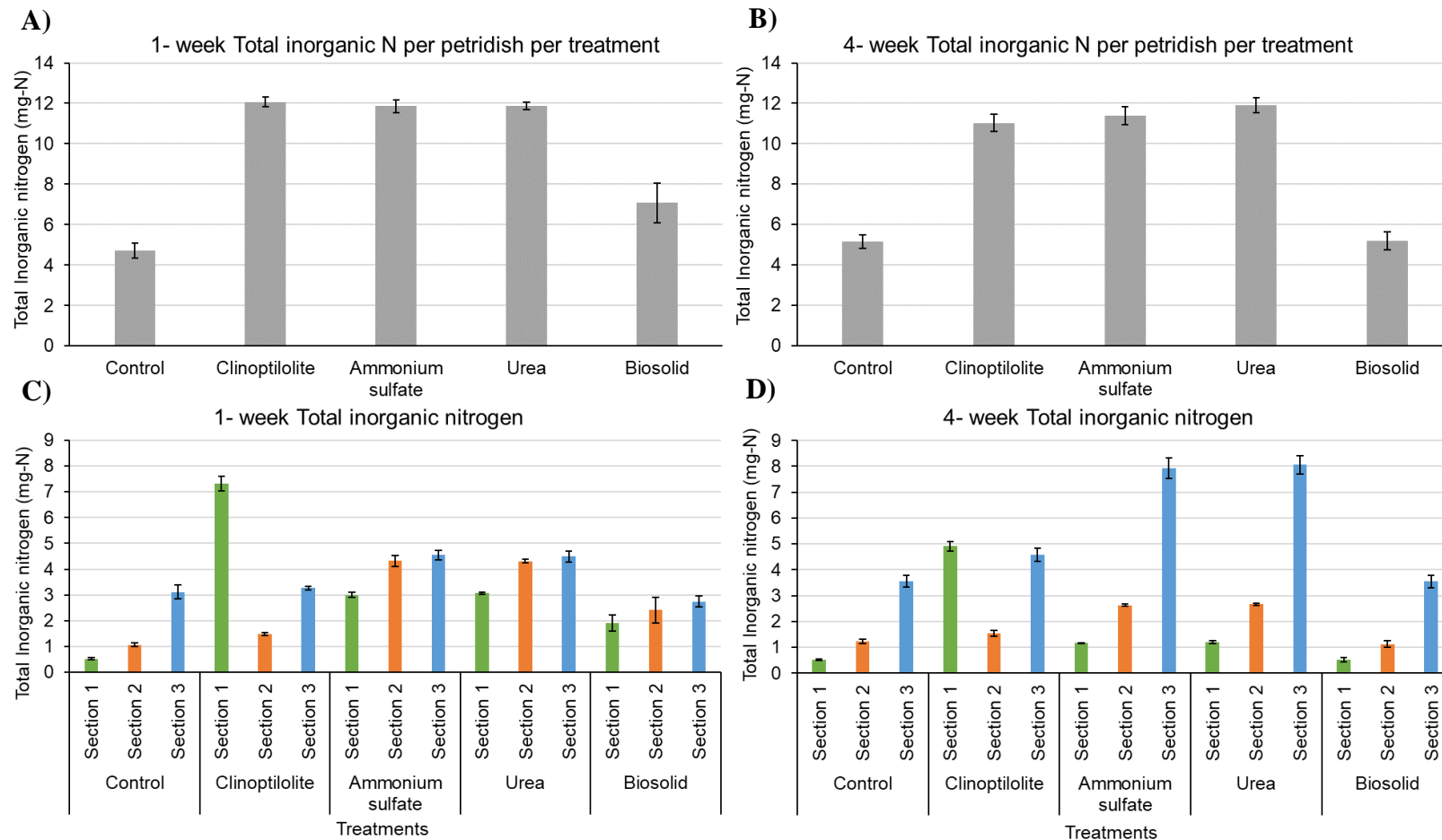
Figure 5.2 A) Total inorganic nitrogen in each treatment dish after 1-week incubation period; B) Total inorganic nitrogen in each treatment dish after 4-weeks incubation; C) Total inorganic nitrogen in each section after 1-week incubation; D) Total inorganic nitrogen in each section after 4 weeks incubation. Error bars represent standard error of five replicates. Results show a clear trend in diffusion of inorganic nitrogen from section 1 (point of N application) to section 3 at the end of 4 weeks incubation.
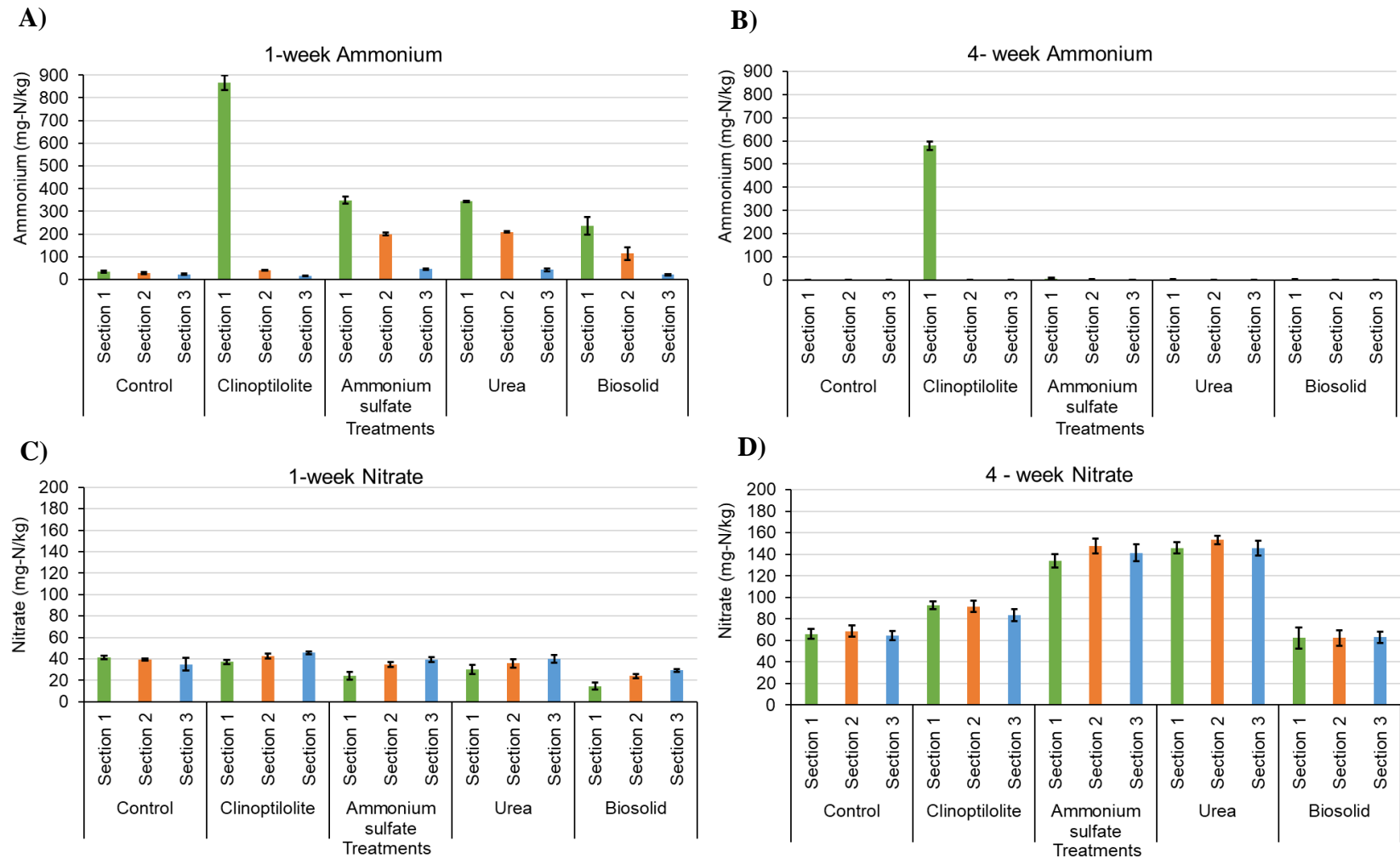
Figure 5.3 Concentration of A) ammonium in each section after 1-week incubation period; B) ammonium in each section after 4 weeks incubation; C) nitrate in each section after 1-week incubation; D) nitrate in each section after 4 weeks incubation. Error bars represent standard error of five replicates. After 1 week incubation, ammonium was the predominant form of nitrogen while nitrate was the predominant form after 4 weeks incubation.

5.3.2 Greenhouse study

Maize plants were harvested 5 weeks after sowing to compare the effect of different treatments on plant nitrogen uptake. Plants take up nitrogen primarily through roots and the nitrogen status of the plant is reflected in the greenness of the leaves (Xiong et al., 2015). In view of this, leaf greenness was measured using a SPAD meter as an indirect measure of chlorophyll content at 3-weeks and 5-weeks. Results summarized in Table 2 showed that SPAD values were within a narrow range for all treatments except T5 (control) which had the lowest value, indicating that all nitrogen treatments had a similar effect on leaf chlorophyll. A similar trend in SPAD readings was observed at 5 weeks, which increased compared to week 3. Such an increase in SPAD value with increasing plant age has been observed in maize (Kandel, 2020). This trend clearly implied that the added nitrogen treatments positively affected leaf greenness and chlorophyll content. To confirm the trends observed in SPAD measurements, chlorophyll estimation was performed at the end of 5 weeks using the harvested plants to determine chlorophyll-a, chlorophyll-b, and total chlorophyll in the leaves and summarized in Table 5.2.

Table 5.2 Variability of physiological and chemical traits in maize across the treatment. (T1 = 100% urea, T2= 90% urea + 10% clinoptilolite, T3 = 80% urea + 20% clinoptilolite, T4 = 100 % clinoptilolite, T5 = No added nitrogen control)

Parameters	T1	T2	T3	T4	T5	p-value
SPAD - 3 Week	42.54 ± 1.48^a	41.68 ± 0.94^a	41.88 ± 0.6^a	41.72 ± 0.94^a	35.14 ± 0.26^b	0.004^{**}
SPAD - 5 Week	44.21 ± 1.4^a	44.21 ± 0.83^a	44.78 ± 0.62^a	45.22 ± 0.88^a	36.47 ± 0.3^b	0.001^{**}
Chlorophyll a (mg/g)	1.8 ± 0.06^a	1.64 ± 0.02^a	1.67 ± 0.1^a	1.53 ± 0.05^a	1.22 ± 0.06^b	0.001^{**}
Chlorophyll b (mg/g)	0.4 ± 0.02^a	0.39 ± 0.01^a	0.35 ± 0.01^a	0.33 ± 0.03^a	0.28 ± 0.02^a	0.066^{ns}
Total Chlorophyll (mg/g)	2.2 ± 0.04^a	$2.03 \pm 0.03^{a,b}$	$2.01 \pm 0.09^{a,b}$	1.87 ± 0.07^b	1.5 ± 0.06^c	0.001^{**}
Total Nitrogen (g/kg)	8.8 ± 0.06^a	7.7 ± 0.06^b	7.7 ± 0.06^b	6.3 ± 0.14^c	7.6 ± 0.00^b	0.000^{**}
pH	8.28 ± 0.12^a	$7.98 \pm .04^{a,b}$	$8.04 \pm 0.08^{a,b}$	7.93 ± 0.04^b	$7.99 \pm 0.03^{a,b}$	0.040^{*}
Total Carbon (g/kg)	$426.7 \pm 0.9^{a,b}$	$428.8 \pm 0.9^{a,b}$	431.3 ± 1.6^a	$428.6 \pm 2.7^{a,b}$	423.1 ± 2.0^b	0.050^{*}
Leaf area (cm²/plant)	2058.61 ± 95.91^a	1935.98 ± 26.61^a	1970.95 ± 118.02^a	1904.99 ± 80.75^a	1695.99 ± 66.84^a	0.162^{ns}

*Significant at P ≤ 0.05; **Significant at P ≤ 0.01

Interestingly, chlorophyll–a had significant differences between the treatments and the control but there was no significant variation in the chlorophyll-b content. However, total leaf chlorophyll content showed significant variation between treatments and control. Treatment 1 had the highest total chlorophyll content (2.2 mg/g), followed by T2 (2.03 mg/g) and T3 (2.01 mg/g). Tukey's post hoc analysis, used to assess the significance of differences between pairs of group means showed that treatments T1 with the highest mean value fell in group 'a', treatments T2 and T3 were grouped together (a,b), and T4 was grouped in group 'b'. Treatment 5 (control) with the lowest total chlorophyll (1.5 mg/g) was grouped separately in group 'c'. The chlorophyll content of the leaves has been linked to the nitrogen status of the plant and used as an indicator to assess the plant nitrogen status at a given point in time (Muñoz-Huerta et al., 2013). Thus, it could be concluded that T1 plants with 100% urea possibly provided the highest nitrogen supply as they had the highest chlorophyll levels, but the mixed treatments of urea + ammonia saturated clinoptilolite (T2, T3) and 100% clinoptilolite (T4) were still similar to urea as a nitrogen source.

The adequate nitrogen supply of clinoptilolite mixtures compared to urea was further confirmed by considering the nitrogen uptake calculated with total nitrogen and total dry biomass (above ground dry biomass) as follows:

Nitrogen uptake (g/plant) = (N concentration in plant tissue * dry weight of biomass)

The ammonium uptake results summarized in Figure 5.4 showed that the treatments had a significant effect on nitrogen uptake.
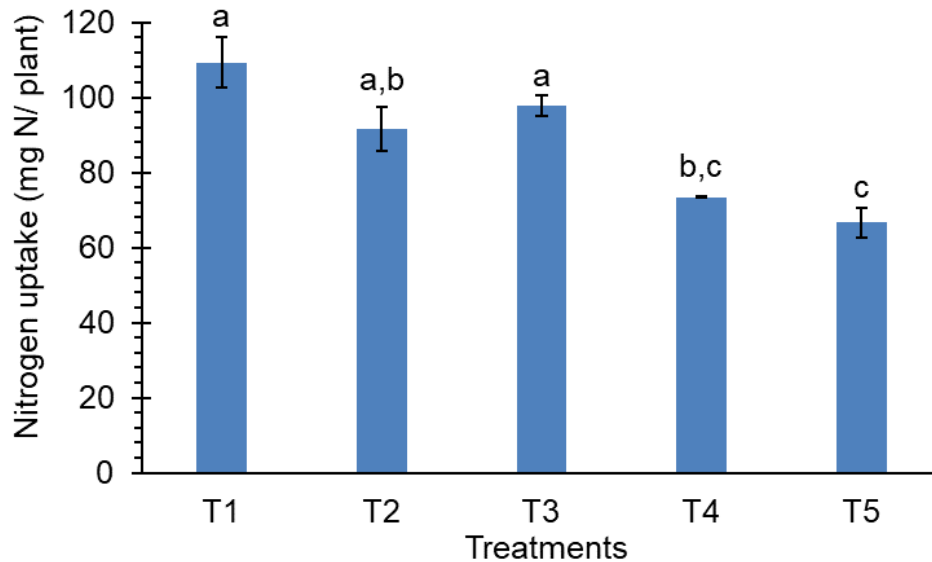
Figure 5.4 Plant nitrogen uptake for different treatments in the greenhouse study. T1= 100% Urea; T2 = 90% Urea + 10% ammonia saturated clinoptilolite; T3 = 80% Urea + 20% ammonia saturated clinoptilolite; T4 = 100% ammonia saturated clinoptilolite; T5 = Control with no added nitrogen. Error bars represent standard error of three replicates. Means within response variable containing the same letter are not significantly different at $P \leq 0.05$.

The maximum nitrogen uptake of 109.3 mg/plant was observed with urea and the lowest uptake was found with the control with no added nitrogen at 66.6 mg/plant. Among the clinoptilolite treatments, T3 showed N uptake of 97.87 mg/plant, which was higher than T2 (91.67 mg/plant). Although the nitrogen uptake was highest in treatment 1 (100% urea), it was statistically on par with T3 (80% urea + 20% clinoptilolite blend) since both means are grouped together (Figure 5.4), indicating that T3 was as good as T1. These results show that N uptake in T1, T2, and T3 are not significantly different and substitution of urea by ammonia sorbed clinoptilolite can be done without compromising N uptake. A 20 % reduction in urea application will significantly reduce the negative impact of urea on the environment and also reduce the cost of crop production. Additionally, the yields of major food grains of the world (wheat, maize and

rice) were shown to increase by 10 to 19% with 15 to 19% reduction in N application (Ren, 2022). In the case of corn, excess nitrogen application reduces the nitrogen use efficiency without any increase in the maize grain yield (Zhang et al. 2015).

However, plant uptake is lower at 73.5 mg/plant when nitrogen is supplied solely by ammonia-saturated clinoptilolite (T4) compared to urea mixed treatments (T1, T2, T3). The lower nitrogen uptake in T4 could be due to the slow nutrient release property of the zeolite, which may not provide enough nitrogen during the initial stages of plant growth while it can release the nutrients to meet the plant's nitrogen needs in the later stages of plant growth. A similar trend was observed by Li et al. (2013), who reported a downward trend in exchangeable and water-soluble NH4-N in zeolite treatments without conventional fertilizers in the first three weeks of their study, while long-term water-soluble NH4 concentrations were higher in zeolite-enriched soils. Therefore, a blend of conventional fertilizer such as urea with ammonia saturated clinoptilolite (T2 and T3) evaluated in the present study could provide a balanced nutrient supply without excessive nitrogen losses.

The dry biomass data summarized in Figure 5.5 showed that the biomass was significantly different between the control and nitrogen treatments, while means of the total dry biomass were grouped together for treatments T1 to T4 indicating that the biomass was not significantly impacted by the different nitrogen treatments. All treatment means (T1 to T4) were grouped together while the control was grouped separately. The slow release of N from T4 (100% clinoptilolite) did not significantly affect plant biomass growth and it would be interesting to see the long term effect of clinoptilolite treatments on N release, plant uptake and cropy yield.

Additionally, the dry biomass weight for T3 (80% urea + 20% clinoptilolite blend) was highest at 12.71 g/plant, followed by urea (12.41 g/plant). The control had the lowest dry

biomass content of 8.77 g possibly due to the lack of sufficient nitrogen. Overall, the present

investigation of evaluating clinoptilolite as a source of nitrogen to support plant growth was

promising. The influence of clinoptilolite on the maize yield and long term nitrogen use

efficiency will be interesting to explore. Therefore, to realize the full potential of clinoptilolite as

a nitrogen source, additional experiments for a longer growing period with different crop types

must be carried out.
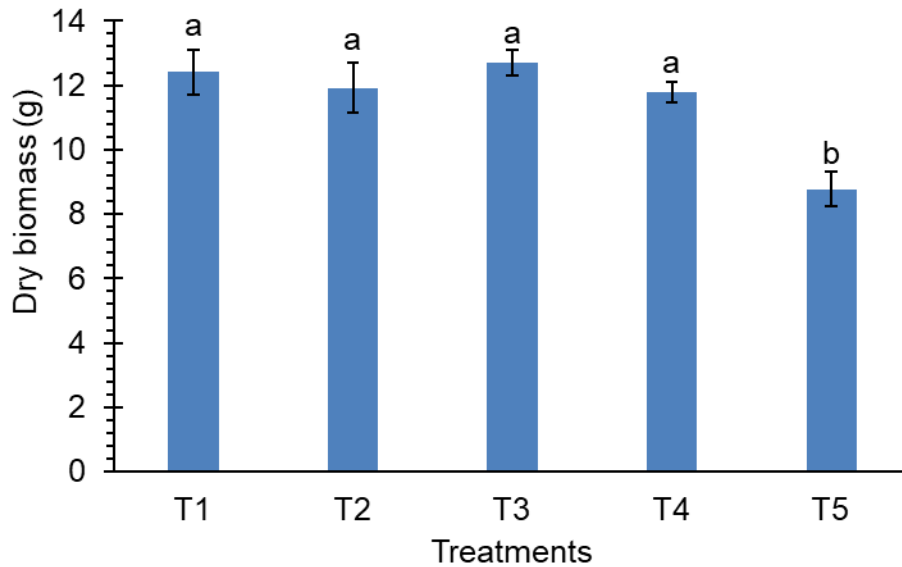
Figure 5.5 Plant dry biomass for different treatments in the greenhouse study. T1= 100% Urea; T2 = 90% Urea + 10% ammonia saturated clinoptilolite; T3 = 80% Urea + 20% ammonia saturated clinoptilolite; T4 = 100% ammonia saturated clinoptilolite; T5 = Control with no added nitrogen. Error bars represent standard error of three replicates. Means within response variable containing the same letter are not significantly different at P ≤ 0.05.

5.3.2.1 Impact of N treatments on soil microbial community

Soil microbial community analysis was performed to identify impact of different N

fertilizer treatments on bacterial and archaeal communities. In this regard, the microbial

community at various taxonomic levels were classified and their relative abundances were

calculated. The phylum level relative bacterial abundance is represented in Figure 5.6.

Among all the different phyla, *Proteobacteria* had the highest relative bacterial abundances in all samples, followed by *Acidobacteria*, *Bacteroidetes*, and *Verrucomicrobia*. These phyla together accounted for >67% in each of the samples. These phyla are metabolically diverse and have important roles to play in nitrogen assimilation and transformation in soil. The genus *Nitrospira,* belonging to Nitrospirae phylum was consistently present in samples belonging to all treatments and had a relative abundance ranging from 1.33% in T5 control, 1.21% in T1 urea, 1.17% in T2 (Appendix Figure C.1). Species belonging to *Nitrospira* genus are known to be nitrite oxidizers (Daims & Wagner, 2018).

Archaea were found to account for 8% to 19% of the total relative abundance in the different treatments. The archaeal relative abundance was predominantly represented by the phylum *Crenarchaeota* comprising >98% of the relative archaeal abundance. The genus *Candidatus Nitrosphaera* belonging to *Nitrososphaeraceae* family and *Crenarchaeota* phylum is known to be ammonia oxidizing archaea (AOA) and could have been a key player in ammonia oxidation during nitrification (Zhalnina et al., 2014). The remaining archaeal abundance at the phylum level was composed of *Euryarchaeota* and *Parvarchaeota* phyla

In general, the composition of the bacterial community was not very different between the treatments, indicating resilience of the communities irrespective**.** The microbial community diversity was evaluated by computing the Shannon index-based metric of Alpha Diversity analysis, which calculates the microbial richness and diversity within each sample by considering both the abundance and evenness of the taxa present. Results of the alpha diversity Shannon index summarized in Table 5.3 showed that overall diversity within each sample was in the same range indicating that the overall richness and diversity was similar in all treatment samples indicating that the N treatments did not greatly influence the soil microbial community.
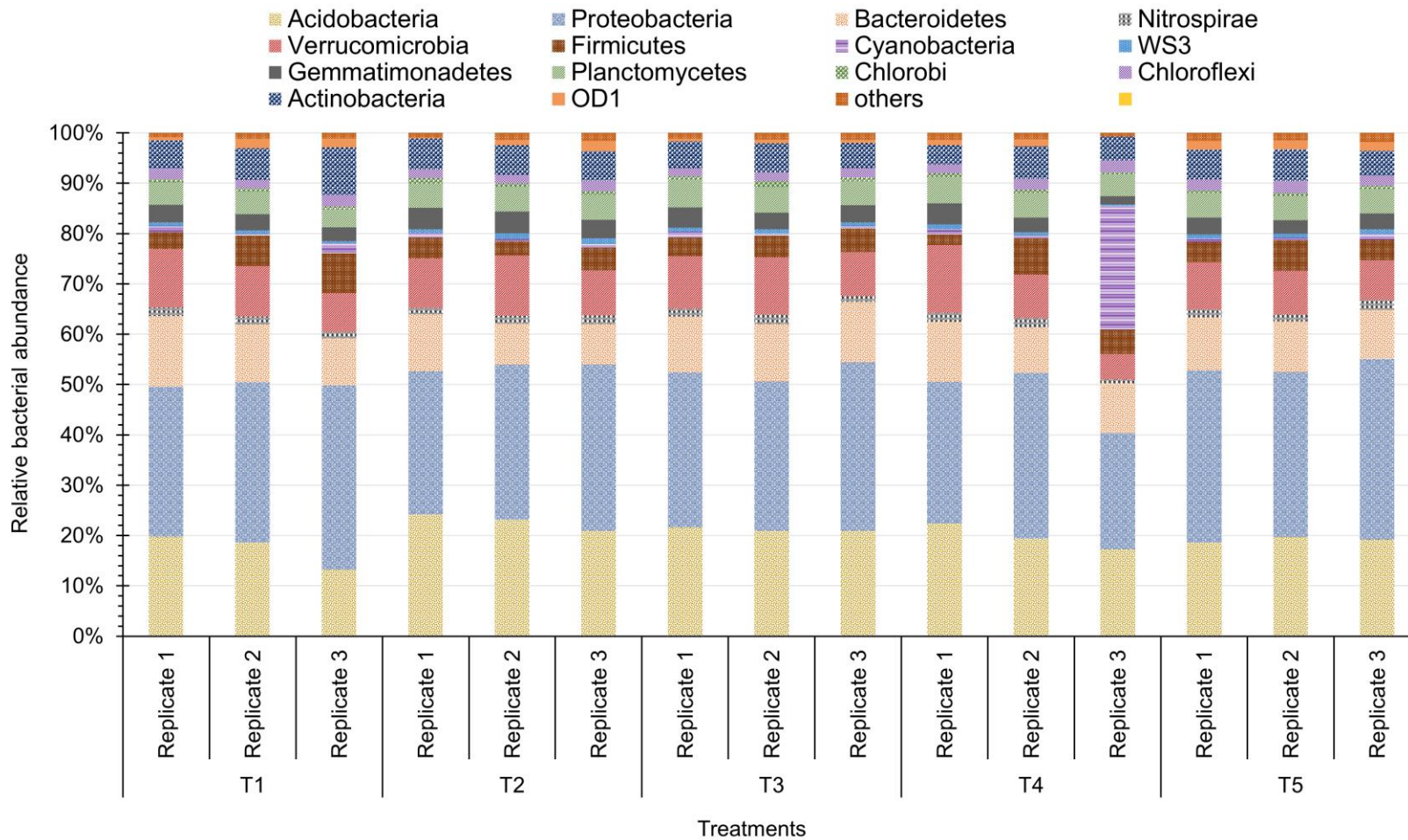
Figure 5.6 Phylum level relative bacterial abundance in soil samples collected from different N treatments. T1= 100 urea treatment; T2 = 90% Urea + 10% clinoptilolite; T3 = 80% Urea + 20% clinoptilolite; T4 = 100% Urea; T5 = Control with no added N

Table 5.3 Summary of Shannon index alpha diversity analysis. Values shown are mean of three replicates

Treatment	Shannon index	
	Mean	SD
T1	9.05	0.33
T2	8.83	0.24
T3	9.06	0.08
T4	8.97	0.32
T5	9.33	0.06

This was further supported by the Kruskal Wallis pairwise comparison of microbial communities between each treatment group (Table 5.4), which showed that there was no statistically significant effect of N treatment on soil microbial composition and microbial diversity. In the present study, it was observed that the different nitrogen fertilizers did not really alter the microbial community within the 5-week duration of the study. The findings are in line with a previous study that reported that fertilizer application mostly had no measurable effects on soil microbial communities (Lupwayi et al., 2010). The findings of microbial community analysis in the present study needs additional evidence to clearly understand the impacts of the different N treatments on soil microbiome. Functional gene based quantitative- PCR would help to observe clear differences in the microbial community. No data on soil nutrient characteristics was taken at the end of the 5-week incubation period. Data on C/N ratio, soil N concentrations at the end of the incubation period could have helped in making correlations between various factors and the microbial community.

Table 5.4 Pairwise comparison of Shannon Index alpha diversity by Kruskal-Wallis test

Group 1	Group 2	H	p-value	q-value
T4 100% Clinoptilolite (n=3)	T5 Control (n=3)	1.190	0.275	0.550
T4 100% Clinoptilolite (n=3)	T1 Urea (n=3)	0.429	0.513	0.570
T4 100% Clinoptilolite (n=3)	T3 Urea/clinoptilolite (80/20) (n=3)	0.429	0.513	0.570
T4 100% Clinoptilolite (n=3)	T2 Urea/ clinoptilolite (90/10) (n=3)	0.429	0.513	0.570
T5 Control (n=3)	T1 Urea (n=3)	1.190	0.275	0.550
T5 Control (n=3)	T3 Urea/ clinoptilolite (80/20) (n=3)	3.857	0.050	0.248
T5 Control (n=3)	T2 Urea/clinoptilolite (90/10) (n=3)	3.857	0.050	0.248
T1 Urea (n=3)	T3 Urea/clinoptilolite (80/20) (n=3)	0.048	0.827	0.827
T1 Urea (n=3)	T2 Urea/clinoptilolite (90/10) (n=3)	0.429	0.513	0.570
T3 Urea/clino (80/20) (n=3)	T2 Urea/clinoptilolite (90/10) (n=3)	2.333	0.127	0.422

5.4 Conclusion

- Overall, the soil incubation study results demonstrate that ammonia saturated clinoptilolite exhibits slow N release properties. Ammonium diffused from the point of nitrogen application to section 3 and transformed into nitrate at the end of the 4 weeks in all the treatments except clinoptilolite.

- Nitrate was the predominant form of inorganic N at the end of 4-week incubation in urea and ammonium sulfate.

- Greenhouse experiments showed that the use of ammonia sorbed clinoptilolite blended with urea had similar plant biomass N uptake compared to 100% urea. This can be beneficial in sustaining nutrient supply without the need for excess urea application.

- The impact of N fertilization on soil microbial community composition and diversity was not significant. Additional functional gene based microbial monitoring would help understand the actual impact of N on the microbial community.

- The greenhouse experiment duration in the present study was for 5-week after sowing. Longer plant growth period is needed to fully evaluate the long term N release pattern from the ammonia sorbed clinoptilolite.

Chapter 6 - Recovery of high-quality Calcium phosphate fertilizer products from anaerobic membrane bioreactor treated swine wastewater

This chapter has been published in *Chemical Engineering Journal.* The citation is as follows:

Damodara Kannan, A., Dillavou, J., H.H. Gamage, K., Randig, E., M. Hettiarachchi, G., & Parameswaran, P. (2023, 2023/02/01/). Recovery of high-quality calcium phosphate fertilizer products from anaerobic membrane bioreactor treated swine wastewater. *Chemical Engineering Journal, 453*, 139539.

6.1 Introduction

Phosphorus, a non-renewable resource, is an essential macronutrient that supports all life forms and is used extensively in a variety of applications such as fertilizers, soft drinks, pharmaceuticals, biomaterials, and flame retardants (Arita et al., 1995; Boer et al., 2019; Duhamel et al., 2021; Jupp et al., 2021; Qiu et al., 2019). The main source of P for societal use is from the mining of phosphate rock. Such mineral phosphate rock reserves are predominantly located in just a handful of countries, increasing supply chain dependency and impact on global food security (Blackwell et al., 2019; Cordell & Neset, 2014; Golroudbary et al., 2019). While mineral fertilizers are essential for agriculture and food production, not all the applied nutrients are utilized by plants and a large proportion is wasted or lost to the environment (Tilman et al., 2002). Such fertilizer nutrient losses increase agricultural costs, waste energy, negatively impact global climate, and pollute the environment, thereby affecting the sustainability of modern agriculture (Chen et al., 2018).

On the other hand, there is great potential to recover the nitrogen and phosphorus and other value-added products from wastewater through appropriate treatment technologies. The primary focus of current mainstream wastewater treatment is nutrient removal and not beneficial recovery. Current treatment methods for phosphorus removal can be categorized as physical,

biological, and chemical removal technologies. Physical technologies include adsorption, sand filtration for particulate P removal, ion exchange, and membrane filtration. Biological technologies include Enhanced biological phosphorus removal (EBPR), photosynthetic microbes immobilized on cellulose, ceramic, or gel carriers, and phosphate binding proteins (Azam et al., 2019). Although biological methods can achieve excellent P removal efficiencies greater than 95% (Gebremariam et al., 2011; Ong et al., 2014), it has certain limitations. Unpredictability of system failure, inability to treat very high phosphorus concentration in wastewaters, need for skilled manpower, and operational instability make it challenging to operate at locations requiring stringent effluent P concentrations (Hasan et al., 2021; Omwene et al., 2018). For these reasons, biological P removal is often implemented along with chemical precipitation for effective P removal since chemical precipitation can achieve very low effluent P concentration (de Haas & Ekama, 2000). Precipitation by metal salts and lime addition, crystallization, coagulation, and flocculation are the most common chemical technologies (Azam et al., 2019). Chemical precipitation of P is achieved by the addition of metal salts of iron, magnesium, and calcium to form mineral precipitates such as struvite ($Mg.NH_4.PO_4.6H_2O$), vivianite $Fe_3(PO_4)_2.8H_2O$ and calcium phosphates including Hydroxyapatite (Hap) ($Ca_{10}(PO_4)_6(OH)_2$), Brushite ($CaHPO_4$), and amorphous calcium phosphate ($Ca_x(PO_4)_y*nH_2O$) (Angel, 1999; Caddarao et al., 2018; Guo & Li, 2020; Liu et al., 2011; Prot et al., 2020). However, little to none of the chemically recovered phosphorus is amenable to beneficial reuse for diverse applications.

There are several full-scale chemical technologies for P recovery from municipal and industrial wastewaters such as ANPHOS, PHOSPAQ, NuReSys, Phosnix, Ostara Pearl, Airprex, and Seaborne predominantly producing struvite as the final product (Desmidt et al., 2015). Crystalactor is a full scale technology producing calcium phosphate (Eggers et al., 1991). While

struvite is the most common phosphate fertilizer product recovered from wastewater, it is limited

by several shortcomings such as high operational costs, high energy consumption, and large

footprint of the recovery technologies (Ghosh et al., 2019). In addition, struvite is marketed

solely as a slow-release fertilizer and cannot be used for other applications. However, calcium

phosphates recovered from wastewater have P content comparable to mined rock phosphates

which allow their application as direct fertilizers or as raw materials for the fertilizer industry

(Vasenko & Qu, 2017). The final quality of these recovered products is affected by the presence

of suspended particles, heavy metals and other impurities, and it is important to remove the

suspended particles before chemical addition to produce high quality products (Ping et al., 2016).

It is important to note that most of the above applications and published literature have focused

on municipal wastewater or anaerobic digester centrate, which still has considerable amounts of

suspended and colloidal organic matter, with very limited efforts for nutrient recovery from

swine lagoon wastewater or other animal agriculture streams. Most studies on phosphorus

removal from animal wastewater including swine and dairy wastewater have primarily focused

on recovery of struvite (Huang et al., 2016; Le et al., 2021; Rabinovich et al., 2018). There are

very few studies on the exclusive recovery of calcium phosphate from swine wastewater (Szogi

et al., 2018). Additionally, no studies are known on the recovery of calcium phosphate as a high-

value nutrient product along with energy recovery and the production of high-quality water for

reuse.

A novel emerging technology that can facilitate production of high-quality nutrient

products is the Anaerobic Membrane Bioreactor (AnMBR), which has shown promise for energy

positive treatment of a variety of wastewaters (Abuabdou et al., 2020; Lim et al., 2019).

Anaerobic membrane bioreactor (AnMBR) treatment of wastewater offers the benefit of

simultaneous resource recovery as energy and water for indirect potable reuse, along with the

potential for mobilizing nutrients for subsequent controlled capture of nitrogen (as ammonium)

and phosphorus (as orthophosphate) using different techniques such as coagulation, flocculation,

chemical precipitation, and ion exchange (Kannan & Parameswaran, 2021). Recent studies have

shown that chemical addition can be highly effective for P removal from AnMBR treated

municipal wastewater permeate (Heronemus et al., 2021; Lim et al., 2019). Factors including

total alkalinity, pH, presence of impurities such as dissolved organic matter (humic and fulvic

acids) and interfering ions such as carbonate (CO_3^{2-}), aluminum (Al^{3+}), magnesium (Mg^{2+}) affect

final fertilizer product quality and purity along with other non-specific product formation

($CaCO_3$ or $MgCO_3$) (Cao & Harris, 2008; Zhou et al., 2015). Thus, the composition of the treated

wastewater significantly influences the type of final recovered nutrient products (RNP) formed

and its subsequent reuse as fertilizers.

The main objectives of the present study are to demonstrate feasible recovery of high-quality

calcium phosphate fertilizer products from AnMBR treated swine permeate using different Ca/P

molar ratios. The characteristics of the RNP for fertilizer applications were evaluated. Finally,

certain process modifications were also explored to fine tune product quality with an aim to

circumvent undesired carbonate ions and dissolved organic matter (DOM) interference, thereby

preventing other non-specific product formation, and enhancing the overall P content and

solubility for fertilizer applications.

6.2 Materials and Methods

6.2.1 Collection of Anaerobic Membrane bioreactor (AnMBR) treated actual swine permeate samples

AnMBR treated swine permeate was collected during the day of testing from a lab-scale Anaerobic Membrane Bioreactor (AnMBR) located at Kansas State University treating real swine lagoon wastewater. The lab scale AnMBR system had a COD removal efficiency > 80% and BOD_5 removal efficiency >95% under steady state conditions (Appendix Figure D.1). The configuration of the lab scale AnMBR used in the present study is summarized by Lim (2021). The characteristics of AnMBR treated actual swine permeate for samples collected on two separate days are summarized in Table 1. As noted in Table 1, the swine permeate has both ammonia-N and phosphate-P and this study focused on recovering primarily the phosphorus, while successful ammonia recovery from the permeate is described in Chapter 3 (Kannan & Parameswaran, 2021).

Table 6.1 Composition of AnMBR treated actual swine permeate for samples collected on two separate days

	Real swine permeate sample 1	Real Swine permeate sample 2
COD (mg/L)	658	573
Zinc, Zn (mg/L)	0	0
Ammonium, NH_4-N (mg/L)	584.59	587.58
Nitrate, NO_3-N (mg/L)	<.0.01	<.0.01
Chloride, Cl (mg/L)	452.34	451.78
Aluminum, Al (mg/L)	<0.01	<0.01
Phosphorus, P (mg/L)	65.5	65
Calcium, Ca (mg/L)	99.73	94.81
Magnesium, Mg (mg/L)	25.85	25.17
Sodium, Na (mg/L)	14.23	15.07
Potassium, K (mg/L)	551.21	556.11
Copper, Cu (mg/L)	<0.01	<0.01
Iron, Fe (mg/L)	0.07	0.03
Manganese, Mn (mg/L)	0.05	0.05
Sulfur, S (mg/L)	23.01	29.66
pH	7.52	7.57
Alkalinity mg/L as $CaCO_3$	3380	2950

6.2.1.1 Coagulation experiments with real AnMBR swine permeate

Coagulation experiments with real swine permeate collected from the lab scale AnMBR system were performed using the 100% Calcium Oxide (CaO) and 50/50 calcium chloride/calcium oxide coagulant mixture. The experiments were performed using coagulants added in varying molar ratios of Ca/P ranging from 1/1 to 12/1. Due to practical reasons, experiments were performed in three different batches using permeate collected on three respective days. Batch 1 involved testing the Ca/P molar ratios from 1/1 to 4/1, followed by 5/1 to 8/1 in batch 2, and finally testing the range from 9/1 to 12/1. After establishing the dosing curve with real swine permeate in the first round, another round of jar tests was performed with

fresh real swine permeate at the Ca/P molar ratios of 2/1, 4/1, 6/1, 8/1 and 10/1 to confirm the P

removal efficiency trends from the previous round. The experimental procedure using the bench

scale jar test apparatus is given in Appendix D.

6.2.2 Permeate alteration for carbonate sequestration

To prevent competitive interference of carbonate alkalinity which induced calcite

formation and to enhance the final product phosphorus content, the permeate characteristics were

altered to remove the carbonate alkalinity from the permeate solution. First, the pH of the

permeate was reduced to around 4.5 by adding 18 M concentrated sulfuric acid (H_2SO_4) to

convert the bicarbonate alkalinity to carbonic acid (H_2CO_3), a weak, unstable acid. After pH

adjustment, the permeate was aerated overnight to strip the CO_2 gas generated within the

solution. The total alkalinity was measured again after overnight aeration to confirm the

effectiveness of permeate alteration in removing alkalinity.

6.2.3 Chemical analyses

Total phosphorus was measured with HACH TNT 844 and TNT 845 kits (concentration

range 0.5 -5 mg/L-P and 2-20 mg/L-P, respectively) using the HACH DR 3900

spectrophotometer (Loveland, CO, USA). Total chemical oxygen demand (TCOD) was analyzed

using HACH TNT 822 kits (20–1500 mg/L). pH was measured using Fisherbrand™ accumet™

AB150 pH Benchtop Meters. Total Alkalinity was measured using HACH TNT 870 kit (25 –

400 mg/L $CaCO_3$). Initial permeate Ca^{2+} and Mg^{2+} concentrations were measured using the

Dionex ICS 5000+ Ion chromatography instrument. Chemical analyses of certain other

components including Zn, Cl, Al, Cu, Fe, Mn, and S in the permeate before coagulant addition

were performed at the Soil Testing Lab at Kansas State University Agronomy department.

6.2.4 Recovered nutrient product characterization: P content, Citric Acid (CA) solubility analysis, X-Ray Diffraction (XRD) analysis

Semi-solid nutrient-rich samples obtained from real swine wastewater were characterized for P content, CA solubility, and X-Ray diffraction analysis. The original samples were freeze-dried and digested using the EPA3051A method in a microwave digestion unit. The freeze-dried products were analyzed for the total P according to (Zarcinas et al., 1996), which was then modified to use a digestion block instead of a microwave using an Inductively Coupled Plasma Optical Emission Spectrometer (ICP-OES, Varian 720-ES, Santa Clara, CA). Calcium content in the final products was also analyzed in the ICP-OES using the same processed samples used for P analysis. A powder X-ray Diffraction (XRD) analysis of freeze-dried products was conducted using a PANalytical Empyrean Multi-Purpose X-Ray Diffractometer (Spectris Company, Egham, Surrey, UK) with a copper anode material and generator settings of 35 eV and 20 mA. Solubility tests using 2% (w/v) citric acid were conducted using a modified method used by the Association of Official Agricultural Chemists (Chemists & Lepper, 1945) for the freeze-dried products.

6.2.5 Excitation-Emission Matrix (EEM) fluorescence analysis

Permeate samples collected after coagulation experiments involving the pH altered swine permeate were scanned in quartz cuvettes (Starna 3-Q-10, Ilford, UK) and analyzed using a Horiba Aqualog fluorometer (Horiba, Kyoto, Japan) to generate excitation-emission matrices (EEMs). EEM interpretation was done through visual peak identification of fluorescent peaks. EEM spectra was composed of four peaks commonly found in wastewaters and include: Peak B representing tyrosine-like fluorescence (Ex: 275nm, Em: 310 nm), Peak T representing tryptophan-like fluorescence (Ex: 275nm, Em: 340nm), Peak C representing Humic-like

fluorescence (Ex: 300-360nm, Em: 420-460nm), and Peak A representing fulvic-like

fluorescence (Ex: 230-260nm, Em: 400-500nm) (Coble, 2007; Hudson et al., 2007).

6.3 Results and Discussion

6.3.1 Coagulation experiments with real swine permeate

Coagulation experiments with varying doses of 50/50 CaO/ CaCl$_2$ mixture ranging from

Ca/P molar ratios of 1/1 to 12/1 were used to evaluate phosphorus removal from the lab-scale

AnMBR treated real swine permeate. Figure 6.1A showed that the P removal efficiency at lower

coagulant Ca/P doses of 1/1, 2/1, 3/1, and 4/1 were 13.9%, 15%, 22%, and 36%, respectively.

These removal efficiencies were lower than the synthetic swine permeate for similar Ca/P molar

ratios previously reported by (Damodara Kannan et al., 2022). This could possibly be attributed

to the complex nature of real swine permeate which comprises of several impurities including

dissolved organic matter and other interfering ions. However, the removal efficiency at higher

doses starting from Ca/P of 5/1 reached 82% and continued to increase, with the higher doses

reaching a maximum of 93% at the 8/1 (Ca/P) ratio.

A)

B)

C)
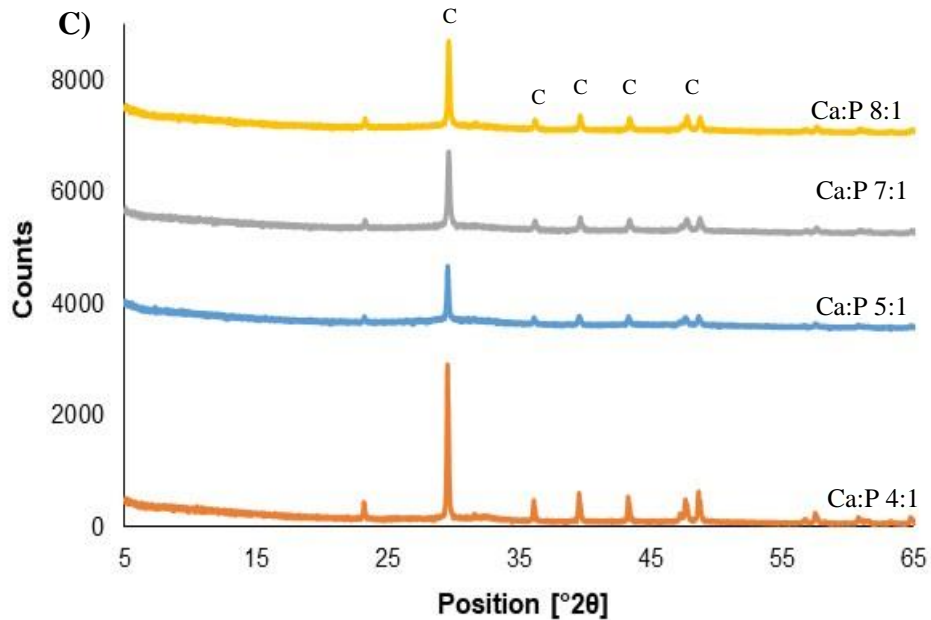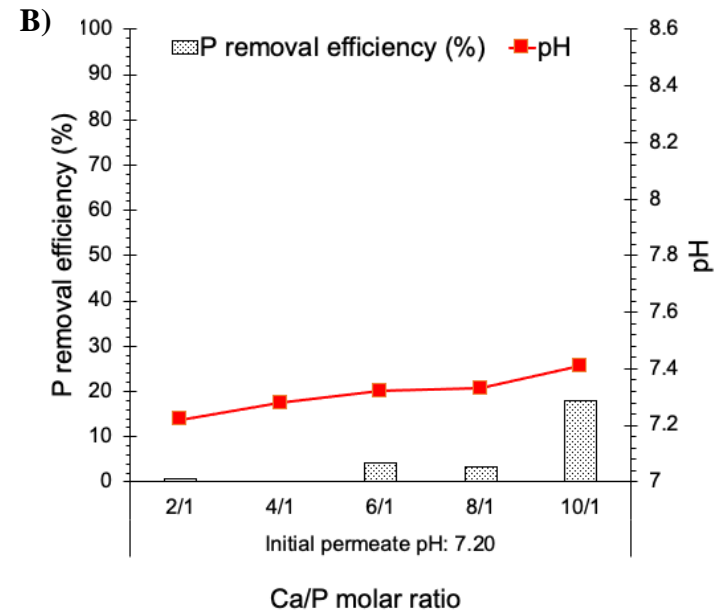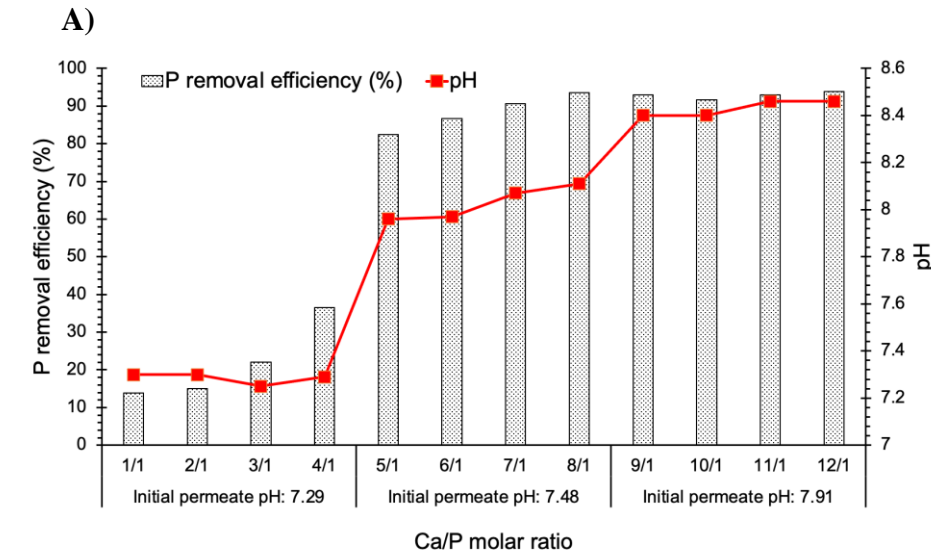
Figure 6.1 A) Phosphorus removal efficiency and final solution/product pH in AnMBR treated real swine permeate Trial 1, and B) Trial 2, at varying P:Ca ratios using calcium oxide and calcium chloride mixture (50% CaO + 50% CaCl2). Phosphorus removal efficiency of around 93% was observed in Trial 1 with the P: Ca coagulant doses of 1:8, 1:9, 1:11, and 1:12. However, negligible phosphorus removal was observed in Trial 2 for all P:Ca doses. Figure 6.1C: XRD pattern of recovered nutrient products obtained from unaltered permeate showing clear calcite peaks indicating calcite presence in the

In addition, the P removal efficiency did not increase any further and was around the same range at doses greater than 8/1 (Figure 6.1A). Although the calcium coagulant mixture was able to efficiently remove the P from the swine wastewater, the need for a higher calcium dose may also be explained by the need to achieve significant apparent supersaturation conditions and induce precipitation within the short duration of the flocculation experiments with the swine permeate. This need to achieve significant apparent supersaturation to induce precipitation is mainly due to ion association effects, where the concentration of free ions contributing to saturation is significantly lower than the total ion concentration (Valsami-Jones, 2001). Thus, it is reasonable to expect that spontaneous precipitation of calcium phosphate does not occur in most cases or requires very high oversaturation. Additionally, the kinetics of calcium phosphate precipitation plays a major role than thermodynamic equilibrium considerations (Cornel & Schaum, 2009). A previous study by (Song et al., 2002) (at Ca/P ~ 3.3/1, pH 8) reported a sigmoidal trend in P removal with rapid precipitation (~20% P removal) occurring in the initial 10 minutes followed by an accelerated phase after 4.5 hours due to the formation of new calcium phosphate phase. Thus, precipitation kinetics governs the type of calcium phosphate phase formed depending on the residence time (Valsami-Jones, 2001).

To confirm the P removal trends observed in the first round of testing with real swine permeate, the experiments were repeated with varying doses of Ca/P molar ratio added as a 50/50 mixture of CaO and CaCl$_2$. The results shown in Figure 6.1B were in contrast to the previous trial (Figure 6.1A) as the removal efficiency was negligible or minimal under all different conditions. The initial solution pH was 7.29 for Ca/P doses 1/1 to 4/1 (phase 1), pH 7.48 for the ranges 5/1 to 8/1 (phase 2), and pH 7.91 for final batch of Ca/P molar doses ranging from 9/1 to 12/1 (phase 3). This seems to indicate that P removal efficiency is strongly

107

influenced by the initial solution pH, with lower removal efficiencies observed at pH 7.29 and highest removal at an initial pH of 7.91. Additionally, a higher initial pH of the solution allowed alkaline pH conditions to be reached easily, favoring precipitation to occur, while the pH 7.29 permeate solution showed no variation in pH after coagulant addition and consequent minimal P removal.

The effect of initial pH on precipitate formation was further observed in the experiments of Run 2, which were performed using the treated permeate at pH 7.2 and showed no visible phase changes with negligible P removal although the solution is supersaturated after coagulant addition (Figure 6.1B). This theory is in line with previous research which has shown that strong buffers inhibit the increase of pH thereby preventing CaP precipitation (Lei et al., 2018).

In an attempt to achieve a higher solution pH and consequently higher P removal, the experiments were repeated with 100% CaO, since the solution pH is expected to be higher than 50/50 CaO/CaCl$_2$ mixture. Appendix Figure D.2A and Appendix Figure D.2B summarize the results of the replicate experiments with 100% CaO as coagulant. Although the final pH of the solution was slightly higher than that achieved with the CaO/CaCl$_2$ mixture, it was still below 8. There were also slight improvements in the P removal efficiency at the lower Ca/P doses compared to the CaO/CaCl$_2$ mixture experiments. These results further demonstrate that the buffering capacity of the solution resists pH increases to alkaline conditions ideal for phosphorus precipitation, thereby compromising overall P removal.

The treated swine permeate used in the present study consistently had a total alkalinity in the range of 1660 - 3300 mg/L CaCO$_3$, likely contributed by the presence of high concentrations of carbonate/bicarbonate and ammonia, which both function as buffers, thereby increasing the coagulant dose requirements for pH adjustment (Vasenko & Qu, 2019). Additionally, the

presence of competing CO_3^{2-} ions in the permeate utilizes the excess Ca^{2+} to form calcium

carbonate (calcite, $CaCO_3$) while having an inhibitory effect on calcium phosphate formation

(Van Der Houwen & Valsami-Jones, 2001). Therefore, the role of carbonate alkalinity on

calcium phosphate precipitation in wastewater nutrient recovery systems cannot be ignored as it

affects the calcium coagulant dose requirements, P removal efficiency, and potentially the

quality of the final recovered product.

6.3.1.1 Characterization of recovered nutrient products from real unaltered swine

permeate

Further analyses to characterize the phosphorus content in the RNP from Trial 1 and their

suitability as fertilizers were performed by assessing their solubility in citric acid solution. The

total P content in various samples and corresponding citric acid solubility results are summarized

in Table 6.2. The total P content of 8.6% (19.7% as P_2O_5) in the 4/1 (Ca/P) RNP sample was

higher than the 8/1 sample (5.8%), although the latter had very high P removal efficiency from

the permeate compared to the former. This indicates that higher P removal does not necessarily

translate to a higher P content in the RNP. Additionally, the 2% citric acid solubility of the

products was in the range of 2.3 – 3.5 (% of Total P) while the calcium content was also very

high compared to the phosphorus content. As a result, the Ca/P molar ratio in the recovered

products was generally higher than the theoretical ratio of hydroxyapatite (HAP) 1.67.

Table 6.2: Total P content and citric acid solubility of recovered nutrient products from unaltered swine permeate

Permeate type	Coagulant type	Ca:P molar dose ratio	Total P (wt %)	Ca (wt %)	Ca/P molar ratio in final product	2% Citric acid solubility (As a % of total P)
Unaltered real swine permeate	CaO/CaCl$_2$ (50/50) mixture	4:1	8.6	53.2	4.8	2.3
		5:1	7.7	60.3	6.1	2.7
		6:1	6.8	22.3	2.5	2.9
		7:1	5.3	40.6	5.9	3.9
		8:1	5.8	41.1	5.5	3.5

Phase analysis of the recovered products using XRD analysis were performed using samples collected from the experimental solutions having Ca/P ratios of 4/1,5/1, 7/1, and 8/1. As shown in Figure 6.1C, XRD patterns showed distinct peaks representing calcite (CaCO$_3$) mineral. There were no identifiable peaks representing calcium phosphate minerals such as HAP. Clear calcite peaks indicate that carbonate ions affect the formation of calcium phosphate minerals and increase the calcium dose required to achieve low residual phosphorus concentrations in the treated water. Interestingly, the solubility product of calcium phosphate ($1.0*10^{36}$) is significantly lower compared to calcite ($3.8*10^9$), meaning that calcite is more soluble than calcium phosphate. However, the preferential precipitation of calcite over calcium phosphate in the permeate solution indicates that calcite precipitation may be kinetically more favorable (Tervahauta et al., 2014). These findings are in accordance with previous studies which identify carbonate co-precipitation to impact calcium phosphate formation (Monballiu et al., 2019; Monballiu et al., 2020; Song et al., 2002).

Overall, phosphorus removal from the treated swine permeate by calcium coagulants was highly variable and significantly dependent on the initial solution pH and total alkalinity. The quality of the recovered products from Trial 1 in terms of the phosphorus content and solubility

was poor due to calcium carbonate co-precipitation. Thus, there is a need to address the carbonate ions' interference to enhance P content in the RNP and lower the calcium dose requirements.

6.3.2 Coagulation experiments with reduced carbonate alkalinity in pH regulated swine permeate

To remove the carbonate alkalinity from the AnMBR treated swine permeate, pH of the solution was lowered to around 4.5 by adding concentrated sulfuric acid, H_2SO_4. The hypothesis for this approach was that lowering pH of the permeate would convert the carbonate species to carbonic acid and eventually to carbon dioxide gas in the solution. After pH adjustment, the permeate was aerated overnight to strip the CO_2 gas generated within the solution to achieve a final pH of 5.5. Correspondingly, the total alkalinity in the pH regulated aerated permeate reduced by almost 97% from 2950 mg/L $CaCO_3$ to 69 mg/L $CaCO_3$ in Trial 1 showing that this could be an effective method for reducing carbonate alkalinity in wastewater nutrient recovery systems.

To evaluate the P removal efficiency, different doses (2/1, 4/1, 6/1, 8/1, 10/1 of Ca/P ratio) of 100% CaO was added to the different beakers containing the aerated pH adjusted permeate. Calcium oxide was chosen because of its ability to raise the pH (which goes from 4.5 to ~5.5 after overnight aeration of the altered permeate) and achieve alkaline conditions (pH > 8) in the solution. The phosphorus removal efficiency shown in Figure 6.2A increased with increasing dose of coagulants. The highest P removal of 97% was achieved with the 10/1 Ca/P dose resulting in a residual phosphorus concentration in the final permeate to be around 1.35 mg– P/L.

Comparing the latest results with the P removal efficiencies from unaltered permeate reported in the previous section, there was a profound improvement in removal efficiency. The phosphorus removal efficiencies in the pH regulated permeate far exceeded the removal efficiencies with unaltered permeate at lower Ca/P ratio. For instance, at the Ca/P ratio of 2/1, almost 70% P removal (Figure 6.2A) was achieved compared to just 15% P removal (Figure 6.1A) in the unaltered permeate. Similarly, 84% P removal efficiency in the altered permeate was observed compared to 36% in the unaltered permeate using Ca/P ratio of 4/1. The better P removal performance is also closely related to the solution pH, which ranged from 8.6 for Ca/P ratio of 2/1 to 12.5 units for 10/1.

A)
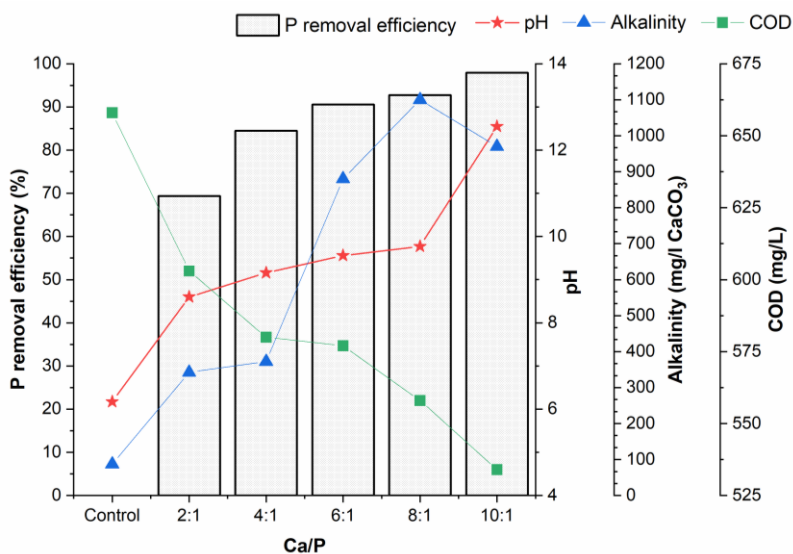
B)
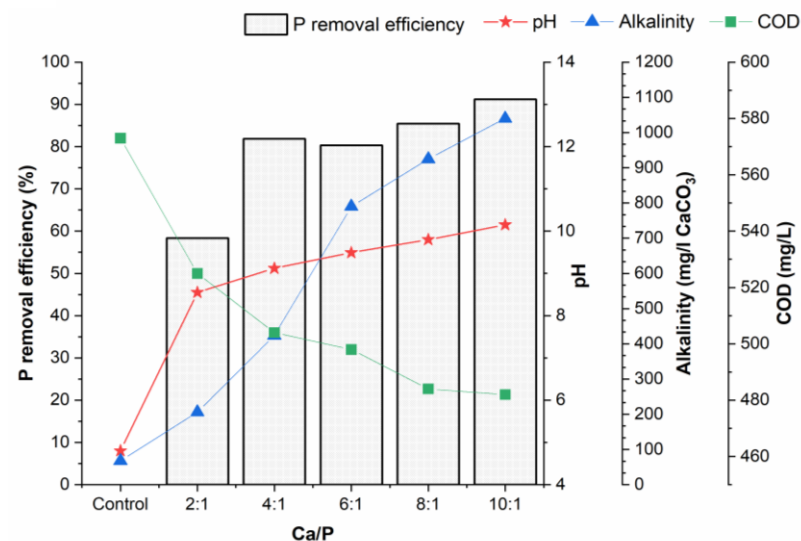
C)
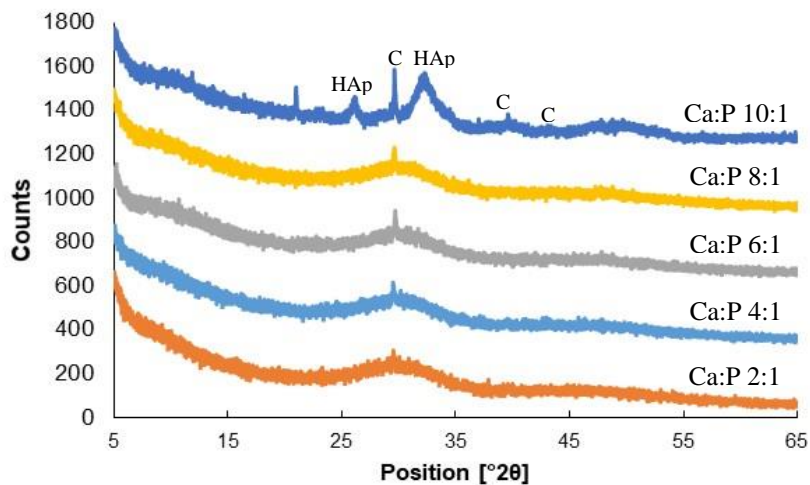
Figure 6.2 A) Phosphorus removal efficiency and final solution/product pH in AnMBR treated pH altered aerated permeate real swine permeate for Trial 1; B) Trial 2 at varying Ca:P ratios using calcium oxide coagulant. Maximum phosphorus removal efficiency of 97% observed with the 10:1 Ca:P coagulant dose in Trial 1. Figure 6.2C): XRD pattern of recovered nutrient products obtained from pH altered aerated permeate at different Ca:P ratios. The XRD pattern of recovered nutrient products obtained from the pH altered aerated permeate had weaker, broad, and wider peaks indicating the absence of calcite formation and presence of hydroxyapatite. C- Calcite, HAp – Hydroxyapatite.

The loss of carbonate alkalinity in the pH regulated aerated permeate resulted in higher availability of the Ca^{2+} ions to participate in phosphate precipitation reactions. Additionally, the buffering capacity of the altered permeate is significantly reduced in the absence of carbonate alkalinity, making it easier for calcium oxide to reach alkaline conditions.

The experiment was repeated as trial 2 with fresh permeate at the same coagulant dosing to check reproducibility and confirm the P removal trends. Interestingly, the P removal trends shown in Figure 6.2B were similar, although the maximum P removal with the 10/1 Ca/P dose was slightly lower at 91%. The differences in P removal rates between the two replicate runs could likely be due to the dynamic variability in the composition of the real swine permeate. Overall, the results achieved demonstrate the effectiveness of this method of permeate alteration in removing carbonate alkalinity prior to phosphorus capture.

6.3.2.1 P content, Citric Acid (CA) solubility analysis, X-Ray Diffraction (XRD) analysis of nutrient product recovered from pH regulated altered permeate

Further analyses comparing the quality and P content of the solid phase nutrient products recovered from these altered swine permeate solutions are summarized in Table 6.3. The RNP appeared to be amorphous in nature. The total P content in the RNP obtained from the altered permeate was higher than those obtained from unaltered permeate, with the highest value of 11.8% P (27% P_2O_5) reported for RNP from Ca/P ratio of 2/1. At the Ca/P dose of 4/1, the P content in the RNP from altered permeate was 10.9% compared to the 8.6% in the unaltered permeate. The P content in the altered permeate products was comparable or even higher than other wastewater-derived nutrient products reported in previous studies. For instance, Rech et al. (2018) recovered struvite from swine wastewater containing 12.8% of total P%. In another study treating black water, Cunha et al. (2020) recovered CaP granules with 10 ± 2 % of average total

P. Similarly, Szogi et al. (2018) produced swine lagoon sludge derived products with P content in the range of 14.5% - 15.5% P (33.2 – 35.5 % P_2O_5). It is likely that the products formed with the altered permeate were amorphous calcium phosphate (ACP) which have a Ca/P molar ratio between 1 and 2.2 (Sergey V. Dorozhkin, 2010), as shown by the Ca and P weight percentages in the recovered products (Table 6.3).

After determining the P content and Ca/P molar ratios in the RNP, the citric acid solubility was also determined to assess the agronomic value of these products (Table 6.3). The citric acid solubility for all Ca/P doses except 10/1, was in the range of 9.3% to 11.4% (solubility as a % of total P). The solubility of RNP from the altered permeate showed about two times increase compared to the unaltered permeate derived RNP. As a reference, soft rock phosphate's 2% citric acid solubility is 30%, and TSP is 88% of total P (Christiansen et al., 2020). Different factors such as crystallinity of the products and the substitution of ions such as Al and Fe affect the 2% citric acid solubility (Braithwaite et al., 1990). The amorphous nature of this product suggests that this could have better P dissolution and greater plant P bioavailability and uptake. These RNP could be used as a good candidate for direct fertilizer application depending on soil and crop types. The solubility, transformations, and reaction products of this RNP need to be further investigated using soil incubation studies.

After determining the P content in the recovered products, XRD analysis was performed for phase identification of the precipitates and the results are shown in Figure 6.2C. The XRD patterns of the products obtained from different Ca/P molar ratios from 2/1 to 10/1 were mostly similar with no clear, distinct peaks indicating that the products formed were non-crystalline and amorphous. In addition, no clear calcite peaks were seen in the products formed in the altered permeate. Correlating the P content reported in Table 6.3 with the XRD patterns in Figure 6.2C,

the precipitates could most likely contain amorphous calcium phosphate. The XRD patterns of products from all Ca/P doses tested had a broad peak between 25° and 35° 2θ position, which is associated with the amorphous P phase as reported in previous studies (Daneshgar et al., 2018; S. V. Dorozhkin, 2010). It is also to be noted that this broad amorphous P peak in the XRD analysis was not observed at any condition for the unaltered permeate studies presented earlier in Figure 6.1C.

At 2/1 Ca/P, the P content was highest and the XRD pattern showed no clear relevant peaks for hydroxyapatite and calcite. This observation could be related to the P content in the products (Table 6.3), where the product quality in terms of P content is higher at lower Ca/P dose and consists of amorphous calcium phosphate as the main product phase. Amorphous calcium phosphate is considered to be one of the most common precursor phases for the formation of crystalline hydroxyapatite (HAP) and is thermodynamically less stable than the latter (Barat et al., 2009). The amorphous calcium phosphate transforms to crystalline hydroxyapatite with sufficient nucleation induction time (Li et al., 2022).

Table 6.3 Total P content and citric acid solubility of recovered nutrient products from pH altered swine permeate

Permeate type	Coagulant type	Ca:P molar dose ratio	Total P (wt %)	Ca (wt %)	Ca/P molar ratio in final product	2% Citric acid solubility (As a % of total P)
pH altered aerated swine permeate	CaO	2:1	11.8	21.1	1.4	10.9
		4:1	10.9	23	1.6	11.4
		6:1	11.2	24.4	1.7	9.3
		8:1	10.6	21.7	1.6	10.4
		10:1	7.5	18.6	1.9	2.1

6.3.3 COD removal and EEMS correlation

Characterization of the final altered permeate after flocculation and P recovery revealed additional removal of COD from the permeate, with an increase in COD removal with increasing calcium dose. Similar phenomenon has been observed in previously reported coagulation studies on different types of wastewaters (Boguniewicz-Zablocka et al., 2019). In the present study, the AnMBR system under steady state operation achieves >80 % COD removal and almost 95% BOD_5 removal, and the permeate was free of suspended organic matter. Any remaining soluble organic content in the permeate is likely to consist of poorly bioavailable dissolved organic matter (DOM) including humic-like substances and amino acid substances (Dong et al., 2021). In the coagulation experimental trial 1, the COD was reduced by almost 19% from 658 mg/L in control to 534 mg/L at Ca/P molar ratio of 10/1 (Figure 6.2A). Similarly, 16% removal was observed in trial 2 with the same dose of 10/1 Ca/P (Figure 6.2B).

The dissolved organic matter in the treated wastewater effluent is mainly present as soluble microbial products such humic acids, polysaccharides, proteins, nucleic acids, organic acids, amino acids, exocellular enzymes, structural components of cells and products of energy metabolism (Kunacheva & Stuckey, 2014). Humic acids have high affinity for Ca^{2+} ions in solution. At higher pH conditions and excess calcium concentrations, the presence of humic acids leads to amorphous calcium precipitates that delay the formation of more crystalline hydroxyapatite (Alvarez et al., 2004). Similarly, the binding of amino acids to calcium phosphates was reported in a previous study, which concluded that alanine and aspartate weakly bind to calcium sites on the apatite surface through their amino acid carboxylates (Palazzo et al., 2009). In addition, surface bound amino acids can promote hydroxyapatite precipitation by attracting Ca^{2+} and PO_4^{3-} ions and increasing local supersaturation (Tavafoghi & Cerruti, 2016).

Thus, the likely mechanism of COD removal during flocculation was that dissolved organic matter such as amino acids and humic substances were bound to the surface of the precipitating solid phases.

To understand the nature of the organic compounds removed from the altered permeate during coagulation, fluorometry based EEMS characterization of the supernatant permeate samples collected after sludge settling was performed. The EEM data results summarized in Figure 6.3 show the peak intensities for three visually identified peaks (Peak B, Peak T, and Peak C representing tyrosine, tryptophan, and humic like materials, respectively). The results show that with increasing calcium dosage, there was a greater removal in the tyrosine and tryptophan like fluorescence. With the highest chemical dose, the tyrosine-like fluorescence showed a removal rate of 60 % and the tryptophan-like fluorescence achieved a removal rate of 30% (Appendix Table D.1). These removal trends could be qualitatively correlated to the observed COD reduction after coagulation.
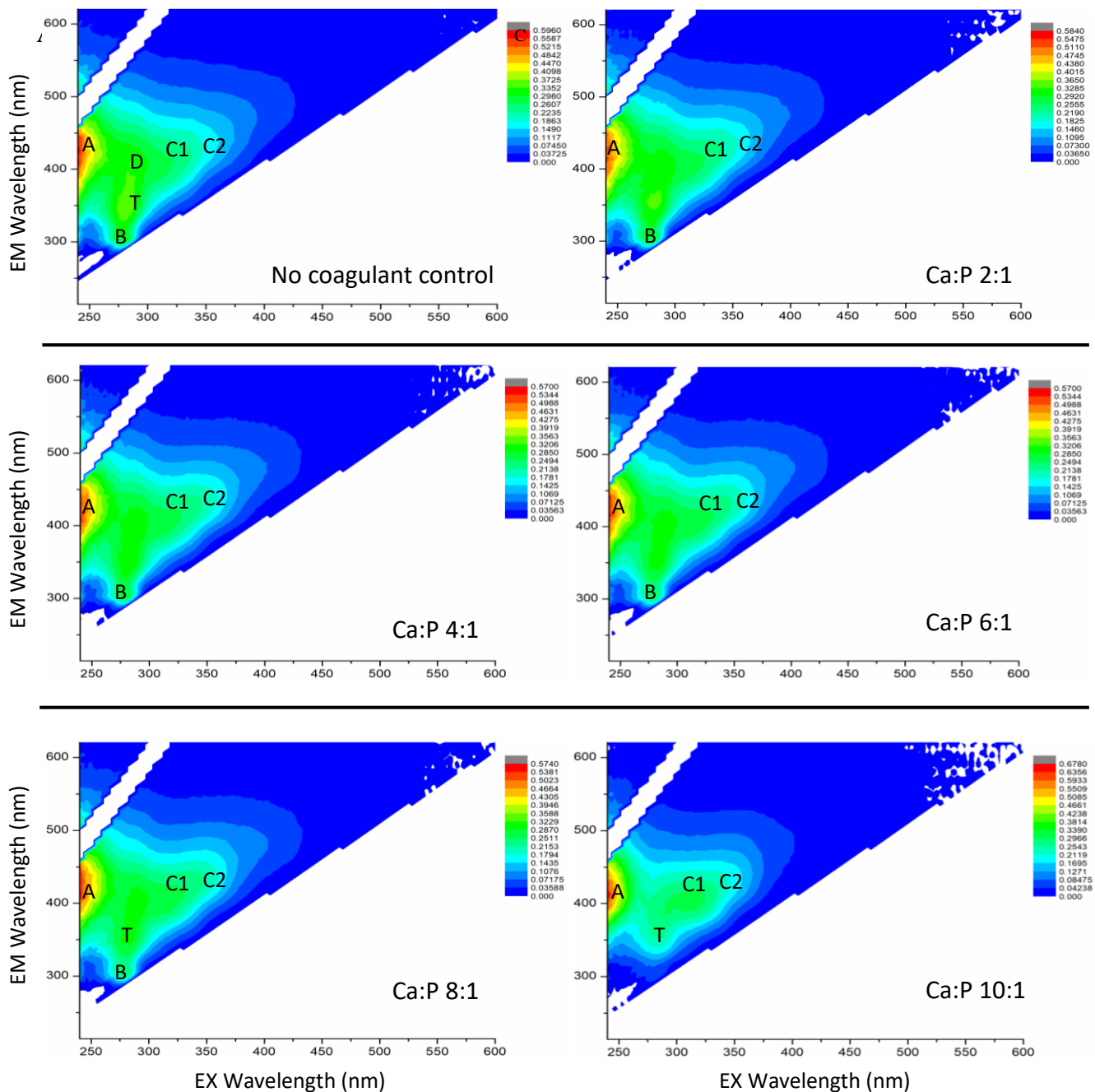
Figure 6.3 EEMs from the pH altered aerated permeate collected after addition of varying molar Ca:P dose. The results show that with increasing coagulant dosage, there is a greater removal in the protein-like fluorescence or the tyrosine (B) peaks and tryptophan (T) like fluorescence peaks.

6.4 Outlook

P-products recovered from wastewater by commercial technologies are currently marketed as fertilizers, with little focus on product solubility and plant bioavailability. There is a need to selectively increase the P content in the end products and its solubility for plant availability or other potential end uses for the Phosphorus. This need is addressed in the present study using the permeate modification method, which produced an improved CaP product with P content comparable to mineral phosphates. In addition, the alkaline pH of the final permeate can eliminate the need for disinfection before spreading the product on land or reusing the treated water as non-potable water, since alkaline conditions can effectively inactivate pathogens (Viancelli et al., 2015). The quality of the final permeate after P recovery can be further improved by recycling the stripped CO_2 to remove residual calcium hardness in the water and lower the final pH to meet discharge standards, as shown in Figure 6.4. Such recycling of CO_2 along with efficient recovery of energy from the AnMBR as biogas offsets all carbon emissions and a portion of the energy footprint of the nutrient recovery process, likely making the platform environmentally safe and economically viable. Overall, the results of the present study support AnMBRs as a robust sustainable nutrient recovery platform that can enable tailored recovery of high-quality nutrients despite any fluctuations in influent wastewater properties..
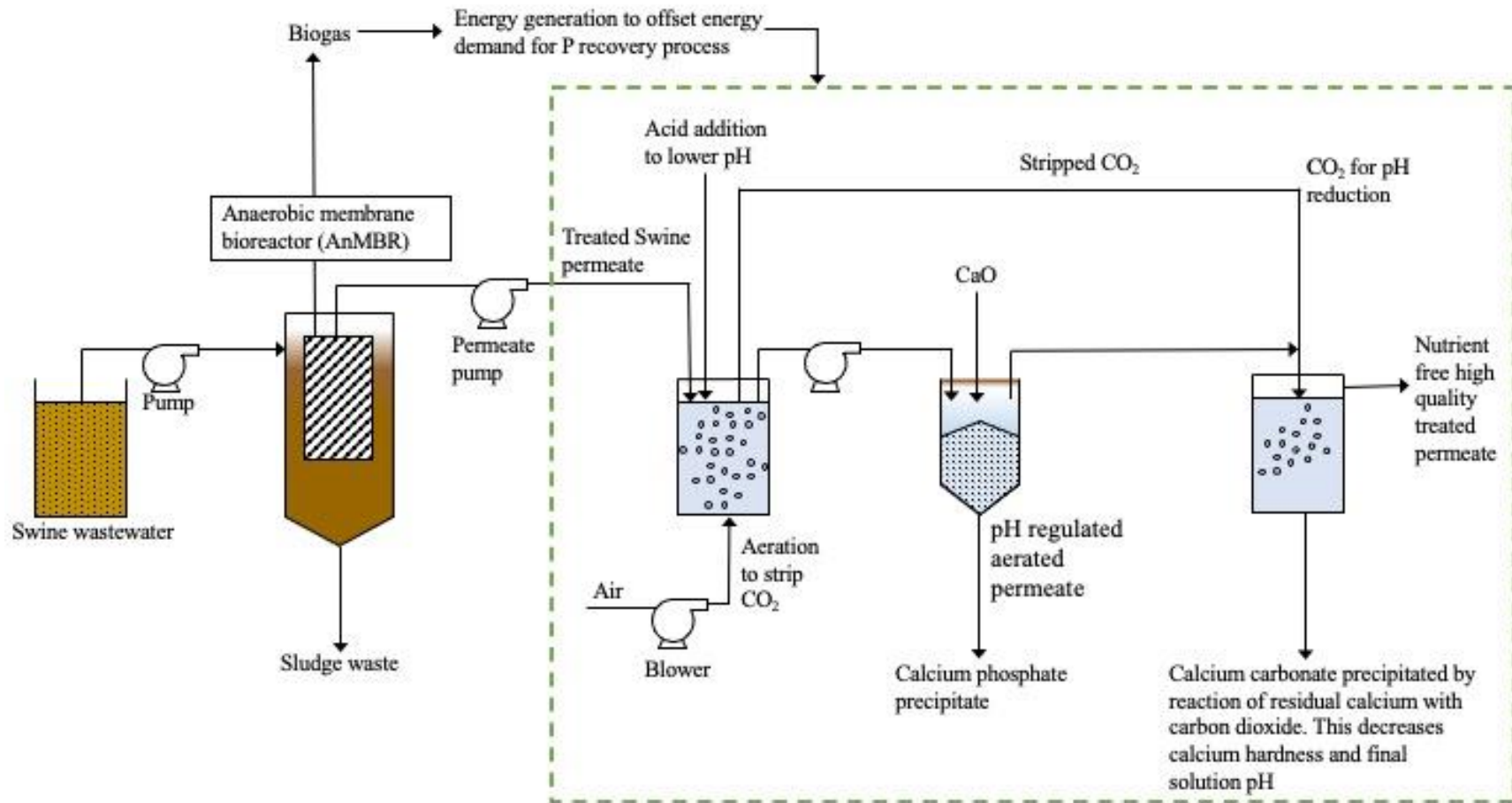
Figure 6.4 Process schematic of the sustainable phosphorus recovery system integrated AnMBR system for tailored capture of phosphorus as high quality calcium phosphate. Additionally, a novel CO_2 recycling process for final effluent polishing by removal residual calcium hardness and reducing final pH is also proposed.

6.5 Conclusions

- This study successfully demonstrated the use of calcium coagulants for high-quality P recovery from AnMBR treated swine wastewater permeate which is free of colloidal and particulate organics.

- Carbonate alkalinity had the greatest impact on the efficiency of P removal and quality of product recovered from swine permeate because of co-precipitation of calcium carbonate.

- Process modifications involving stripping the CO_2 by pH adjustment and aeration to remove carbonate species from the permeate (treated water) prior to P recovery to avoid non-essential co-precipitates significantly improved the P removal efficiency from the permeate as well as the total and citric acid soluble P content in the final recovered nutrient product. This is a significant finding.

- Amorphous calcium phosphates (ACPs) were the main products formed with the altered permeate and could possibly be recovered as HAP by allowing sufficient induction time for crystallization. ACP can also be used as is because of its better solubility.

Chapter 7 - Sequential recovery of Struvite and Calcium phosphate as high value nutrient products from swine permeate

7.1 Introduction

Struvite ($NH_4 Mg PO_4 \cdot 6 H_2O$), an important phosphate mineral found in natural and engineered systems, can precipitate and form scales in distribution systems and different parts of wastewater systems (Petzet & Cornel, 2012). Struvite formation occurs in wastewater treatment plants due to the characteristics of the wastewater. There are three primary components of struvite formation such as magnesium (Mg^{2+}), ammonium (NH_4^+) and phosphorus (PO_4^{3-}). Struvite precipitates and crystalizes in wastewater treatment plants when magnesium, ammonium, and phosphorus react in water in a 1:1:1 ratio ($Mg^{2+} + NH_4^+ + PO_4^{3-} + H_2O \rightarrow MgNH_4PO_4 \cdot 6H_2O(s)$)(Doyle & Parsons, 2002). Uncontrolled struvite formation increases operating and maintenance costs and reduces the hydraulic capacity of distribution systems and equipment by reducing pipe diameter (Achilleos et al., 2022; Parsons & Doyle, 2004). While uncontrolled precipitation of struvite is detrimental, its controlled precipitation is economically and ecologically beneficial as it can be used as a fertilizer due to its excellent slow release properties (Melia et al., 2017). In view of this, most commercial P recovery technologies have focused on recovering struvite as the final product from municipal wastewaters without much focus on calcium phosphate.

There are no known studies in the literature that have reported the sequential recovery of struvite and calcium phosphate from swine permeate or other types of wastewaters including municipal wastewater. No prior study has attempted to validate this approach and the proposed study will be one of the first attempts to explore this possibility and present preliminary results. The results of the experiments discussed in Chapter 6 showed successful recovery of high quality calcium phosphate products from the swine permeate. To further explore the possibility of

tailored nutrient recovery in the AnMBR system, the present study focused on the recovery of P as two different products of struvite and calcium phosphate in the same process train in a sequential manner. The main objective of this chapter is to recover struvite by adding magnesium chloride at different molar ratios of Magnesium (Mg)/Phosphorus (P) followed by calcium phosphate precipitation by calcium chloride addition.

7.2 Materials and Methods

7.2.1 AnMBR swine permeate collection and modification

Swine permeate collected from the lab scale AnMBR was modified to remove the carbonate alkalinity by adding H_2SO_4 to lower pH to 4.5 followed by overnight aeration to strip the CO_2 (Damodara Kannan et al., 2023). Alkalinity was measured both before and after swine permeate modification to understand P removal.

7.2.2 Struvite and calcium phosphate precipitation experiments

Two-stage sequential precipitation of struvite and calcium phosphate from the pH modified CO_2 stripped swine permeate was performed at two different pH values of 9.5 and 8.5. First, varying molar dose ratios of magnesium/phosphorus (Mg/P) of 1/1, 1.5/1, 2/1, 4/1 was added to 200 mL of swine permeate using $MgCl_2$. The magnesium was added from a stock solution of 0.5 M $MgCl_2$. The pH of the solution after Mg addition was raised to 9.5 using 4 M NaOH solution. The pH adjusted solutions after Mg addition were placed on an orbital shaker for 24 hours at 100 rpm. After 24 hours, the solutions were checked for any solids precipitation and were centrifuged in an Eppendorf centrifuge 5920 R (Hauppauge, New York, USA) at 10000 rpm for 10 minutes. The supernatant was transferred to new flasks and the settled solid precipitates were air dried at room temperature for use in further phase identification analysis. The residual phosphorus concentration in each of the samples was measured 24 hours after Mg

addition to estimate P removal efficiency. Next, calcium was added using 0.5 M calcium

chloride ($CaCl_2$) solution in a Ca/P molar ratio of 4/1 based on the residual phosphorus

concentration remaining after the first stage precipitation with Mg. The Ca/P molar ratio of 4/1

was chosen because it gave >80% P removal as reported in chapter 6. The solutions were placed

on an orbital shaker for 24 hours to allow calcium-based precipitation reactions. Finally, the

precipitate formed after Ca addition was separated by centrifuging the solution at 10000 rpm for

10 minutes and air dried separately. The final phosphorus concentration was measured to

calculate the P removal efficiency. The next set of experiments at pH 8.5 follows the same

experimental procedure as described above.

7.2.3 Phase identification using X-Ray diffraction (XRD)

A powder X-ray Diffraction (XRD) analysis of air-dried precipitates was conducted using

a PANalytical Empyrean Multi-Purpose X-Ray Diffractometer (Spectris Company, Egham,

Surrey, UK) with a copper anode material and generator settings of 35 eV and 20 mA. Due to

logistical issues and instrument access limitations, only the precipitate product obtained after Mg

addition from the pH 9.5 experiment was used for phase analysis. The XRD data file was

processed using Profex software (Doebelin & Kleeberg, 2015) for peak identification and

subsequent phase matching was performed in QualX software (Altomare et al., 2015) using the

POW_COD database.

7.2.4 Chemical analysis

Total phosphorus was measured with HACH TNT 844 and TNT 845 kits (concentration

range 0.5 -5 mg/L-P and 2-20 mg/L-P, respectively) using the HACH DR 3900

spectrophotometer (Loveland, CO, USA). Total Alkalinity was measured using HACH TNT 870

kit (25 – 400 mg/L CaCO3). pH was measured using Fisherbrand™ accumet™ AB150 pH Benchtop Meters.

7.3 Results and discussion

7.3.1 Sequential P removal efficiency

The results of chemical precipitation at pH 9.5 showed that P removal after Mg addition was highest at 56% using the 2/1 Mg/P dose as shown in Figure 7.1. The initial phosphate concentration was found to be 61.9 mg/L – P. The P removal decreased to 52% at the 4/1 dose indicating that higher Mg dose did not improve P removal. Similar observations have been reported by (Kemacheevakul et al., 2015) where optimum Mg/P ratio for maximum struvite removal was found to be 2/1. Calcium addition at Ca/P dose of 4/1 achieved further P removal of 56.5% in the 2/1 Mg/P dose solution. The combined P removal from each stage of Mg and Ca addition resulted in an overall removal efficiency of greater than 97% in each of the Mg/P dosing solutions.
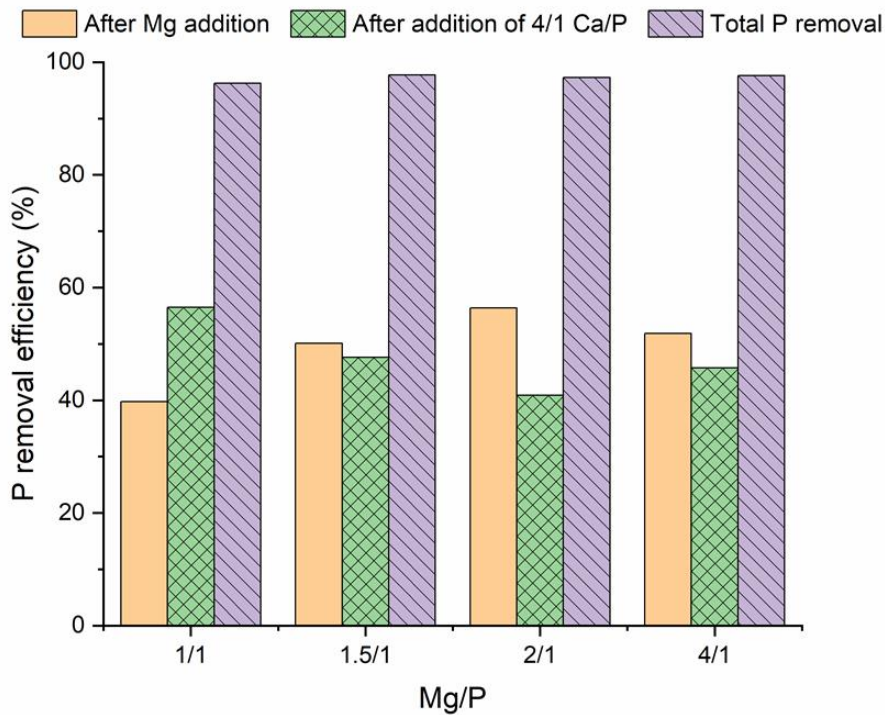
Figure 7.1 P removal efficiencies at different Mg/P doses and subsequent Ca/P dose of 4/1 at initial pH of 9.5. The results showed a combined P removal efficiency of more than 97% in all different solutions.

The results of P removal efficiencies at pH 8.5 summarized in Figure 7.2 showed that removal efficiency after Mg addition was highest at 42% in the 2/1 Mg/P dose compared to other Mg doses. The initial phosphate concentration in the solution was 60.5 mg/L-P. Compared to the pH 9.5 experiment, Mg addition at pH 8.5 resulted in lower P removal efficiency and can be explained by the decline in struvite crystal solubility with increasing solution pH (Liu et al., 2018). Subsequent Ca addition at the 4/1 Ca/P dose resulted in negligible P removal in the 2/1 and 4/1 Mg/P dosing solutions, although a 46% removal in the 1/1 Mg/P dosing solution was observed.
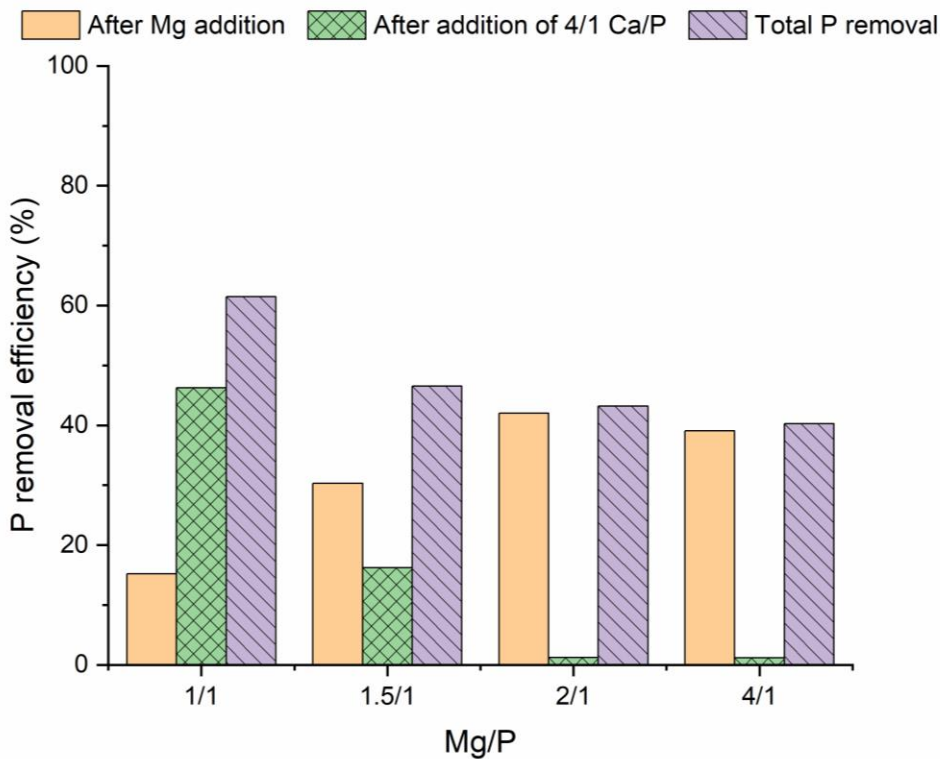
Figure 7.2 P removal efficiencies at various Mg/P doses and subsequent Ca/P dosing of 4/1 at initial pH of 8.5. Results showed a combined maximum P removal efficiency of 61% at 1/1 Mg/P and 4/1 Ca/P doses. In solutions dosed with Mg/P of 2/1 and 4/1, calcium addition resulted in negligible further P removal.

The negligible P removal after Ca addition in the Mg/P dosing solutions of 2/1 and 4/1 was probably because of decrease in solution pH after Mg addition. The pH values measured 24 hours after Mg addition decreased from the initial value of 8.5 to 8.17, 8.02, 7.78, and 7.73 in the1/1, 1.5/1, 2/1, and 4/1 Mg/P dosing solutions, respectively. The decrease in pH of the solution is due to proton generation during struvite formation reactions as shown below

$H_nPO_4^{3-n} + Mg^{2+} + NH^{4+} + 6H_2O \rightarrow MgNH_4PO_4.6H_2O + nH^+$

This decrease in solution pH impacted subsequent P removal with Ca, resulting in less than 2% removal after Ca addition in the 2/1 Mg/P (pH 7.78) and 4/1 Mg/P (pH 7.73) dosing solutions. As discussed in Chapter 6, calcium-based P removal is highly dependent on solution pH to induce precipitation reactions, which are ideal at alkaline pH. It has been previously

reported that no calcium-based precipitation was observed when the solution pH ≤ 8.5 (Hao et al., 2008) Therefore, other sources of calcium such as quick lime or calcium hydroxide can be used as alternative sources of calcium as these chemicals can increase the pH of the solution and induce calcium phosphate precipitation.

7.3.2 Phase analysis of recovered phosphorus products

The results of the XRD analysis, shown in Figures 7.3A and 7.3B, represent the XRD pattern of the precipitate formed after Mg addition in the pH 9.5 experiment at Mg/P ratios of 1/1 and 2/1, respectively. Phase analysis of the precipitates showed peak matching with struvite mineral confirming struvite formation. However, the peak noise pattern indicates there may be other mineral phase contaminants that could not be identified by exact peak matches in the database search process. The high intensities of the peaks seen around 15-16° angles compared to the pure struvite pattern were reported in a previous study and observed with increasing pH (7.8-9) and increasing Mg/P ratio (Liu et al., 2018).

A)
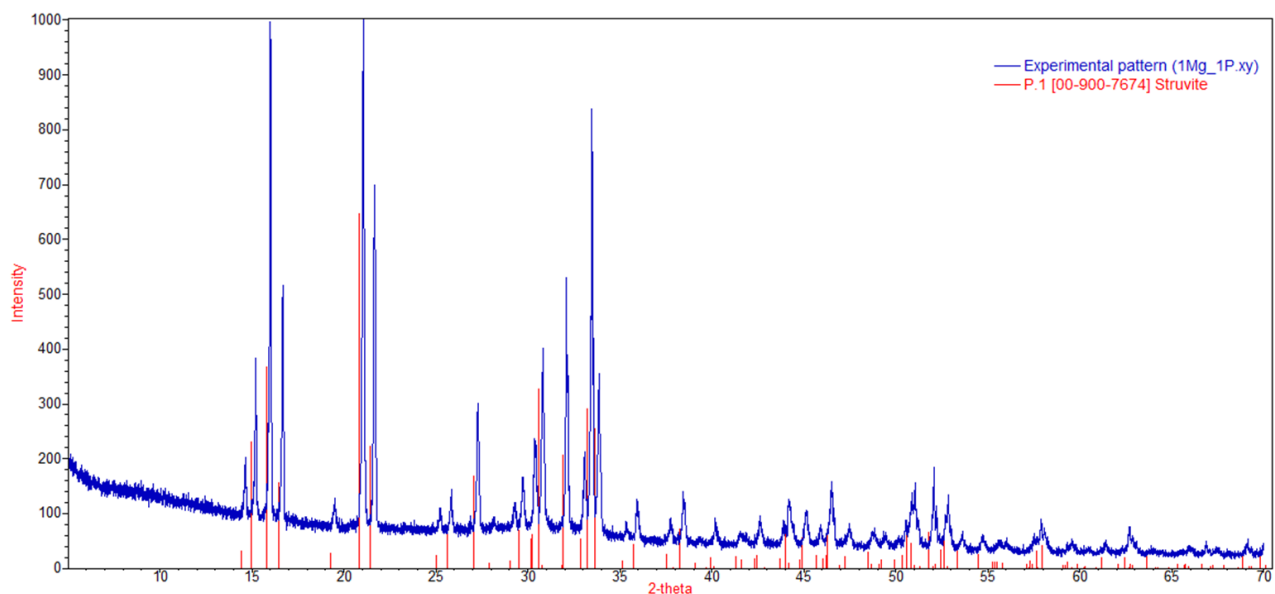
B)
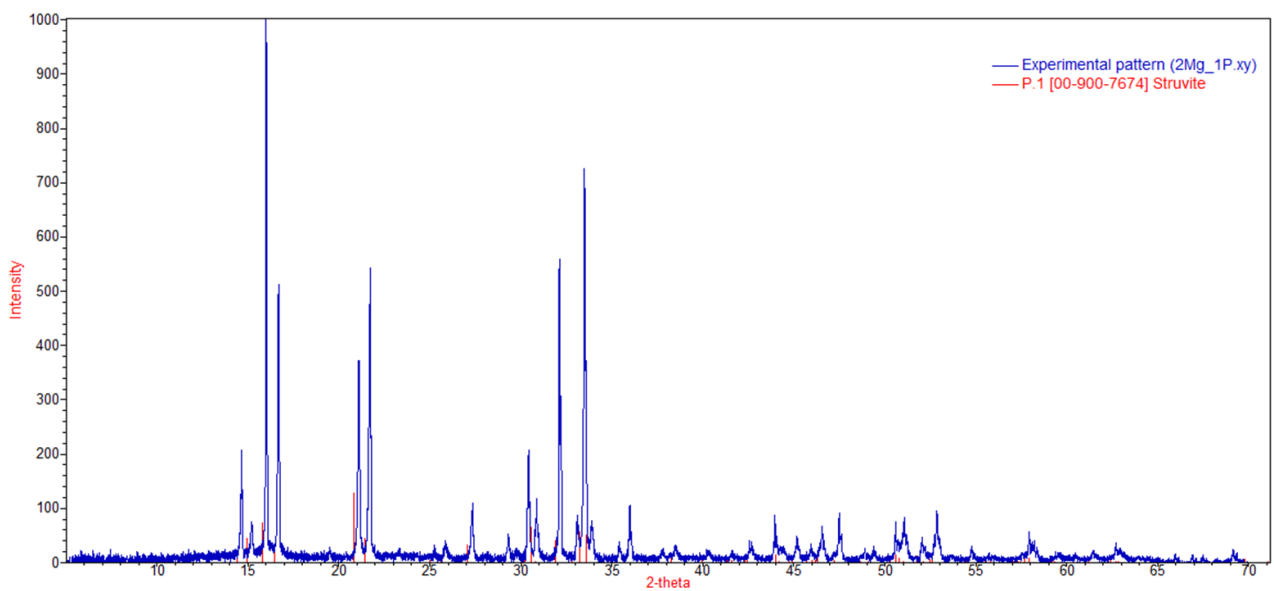
Figure 7.3 XRD pattern of precipitates formed at pH 9.5 for A) Mg/P dose of 1/1 and B) Mg/P dose of 2/1.

7.3.3 Limitations and Uncertainties

The results reported in this chapter are preliminary proof of concept showing efficient P removal resulting in tailored products at low chemical doses and provide a new perspective on the tailored recovery of phosphorus products. However, with this limited study, not much can be concluded about the mineral phases formed after calcium addition. Ammonia removal data could not be measured due to logistical issues affecting the availability of test kits. Such data would be useful to understand the ammonia removal, mineral composition of the formed precipitate, and its struvite content. Additionally, the phosphorus content of the formed precipitate needs to be analyzed by dissolution method and analyzed using the ICP as reported in chapter 6 on calcium phosphate recovery. It is also important to characterize the ionic composition of the swine permeate to understand the impact of cations and anions on P removal and purity of the struvite and calcium phosphate precipitates formed. Finally, there is a need to demonstrate the impact of alternate calcium coagulants (calcium oxide and calcium hydroxide) and the pH dependence of the permeate needs to be addressed. Overall, these limitations should be addressed in future studies.

7.4 Conclusion

In conclusion, this study shows efficient P removal from swine permeate using magnesium and calcium chemicals for sequential recovery of tailored phosphorus products. A combined P removal >97% was observed after magnesium and calcium addition at an initial pH of 9.5. The Mg/P molar dose of 2/1 was found to be the optimum dose resulting in a maximum P removal of 56% and 42% at pH 9.5 and pH 8.5, respectively. Despite some limitations, the findings of this study support the hypothesis that both struvite and calcium phosphate may be recovered in the same process stream.

Chapter 8 - Summary and Recommendations for Future Research

8.1 Summary

The recovery of high-quality nutrient products from wastewater remains a major challenge, largely due to current treatment systems focusing on nutrient removal than recovery. Anaerobic membrane bioreactors are an emerging environmental biotechnology with the greatest potential to enable municipal, agricultural, and industrial wastewater treatment to simultaneously achieve energy-positive treatment, water recovery for reuse and more importantly, tailored recovery of high-quality nutrient products from the treated permeate for subsequent useful applications. Targeted capture of ammonia from real swine wastewater using clinoptilolite from real swine wastewater was demonstrated in Chapter 3. The experimental results showed that clinoptilolite can be an effective natural adsorbent material for capturing ammonia while modeling results provided deeper insights into the mechanistic understanding of ammonia adsorption on clinoptilolite.

Chapter 4 presents the microbial community structure analysis in anaerobic sludge of the AnMBR in an effort to understand the potential microbial interactions with the soil microbiota for beneficial land/crop application. Results showed that the microbial community of the sludge was dominated by a core group of bacteria and was not influenced by the influent wastewater microbial community.

The anaerobically digested biosolids from wastewater together with ammonia sorbed clinoptilolite were evaluated for their fertilizer suitability in soil incubation and greenhouse studies (Chapter 5). The ammonia sorbed clinoptilolite exhibited slow nutrient release by slowly diffusing nitrogen compared to conventional fertilizers such as urea and ammonium sulfate.

However, the anaerobically digested biosolids performed poorly as a nitrogen source, failing to mineralize the organic nitrogen within the duration of the incubation period. Further greenhouse experiments with corn crop showed that urea can be blended with ammonia sorbed clinoptilolite without significantly compromising on the plant nitrogen uptake. This has both significant economic and environmental benefits as it reduces the cost of excess urea and prevents pollution caused by nitrogen losses.

In chapter 6, another demonstration of tailored nutrient recovery in the AnMBR system using calcium-based coagulants for phosphorus recovery as calcium phosphates showed that carbonate alkalinity and pH greatly affected phosphorus precipitation. This limitation was overcome by modifying the swine permeate to remove the carbonate alkalinity by lowering the pH and aerating to strip as CO_2. The resulting product formed with the modified permeate had a higher P content and better citric acid solubility, confirming the effectiveness of the permeate modification process. The results certainly suggest that this is a viable method for producing high quality nutrient products. It is proposed to recycle the generated CO_2 to polish the phosphate-free effluent to remove residual calcium hardness and impart alkalinity to the effluent before discharge. No previous study has investigated this approach, and this can be considered to be a significant step forward in sequestering CO_2 from wastewater treatment plants.

In chapter 7, preliminary results on sequential recovery of phosphorus as struvite ($MgNH_4PO_4.6H_2O$) and calcium phosphate in the pH altered CO_2 stripped swine permeate is presented. The process involved a two-step approach to recovering struvite first followed by calcium phosphate. Despite the success demonstrated with sequential recovery of struvite and calcium-based P removal, these preliminary findings warrant further investigations pertaining to phase identification of the precipitate formed after calcium addition and Ca dose reduction. The

sequential recovery of struvite and calcium phosphate is the first time this approach of sequential P recovery of struvite and calcium phosphate has been explored and offers great potential for large scale commercial implementation. Overall, the results of this dissertation demonstrate that AnMBRs can be a sustainable nutrient recovery platform enabling tailored recovery of nutrient products with commercial value that can be beneficially reused. Furthermore, this dissertation provides a framework for further research directions and application of AnMBRs as a resource recovery platform.

8.2 Recommendations for Future Research

Future research should focus on the following research ideas that are either beyond the scope of this study or were not directly addressed in this study.

- Although clinoptilolite can be very effective for ammonia sorption as shown in Chapter 3, further research is needed to sustainably regenerate the spent clinoptilolite. Currently, brine is the most commonly used regenerant solution, but regeneration efficiency can be improved with novel electrochemical regeneration technologies.

- The greenhouse study in Chapter 5 should be carried out over a longer period of time in order to clearly distinguish the effects of different N treatments on the entire plant growth cycle. It is recommended to conduct the experiments in larger pots to monitor differences in microbial communities between the rhizosphere and the bulk soil. In addition, a functional gene based quantitative polymerase chain reaction (qPCR) based estimation is recommended for a full understanding of the key microbial players involved in the nitrogen cycle. It is also recommended that soil characterization of the soil from the pots be performed at different sampling times during the growth phase of the crop to understand soil nitrogen leaching and transformations. Such time series-based sampling

should also be performed for soil DNA extractions to monitor changes in the microbial community in the long term. Overall, it is highly recommended to conduct greenhouse trials with different N treatments as long-term trials to clearly understand the slow nutrient release properties of ammonia sorbed clinoptilolite.

- In the greenhouse study, the nitrogen contribution of clinoptilolite and urea in the mixture of urea + ammonia sorbed clinoptilolite treatment was not clearly understood. This can be addressed through the use of isotope labeled N in each of the two N sources, which can then be traced to identify the exact source of nitrogen taken up by plants.

- In Chapter 6, the calcium based chemical addition resulted in excellent P removal in the pH altered CO_2 stripped swine permeate. An issue to consider in future studies is how best to reduce the Ca dose without compromising the P removal efficiency. It is expected that seeding the solution with mineral particles can act as nucleation sites for mineral precipitates to aggregate and grow. This could be particularly useful for AnMBR treated permeate that is free of colloidal and suspended particles that might otherwise act as nucleation sites for crystal growth.

- The process modification of the permeate in this study resulted in CO_2 generation. To offset any potential CO_2 emissions, it is recommended to recycle the generated CO_2 back to the treated phosphorus free effluent for further polishing the effluent. Such recycling of CO_2 can help in reducing residual calcium in the permeate due to the initial addition of calcium and lower the pH of the solution from highly alkaline pH to closer to neutral.

- Further investigation is needed to understand the effects of interfering cations and anions on P removal by the calcium coagulants especially magnesium ion.

- The permeate modification in this study was done using H2SO4 acid to lower the pH. However, the possibility of using organic acids generated within the anaerobic bioreactor should be explored as alternatives for lowering the pH in the permeate and subsequently recovering calcium phosphate or other recovered nutrient products.

- The dose of calcium or magnesium required to recover P may be optimized and lowered through the use of electrocoagulation techniques and requires further investigation.

References

Abuabdou, S. M. A., Ahmad, W., Aun, N. C., & Bashir, M. J. K. (2020). A review of anaerobic membrane bioreactors (AnMBR) for the treatment of highly contaminated landfill leachate and biogas production: Effectiveness, limitations and future perspectives. *Journal of Cleaner Production, 255*, 120215.

Achilleos, P., Roberts, K. R., & Williams, I. D. (2022). Struvite precipitation within wastewater treatment: A problem or a circular economy opportunity? *Heliyon, 8*(7), e09862.

Agler, M. T., Wrenn, B. A., Zinder, S. H., & Angenent, L. T. (2011). Waste to bioproduct conversion with undefined mixed cultures: the carboxylate platform. *Trends in Biotechnology, 29*(2), 70-78.

Altomare, A., Corriero, N., Cuocci, C., Falcicchio, A., Moliterni, A., & Rizzi, R. (2015). QUALX2. 0: a qualitative phase analysis software using the freely available database POW_COD. *Journal of Applied Crystallography, 48*(2), 598-603.

Alvarez, R., Evans, L. A., Milham, P. J., & Wilson, M. A. (2004). Effects of humic material on the precipitation of calcium phosphate. *Geoderma, 118*(3), 245-260.

Amini, A., Aponte-Morales, V., Wang, M., Dilbeck, M., Lahav, O., Zhang, Q., Cunningham, J. A., & Ergas, S. J. (2017). Cost-effective treatment of swine wastes through recovery of energy and nutrients. *Waste Management, 69*, 508-517.

Anas, M., Liao, F., Verma, K. K., Sarwar, M. A., Mahmood, A., Chen, Z.-L., Li, Q., Zeng, X.-P., Liu, Y., & Li, Y.-R. (2020). Fate of nitrogen in agriculture and environment: agronomic, eco-physiological and molecular approaches to improve nitrogen use efficiency. *Biological Research*, *53*(1), 47. https://doi.org/10.1186/s40659-020-00312-4

Angel, R. (1999). Removal of phosphate from sewage as amorphous calcium phosphate. *Environmental technology, 20*(7), 709-720.

Antille, D. L., Godwin, R. J., Sakrabani, R., Seneweera, S., Tyrrel, S. F., & Johnston, A. E. (2017). Field-Scale Evaluation of Biosolids-Derived Organomineral Fertilizers Applied to Winter Wheat in England. Agronomy Journal, 109(2), 654-674. https://doi.org/https://doi.org/10.2134/agronj2016.09.0495

Ariesyady, H. D., Ito, T., & Okabe, S. (2007). Functional bacterial and archaeal community structures of major trophic groups in a full-scale anaerobic sludge digester. *Water Research, 41*(7), 1554-1568.

Arita, I. H., Wilkinson, D. S., Mondragón, M. A., & Castaño, V. M. (1995). Chemistry and sintering behaviour of thin hydroxyapatite ceramics with controlled porosity. *Biomaterials, 16*(5), 403-408.

Azam, H. M., Alam, S. T., Hasan, M., Yameogo, D. D. S., Kannan, A. D., Rahman, A., & Kwon, M. J. (2019). Phosphorous in the environment: characteristics with distribution and effects, removal mechanisms, treatment technologies, and factors affecting recovery as minerals in natural and engineered systems. *Environmental Science and Pollution Research, 26*(20), 20183-20207.

Azam, H. M., Alam, S. T., Hasan, M., Yameogo, D. D. S., Kannan, A. D., Rahman, A., & Kwon, M. J. (2019). Phosphorous in the environment: characteristics with distribution and effects, removal mechanisms, treatment technologies, and factors affecting recovery as minerals in natural and engineered systems. *Environmental Science and Pollution Research, 26*(20), 20183-20207.

Bansiwal, A. K., Rayalu, S. S., Labhasetwar, N. K., Juwarkar, A. A., & Devotta, S. (2006). Surfactant-Modified Zeolite as a Slow Release Fertilizer for Phosphorus. *Journal of Agricultural and Food Chemistry, 54*(13), 4773-4779.

Barak, P. (2017). Phosphate recovery from wastewater. In: Google Patents.

Barat, R., Bouzas, A., Martí, N., Ferrer, J., & Seco, A. (2009). Precipitation assessment in wastewater treatment plants operated for biological nutrient removal: a case study in Murcia, Spain. *J Environ Manage, 90*(2), 850-857.

Bei, S., Zhang, Y., Li, T., Christie, P., Li, X., & Zhang, J. (2018). Response of the soil microbial community to different fertilizer inputs in a wheat-maize rotation on a calcareous soil. Agriculture, Ecosystems & Environment, 260, 58-69.

Belova, T. (2019). Adsorption of heavy metal ions (Cu2+, Ni2+, Co2+ and Fe2+) from aqueous solutions by natural zeolite. *Heliyon, 5*(9), e02320.

Berca, M., Robescu, V.-O., Duică, M., & Horoiaş, R. (2019). Nitrogen fertilizers and bioeconomic agriculture–example on wheat. Agrarian economy and rural development-realities and perspectives for romania, 64.

Bhardwaj, D., Sharma, M., Sharma, P., & Tomar, R. (2012). Synthesis and surfactant modification of clinoptilolite and montmorillonite for the removal of nitrate and preparation of slow release nitrogen fertilizer. Journal of Hazardous Materials, 227-228, 292-300.

Bialek, K., Kim, J., Lee, C., Collins, G., Mahony, T., & O'Flaherty, V. (2011). Quantitative and qualitative analyses of methanogenic community development in high-rate anaerobic bioreactors. *Water Research, 45*(3), 1298-1308.

Blackwell, M., Darch, T., & Haslam, R. (2019). Phosphorus use efficiency and fertilizers: future opportunities for improvements. *Frontiers of Agricultural Science and Engineering, 6*(4), 332-340.

Blackwell, M., Darch, T., & Haslam, R. (2019). Phosphorus use efficiency and fertilizers: future opportunities for improvements. *Frontiers of Agricultural Science and Engineering, 6*(4), 332-340.

Boer, M. A. d., Wolzak, L., & Slootweg, J. C. (2019). Phosphorus: reserves, production, and applications. In *Phosphorus recovery and recycling* (pp. 75-100): Springer.

Boguniewicz-Zablocka, J., Klosok-Bazan, I., Naddeo, V., & Mozejko, C. A. (2019). Cost-effective removal of COD in the pre-treatment of wastewater from the paper industry. *Water Science and Technology, 81*(7), 1345-1353.

Bolyen, E., Rideout, J. R., Dillon, M. R., Bokulich, N. A., Abnet, C. C., Al-Ghalith, G. A., . . . Asnicar, F. (2019). Reproducible, interactive, scalable and extensible microbiome data science using QIIME 2. *Nature biotechnology, 37*(8), 852-857.

Bolyen, E., Rideout, J. R., Dillon, M. R., Bokulich, N. A., Abnet, C. C., Al-Ghalith, G. A., Alexander, H., Alm, E. J., Arumugam, M., Asnicar, F., Bai, Y., Bisanz, J. E., Bittinger, K., Brejnrod, A., Brislawn, C. J., Brown, C. T., Callahan, B. J., Caraballo-Rodríguez, A. M., Chase, J., . . . Caporaso, J. G. (2019). Reproducible, interactive, scalable and extensible microbiome data science using QIIME 2. Nature Biotechnology, 37(8), 852-857. https://doi.org/10.1038/s41587-019-0209-9

Bonmatí, A., & Flotats, X. (2003). Air stripping of ammonia from pig slurry: characterisation and feasibility as a pre-or post-treatment to mesophilic anaerobic digestion. *Waste Management, 23*(3), 261-272.

Booker, N., Cooney, E., & Priestley, A. (1996). Ammonia removal from sewage using natural Australian zeolite. *Water Science and Technology, 34*(9), 17-24.

Braithwaite, A., Eaton, A., & Groom, P. (1990). Factors affecting the solubility of phosphate rock residues in 2% citric acid and 2% formic acid. *Fertilizer research, 23*(1), 37-42.

Bremner, J. M. (1996). Nitrogen-total. Methods of soil analysis: Part 3 Chemical methods, 5, 1085-1121.

Britton, A., Sacluti, F., Oldham, W., Mohammed, A., Mavinic, D., & Koch, F. (2007). *Value from waste–struvite recovery at the city of Edmonton's gold bar WWTP.* Paper presented at the Proc. IWA Specialist Conference: Moving Forward–Wastewater biosolids sustainability.

Buhlmann, C. H., Mickan, B. S., Jenkins, S. N., Tait, S., Kahandawala, T. K. A., & Bahri, P. A. (2019). Ammonia stress on a resilient mesophilic anaerobic inoculum: Methane production, microbial community, and putative metabolic pathways. *Bioresource Technology, 275*, 70-77. doi:https://doi.org/10.1016/j.biortech.2018.12.012

Caddarao, P. S., Garcia-Segura, S., Ballesteros, F. C., Huang, Y.-H., & Lu, M.-C. (2018). Phosphorous recovery by means of fluidized bed homogeneous crystallization of calcium phosphate. Influence of operational variables and electrolytes on brushite homogeneous crystallization. *Journal of the Taiwan Institute of Chemical Engineers, 83*, 124-132.

Cantrell, K. B., Ducey, T., Ro, K. S., & Hunt, P. G. (2008). Livestock waste-to-bioenergy generation opportunities. *Bioresource Technology, 99*(17), 7941-7953.

Cao, X., & Harris, W. (2008). Carbonate and Magnesium Interactive Effect on Calcium Phosphate Precipitation. *Environmental science & technology, 42*(2), 436-442.

Çelen, I., Buchanan, J. R., Burns, R. T., Bruce Robinson, R., & Raj Raman, D. (2007). Using a chemical equilibrium model to predict amendments required to precipitate phosphorus as struvite in liquid swine manure. *Water Research, 41*(8), 1689-1696.

Chemists, A. o. O. A., & Lepper, H. A. (1945). *Official methods of analysis*.

Chen, C.-C., Lin, C.-Y., & Lin, M.-C. (2002). Acid–base enrichment enhances anaerobic hydrogen production process. *Applied microbiology and biotechnology, 58*(2), 224-228.

Chen, J., Lü, S., Zhang, Z., Zhao, X., Li, X., Ning, P., & Liu, M. (2018). Environmentally friendly fertilizers: A review of materials used and their effects on the environment. *Science of The Total Environment, 613-614*, 829-839.

Chen, J., Lü, S., Zhang, Z., Zhao, X., Li, X., Ning, P., & Liu, M. (2018). Environmentally friendly fertilizers: A review of materials used and their effects on the environment. *Science of The Total Environment, 613*, 829-839.

Chen, S., Shi, Y., Wang, W., Li, Z., Gao, J., Bao, K., Han, R., & Zhang, R. (2014). Phosphorus removal from continuous phosphate-contaminated water by electrocoagulation using aluminum and iron plates alternately as electrodes. *Separation Science and Technology, 49*(6), 939-945.

Cheng, H., Cheng, D., Mao, J., Lu, T., & Hong, P.-Y. (2019). Identification and characterization of core sludge and biofilm microbiota in anaerobic membrane bioreactors. *Environment international, 133*, 105165.

Christiansen, N. H., Sørensen, P., Labouriau, R., Christensen, B. T., & Rubæk, G. H. (2020). Characterizing phosphorus availability in waste products by chemical extractions and plant uptake. *Journal of Plant Nutrition and Soil Science, 183*(4), 416-428.

Coble, P. G. (2007). Marine optical biogeochemistry: the chemistry of ocean color. *Chemical reviews, 107*(2), 402-418.

Cordell, D., & Neset, T.-S. (2014). Phosphorus vulnerability: a qualitative framework for assessing the vulnerability of national and regional food systems to the multi-dimensional stressors of phosphorus scarcity. *Global Environmental Change, 24*, 108-122.

Cordell, D., Drangert, J.-O., & White, S. (2009). The story of phosphorus: Global food security and food for thought. *Global Environmental Change, 19*(2), 292-305.

Cornel, P., & Schaum, C. (2009). Phosphorus recovery from wastewater: needs, technologies and costs. *Water Science and Technology, 59*(6), 1069-1076.

Cunha, J. R., Schott, C., van der Weijden, R. D., Leal, L. H., Zeeman, G., & Buisman, C. (2020). Calcium phosphate granules recovered from black water treatment: A sustainable substitute for mined phosphorus in soil fertilization. *Resources, Conservation and Recycling, 158*, 104791.

Cusick, R. D., & Logan, B. E. (2012). Phosphate recovery as struvite within a single chamber microbial electrolysis cell. *Bioresource Technology, 107*, 110-115.

Damodara Kannan, A., Dillavou, J., H.H. Gamage, K., Randig, E., M. Hettiarachchi, G., & Parameswaran, P. (2023). Recovery of high-quality calcium phosphate fertilizer products from anaerobic membrane bioreactor treated swine wastewater. *Chemical Engineering Journal, 453*, 139539.

Damodara Kannan, A., Evans, P., & Parameswaran, P. (2020). Long-term microbial community dynamics in a pilot-scale gas sparged anaerobic membrane bioreactor treating municipal wastewater under seasonal variations. *Bioresource Technology, 310*, 123425.

Damodara Kannan, A., Heronemus, E., Gamage, K., Hettiarachchi, G. M., & Parameswaran, P. (2022). *Tailored Recovery of Ammonia and Phosphorus from Anaerobic Membrane Bioreactor (ANMBR) Treated Swine Permeate for Use as Targeted High-Quality Fertilizer.* Paper presented at the WEF Residuals and Biosolids Conference, Columbus, Ohio.

Daneshgar, S., Buttafava, A., Capsoni, D., Callegari, A., & Capodaglio, A. G. (2018). Impact of pH and Ionic Molar Ratios on Phosphorous Forms Precipitation and Recovery from Different Wastewater Sludges. *Resources, 7*(4), 71.

de Boer, M. A., Kabbe, C., & Slootweg, J. C. (2018). Comment on "Application of Struvite Alters the Antibiotic Resistome in Soil, Rhizosphere, and Phyllosphere". *Environmental science & technology*, *52*(24), 14564-14565. https://doi.org/10.1021/acs.est.8b03524

de Haas, D., Wentzel, MC, & Ekama, G. (2000). The use of simultaneous chemical precipitation in modified activated sludge systems exhibiting biological excess phosphate removal-Part 1: Literature review. *Water Sa, 26*(4), 439-452.

DELIN, S., STENBERG, B., NYBERG, A., & BROHEDE, L. (2012). Potential methods for estimating nitrogen fertilizer value of organic residues. Soil Use and Management, 28(3), 283-291. https://doi.org/https://doi.org/10.1111/j.1475-2743.2012.00417.x

Deng, Q., Dhar, B. R., Elbeshbishy, E., & Lee, H.-S. (2014). Ammonium nitrogen removal from the permeates of anaerobic membrane bioreactors: economic regeneration of exhausted zeolite. *Environmental technology, 35*(16), 2008-2017.

Deng, Q., Dhar, B. R., Elbeshbishy, E., & Lee, H.-S. (2014). Ammonium nitrogen removal from the permeates of anaerobic membrane bioreactors: economic regeneration of exhausted zeolite. *Environmental technology, 35*(16), 2008-2017.

Deng, Q., Elbeshbishy, E., & Lee, H.-S. (2016). Simultaneous regeneration of exhausted zeolite and nitrogen recovery using an air stripping method at alkaline pH. *Water Quality Research Journal of Canada, 51*(4), 321-330.

Desmidt, E., Ghyselbrecht, K., Zhang, Y., Pinoy, L., Van der Bruggen, B., Verstraete, W., Rabaey, K., & Meesschaert, B. (2015). Global phosphorus scarcity and full-scale P-recovery techniques: a review. *Critical Reviews in Environmental Science and Technology, 45*(4), 336-384.

Deutz, P. (2020). Circular Economy. In A. Kobayashi (Ed.), *International Encyclopedia of Human Geography (Second Edition)* (pp. 193-201). Elsevier. https://doi.org/https://doi.org/10.1016/B978-0-08-102295-5.10630-4

Devereux, R., He, S.-H., Doyle, C. e. a., Orkland, S., Stahl, D., LeGall, J., & Whitman, W. (1990). Diversity and origin of Desulfovibrio species: phylogenetic definition of a family. *Journal of Bacteriology, 172*(7), 3609-3619.

Doebelin, N., & Kleeberg, R. (2015). Profex: a graphical user interface for the Rietveld refinement program BGMN. *J Appl Crystallogr, 48*(Pt 5), 1573-1580.

Dong, D., Wang, C., Van Zwieten, L., Wang, H., Jiang, P., Zhou, M., & Wu, W. (2020). An effective biochar-based slow-release fertilizer for reducing nitrogen loss in paddy fields. Journal of Soils and Sediments, 20(8), 3027-3040.

Dong, L., Qi, Z., Li, M., Zhang, Y., Chen, Y., Qi, Y., & Wu, H. (2021). Organics and nutrient removal from swine wastewater by constructed wetlands using ceramsite and magnetite as substrates. *Journal of Environmental Chemical Engineering, 9*(1), 104739.

Dorozhkin, S. V. (2010a). Amorphous calcium (ortho)phosphates. *Acta Biomaterialia, 6*(12), 4457-4475.

Dorozhkin, S. V. (2010b). Amorphous calcium (ortho)phosphates. *Acta Biomater, 6*(12), 4457-4475.

Doyle, J. D., & Parsons, S. A. (2002). Struvite formation, control and recovery. *Water Research, 36*(16), 3925-3940.

Dubey, A., & Mailapalli, D. R. (2019). Zeolite coated urea fertilizer using different binders: Fabrication, material properties and nitrogen release studies. Environmental Technology & Innovation, 16, 100452.

Duhamel, S., Diaz, J. M., Adams, J. C., Djaoudi, K., Steck, V., & Waggoner, E. M. (2021). Phosphorus as an integral component of global marine biogeochemistry. *Nature Geoscience, 14*(6), 359-368.

Edgar, R. C. (2018). Updating the 97% identity threshold for 16S ribosomal RNA OTUs. *Bioinformatics, 34*(14), 2371-2375.

Eggers, E., Dirkzwager, A., & Van der Honing, H. (1991). Full-scale experiences with phosphate crystallization in a Crystalactor®. *Water Science and Technology, 23*(4-6), 819-824.

Egle, L., Rechberger, H., Krampe, J., & Zessner, M. (2016). Phosphorus recovery from municipal wastewater: An integrated comparative technological, environmental and economic assessment of P recovery technologies. *Science of The Total Environment*, *571*, 522-542.

Elyasi, S., Amani, T., & Dastyar, W. (2015). A Comprehensive Evaluation of Parameters Affecting Treating High-Strength Compost Leachate in Anaerobic Baffled Reactor Followed by Electrocoagulation-Flotation Process. *Water, Air, & Soil Pollution, 226*(4), 116.

Evans, P. J., Doody, A., Harclerode, M., Brower, A., Vila, P., Parameswaran, P., Lim, K., Bae, J., Shin, J., Lee, P. H., Tan, A., McCarty, P., Parker, W., Guy, K., Page, M., & Maga, S.

(2018). *Anaerobic Membrane Bioreactor for Sustainable Wastewater Treatment. Project ER-201434. Department of Defense Environmental Security Technology Program Final Report.* (ESTCP Project Number ER-201434). Retrieved from https://www.serdp-estcp.org/Program-Areas/Environmental-Restoration/Wastewater-and-Drinking-Water/ER-201434.

Evans, P. J., Doody, A., Harclerode, M., Brower, A., Vila, P., Parameswaran, P., Lim, K., Bae, J., Shin, J., Lee, P. H., Tan, A., McCarty, P., Parker, W., Guy, K., Page, M., & Maga, S. (2018). *Anaerobic Membrane Bioreactor for Sustainable Wastewater Treatment. Project ER-201434. Department of Defense Environmental Security Technology Program Final Report.* (ESTCP Project Number ER-201434). Retrieved from https://www.serdp-estcp.org/Program-Areas/Environmental-Restoration/Wastewater-and-Drinking-Water/ER-201434.

Evans, P. J., Doody, A., Harclerode, M., Brower, A., Vila, P., Parameswaran, P., Lim, K., Bae, J., Shin, J., Lee, P.-H., Tan, A., McCarty, P., Parker, W., Guy, K., Page, M., Maga, S. (2018). *Anaerobic Membrane Bioreactor for Sustainable Wastewater Treatment. Project ER-201434. Department of Defense Environmental Security Technology Program Final Report.* . Retrieved from https://www.serdp-estcp.org/Program-Areas/Environmental-Restoration/Wastewater-and-Drinking-Water/ER-201434.

Evans, P. J., Parameswaran, P., Lim, K., Bae, J., Shin, C., Ho, J., & McCarty, P. L. (2019). A comparative pilot-scale evaluation of gas-sparged and granular activated carbon-fluidized anaerobic membrane bioreactors for domestic wastewater treatment. *Bioresource Technology, 288*, 120949.

Farkaš, A., Rožić, M., & Barbarić-Mikočević, Ž. (2005). Ammonium exchange in leakage waters of waste dumps using natural zeolite from the Krapina region, Croatia. *Journal of hazardous materials, 117*(1), 25-33.

Feng, L., Chen, Y., & Zheng, X. (2009). Enhancement of Waste Activated Sludge Protein Conversion and Volatile Fatty Acids Accumulation during Waste Activated Sludge Anaerobic Fermentation by Carbohydrate Substrate Addition: The Effect of pH. *Environmental Science & Technology, 43*(12), 4373-4380.

Ferguson, R. M., Coulon, F., & Villa, R. (2016). Organic loading rate: A promising microbial management tool in anaerobic digestion. *Water Research, 100*, 348-356.

Fisher, J. C., Levican, A., Figueras, M. J., & McLellan, S. L. (2014). Population dynamics and ecology of Arcobacter in sewage. *Frontiers in microbiology, 5*, 525.

Ganrot, Z., Dave, G., Nilsson, E., & Li, B. (2007). Plant availability of nutrients recovered as solids from human urine tested in climate chamber on Triticum aestivum L. *Bioresource Technology, 98*(16), 3122-3129.

Gebremariam, S. Y., Beutel, M. W., Christian, D., & Hess, T. F. (2011). Research advances and challenges in the microbiology of enhanced biological phosphorus removal—a critical review. *Water Environment Research, 83*(3), 195-219.

Genethliou, C., Triantaphyllidou, I., Giannakis, D., Papayianni, M., Sygellou, L., Tekerlekopoulou, A., Koutsoukos, P., & Vayenas, D. (2021). Simultaneous removal of ammonium nitrogen, dissolved chemical oxygen demand and color from sanitary landfill leachate using natural zeolite. *Journal of hazardous materials, 406*, 124679.

Gharibi, H., Mahvi, A. H., Chehrazi, M., Sheikhi, R., & Hosseini, S. S. (2010). Phosphorous removal from wastewater effluent using electro-coagulation by aluminum and iron plates. *ANALYTICAL & BIOANALYTICAL ELECTROCHEMISTRY, 2*(3), 165-177.

Ghosh, S., Lobanov, S., & Lo, V. K. (2019). An overview of technologies to recover phosphorus as struvite from wastewater: advantages and shortcomings. *Environmental Science and Pollution Research*, *26*(19), 19063-19077. https://doi.org/10.1007/s11356-019-05378-6

Ghosh, S., Lobanov, S., & Lo, V. K. (2019). An overview of technologies to recover phosphorus as struvite from wastewater: advantages and shortcomings. *Environmental Science and Pollution Research, 26*(19), 19063-19077.

Giménez, J., Robles, A., Carretero, L., Durán, F., Ruano, M., Gatti, M. N., . . . Seco, A. (2011). Experimental study of the anaerobic urban wastewater treatment in a submerged hollow-fibre membrane bioreactor at pilot scale. *Bioresource Technology, 102*(19), 8799-8806.

Golroudbary, S. R., El Wali, M., & Kraslawski, A. (2019). Environmental sustainability of phosphorus recycling from wastewater, manure and solid wastes. *Sci Total Environ, 672*, 515-524.

Golroudbary, S. R., El Wali, M., & Kraslawski, A. (2019). Environmental sustainability of phosphorus recycling from wastewater, manure and solid wastes. *Sci Total Environ, 672*, 515-524.

Gouveia, J., Plaza, F., Garralon, G., Fdz-Polanco, F., & Peña, M. (2015). Long-term operation of a pilot scale anaerobic membrane bioreactor (AnMBR) for the treatment of municipal wastewater under psychrophilic conditions. *Bioresource Technology, 185*, 225-233.

Guaya, D., Mendoza, A., Valderrama, C., Farran, A., Sauras-Yera, T., & Cortina, J. L. (2020). Use of nutrient-enriched zeolite (NEZ) from urban wastewaters in amended soils: Evaluation of plant availability of mineral elements. Science of The Total Environment, 727, 138646.

Guo, J. (2016). Adsorption characteristics and mechanisms of high-levels of ammonium from swine wastewater using natural and MgO modified zeolites. *Desalination and Water Treatment, 57*(12), 5452-5463.

Guo, Y., & Li, Y.-Y. (2020). Hydroxyapatite crystallization-based phosphorus recovery coupling with the nitrogen removal through partial nitritation/anammox in a single reactor. *Water Research, 187*, 116444.

Guy, K. A., & Page, M. (2019). Ammonia sequestering system. In: Google Patents.

Hao, X.-D., Wang, C.-C., Lan, L., & Van Loosdrecht, M. (2008). Struvite formation, analytical methods and effects of pH and Ca2+. *Water Science and Technology, 58*(8), 1687-1692.

Harb, M., Xiong, Y., Guest, J., Amy, G., & Hong, P.-Y. (2015). Differences in microbial communities and performance between suspended and attached growth anaerobic membrane bioreactors treating synthetic municipal wastewater. *Environmental Science: Water Research & Technology, 1*(6), 800-813.

Haruna Ahmed, O., Husin, A., & Husni Mohd Hanif, A. (2008). Ammonia volatilization and ammonium accumulation from urea mixed with zeolite and triple superphosphate. Acta Agriculturae Scandinavica Section B-Soil and Plant Science, 58(2), 182-186.

Hasan, M. N., Altaf, M. M., Khan, N. A., Khan, A. H., Khan, A. A., Ahmed, S., Kumar, P. S., Naushad, M., Rajapaksha, A. U., Iqbal, J., Tirth, V., & Islam, S. (2021). Recent technologies for nutrient removal and recovery from wastewaters: A review. *Chemosphere, 277*, 130328.

He, Z. L., Calvert, D. V., Alva, A. K., Li, Y. C., & Banks, D. J. (2002). Clinoptilolite zeolite and cellulose amendments to reduce ammonia volatilization in a calcareous sandy soil. Plant and Soil, 247(2), 253-260.

He, Z., Calvert, D., Alva, A., Li, Y., & Banks, D. (2002). Clinoptilolite zeolite and cellulose amendments to reduce ammonia volatilization in a calcareous sandy soil. Plant and Soil, 247(2), 253-260.

Hedström, A., & Rastas Amofah, L. (2008). Adsorption and desorption of ammonium by clinoptilolite adsorbent in municipal wastewater treatment systems. *Journal of Environmental Engineering and Science, 7*(1), 53-61.

Heronemus, E., Gamage, K. H. H., Hettiarachchi, G. M., & Parameswaran, P. (2021). Efficient recovery of phosphorus and sulfur from Anaerobic Membrane Bioreactor (AnMBR) permeate using chemical addition of iron and evaluation of its nutrient availability for plant uptake. *Science of The Total Environment, 783*, 146850.

Heronemus, E., Gamage, K. H. H., Hettiarachchi, G. M., & Parameswaran, P. (in press). Efficient recovery of phosphorus and sulfur from Anaerobic Membrane Bioreactor (AnMBR) permeate using chemical addition of iron and evaluation of its nutrient availability for plant uptake. Science of the Total Environment.

Heronemus, E., Gamage, K. H. H., Hettiarachchi, G. M., & Parameswaran, P. (2021). Efficient recovery of phosphorus and sulfur from Anaerobic Membrane Bioreactor (AnMBR) permeate using chemical addition of iron and evaluation of its nutrient availability for plant uptake. *Science of The Total Environment, 783*, 146850.

Ho, J., & Sung, S. (2010). Methanogenic activities in anaerobic membrane bioreactors (AnMBR) treating synthetic municipal wastewater. *Bioresource Technology, 101*(7), 2191-2196.

Hofer, S. (2003). QuikChem Method 12-107-06-2-A: Determination of ammonia (salicylate) in 2 M KCl soil extracts by flow injection analysis. Lachat Instrum., Loveland, CO.

Hu, X., Tanaka, A., & Tanaka, R. (2013). Simple extraction methods that prevent the artifactual conversion of chlorophyll to chlorophyllide during pigment isolation from leaf samples. Plant Methods, 9(1), 19. https://doi.org/10.1186/1746-4811-9-19

Huang, H., Xiao, D., Pang, R., Han, C., & Ding, L. (2014). Simultaneous removal of nutrients from simulated swine wastewater by adsorption of modified zeolite combined with struvite crystallization. *Chemical Engineering Journal, 256*, 431-438.

Huang, H., Xiao, X., Yan, B., & Yang, L. (2010). Ammonium removal from aqueous solutions by using natural Chinese (Chende) zeolite as adsorbent. *Journal of Hazardous Materials, 175*(1-3), 247-252.

Huang, H., Xiao, X., Yan, B., & Yang, L. (2010). Ammonium removal from aqueous solutions by using natural Chinese (Chende) zeolite as adsorbent. *Journal of hazardous materials, 175*(1), 247-252.

Huang, H., Xu, C., & Zhang, W. (2011). Removal of nutrients from piggery wastewater using struvite precipitation and pyrogenation technology. *Bioresource Technology, 102*(3), 2523-2528.

Huang, H., Yang, L., Xue, Q., Liu, J., Hou, L., & Ding, L. (2015). Removal of ammonium from swine wastewater by zeolite combined with chlorination for regeneration. *Journal of Environmental Management, 160*, 333-341.

Huang, H., Zhang, P., Zhang, Z., Liu, J., Xiao, J., & Gao, F. (2016). Simultaneous removal of ammonia nitrogen and recovery of phosphate from swine wastewater by struvite

electrochemical precipitation and recycling technology. *Journal of Cleaner Production, 127*, 302-310.

Hudson, N., Baker, A., & Reynolds, D. (2007). Fluorescence analysis of dissolved organic matter in natural, waste and polluted waters—a review. *River research and applications, 23*(6), 631-649.

Inaba, T., Aoyagi, T., Hori, T., Charfi, A., Suh, C., Lee, J., . . . Habe, H. (2019). Long-term acclimatization of sludge microbiome for treatment of high-strength organic solid waste in anaerobic membrane bioreactor. *Biochemical Engineering Journal*, 107461.

Ippersiel, D., Mondor, M., Lamarche, F., Tremblay, F., Dubreuil, J., & Masse, L. (2012). Nitrogen potential recovery and concentration of ammonia from swine manure using electrodialysis coupled with air stripping. *Journal of Environmental Management, 95*, S165-S169.

Ippolito, J. A., Tarkalson, D. D., & Lehrsch, G. A. (2011). Zeolite soil application method affects inorganic nitrogen, moisture, and corn growth. Soil Science, 176(3), 136-142.

İrdemez, Ş., Demircioğlu, N., Yıldız, Y. Ş., & Bingül, Z. (2006). The effects of current density and phosphate concentration on phosphate removal from wastewater by electrocoagulation using aluminum and iron plate electrodes. *Separation and Purification Technology, 52*(2), 218-223.

Jackson, B. E., Bhupathiraju, V. K., Tanner, R. S., Woese, C. R., & McInerney, M. J. (1999). Syntrophus aciditrophicus sp. nov., a new anaerobic bacterium that degrades fatty acids and benzoate in syntrophic association with hydrogen-using microorganisms. *Archives of microbiology, 171*(2), 107-114.

Jaffer, Y., Clark, T. A., Pearce, P., & Parsons, S. A. (2002). Potential phosphorus recovery by struvite formation. *Water Research, 36*(7), 1834-1842.

Jakkula, V., & Wani, S. (2018). Zeolites: Potential soil amendments for improving nutrient and water use efficiency and agriculture productivity. Scientific Reviews & Chemical Communications, 8(1), 1-15.

Jenkinson, D. S., & Powlson, D. S. (1976). The effects of biocidal treatments on metabolism in soil—V: A method for measuring soil biomass. Soil biology and Biochemistry, 8(3), 209-213.

Jordaan, E., Ackerman, J., & Cicek, N. (2010). Phosphorus removal from anaerobically digested swine wastewater through struvite precipitation. *Water Science and Technology, 61*(12), 3228-3234.

Jupp, A. R., Beijer, S., Narain, G. C., Schipper, W., & Slootweg, J. C. (2021). Phosphorus recovery and recycling–closing the loop. *Chemical Society Reviews, 50*(1), 87-101.

Kannan, A. D., & Parameswaran, P. (2021). Ammonia adsorption and recovery from swine wastewater permeate using naturally occurring clinoptilolite. *Journal of Water Process Engineering, 43*, 102234.

Kehrein, P., van Loosdrecht, M., Osseweijer, P., Garfí, M., Dewulf, J., & Posada, J. (2020). A critical review of resource recovery from municipal wastewater treatment plants – market supply potentials, technologies and bottlenecks. *Environmental Science: Water Research & Technology, 6*(4), 877-910.

Kemacheevakul, P., Chuangchote, S., Otani, S., Matsuda, T., & Shimizu, Y. (2015). Effect of magnesium dose on amount of pharmaceuticals in struvite recovered from urine. *Water Sci Technol, 72*(7), 1102-1110.

Kim, J., Kim, K., Ye, H., Lee, E., Shin, C., McCarty, P. L., & Bae, J. (2011). Anaerobic fluidized bed membrane bioreactor for wastewater treatment. *Environmental Science & Technology, 45*(2), 576-581.

Kizito, S., Luo, H., Lu, J., Bah, H., Dong, R., & Wu, S. (2019). Role of nutrient-enriched biochar as a soil amendment during maize growth: exploring practical alternatives to recycle agricultural residuals and to reduce chemical fertilizer demand. *Sustainability, 11*(11), 3211.

Knepel, K. (2003). Determination of nitrate in 2M KCl soil extracts by flow injection analysis. QuikChem method, 12, 107-104.

Kocatürk-Schumacher, N. P., Zwart, K., Bruun, S., Stoumann Jensen, L., Sørensen, H., & Brussaard, L. (2019). Recovery of nutrients from the liquid fraction of digestate: Use of enriched zeolite and biochar as nitrogen fertilizers. *Journal of Plant Nutrition and Soil Science, 182*(2), 187-195.

Kogler, A., Farmer, M., Simon, J. A., Tilmans, S., Wells, G. F., & Tarpeh, W. A. (2021). Systematic Evaluation of Emerging Wastewater Nutrient Removal and Recovery Technologies to Inform Practice and Advance Resource Efficiency. *ACS ES&T Engineering, 1*(4), 662-684.

Koon, J. ufman W J. Ammonia removal from municipal wastewaters by ion exchange. *Journal Water Pollution Control Federation, l, 975*, 448-465.

Kotoulas, A., Agathou, D., Triantaphyllidou, I. E., Tatoulis, T. I., Akratos, C. S., Tekerlekopoulou, A. G., & Vayenas, D. V. (2019). Zeolite as a potential medium for ammonium recovery and second cheese whey treatment. *Water, 11*(1), 136.

Kumar, R., & Pal, P. (2015). Assessing the feasibility of N and P recovery by struvite precipitation from nutrient-rich wastewater: a review. *Environmental Science and Pollution Research, 22*(22), 17453-17464.

Kunacheva, C., & Stuckey, D. C. (2014). Analytical methods for soluble microbial products (SMP) and extracellular polymers (ECP) in wastewater treatment systems: A review. *Water Research, 61*, 1-18.

Kuntke, P., Śmiech, K., Bruning, H., Zeeman, G., Saakes, M., Sleutels, T., Hamelers, H., & Buisman, C. (2012). Ammonium recovery and energy production from urine by a microbial fuel cell. *Water Research, 46*(8), 2627-2636.

Kurama, H., Zimmer, A., & Reschetilowski, W. (2002). Chemical modification effect on the sorption capacities of natural clinoptilolite. *Chemical engineering & technology, 25*(3), 301-305.

Le, V.-G., Vo, D.-V. N., Nguyen, N.-H., Shih, Y.-J., Vu, C.-T., Liao, C.-H., & Huang, Y.-H. (2021). Struvite recovery from swine wastewater using fluidized-bed homogeneous granulation process. *Journal of Environmental Chemical Engineering, 9*(3), 105019.

Lee, S.-H., Kang, H.-J., & Park, H.-D. (2015). Influence of influent wastewater communities on temporal variation of activated sludge communities. *Water Research, 73*, 132-144.

Lei, L., Li, X., & Zhang, X. (2008). Ammonium removal from aqueous solutions using microwave-treated natural Chinese zeolite. *Separation and Purification Technology, 58*(3), 359-366.

Lei, X., Sugiura, N., Feng, C., & Maekawa, T. (2007). Pretreatment of anaerobic digestion effluent with ammonia stripping and biogas purification. *Journal of Hazardous Materials, 145*(3), 391-397.

Lei, Y., Song, B., Saakes, M., van der Weijden, R. D., & Buisman, C. J. (2018). Interaction of calcium, phosphorus and natural organic matter in electrochemical recovery of phosphate. *Water Research, 142*, 10-17.

Lens, P., Visser, A., Janssen, A., Pol, L. H., & Lettinga, G. (1998). Biotechnological treatment of sulfate-rich wastewaters. *Critical Reviews in Environmental Science and Technology, 28*(1), 41-88.

Letunic, I., & Bork, P. (2019). Interactive Tree Of Life (iTOL) v4: recent updates and new developments. *Nucleic acids research*.

Lew, B., Tarre, S., Beliavski, M., Dosoretz, C., & Green, M. (2009). Anaerobic membrane bioreactor (AnMBR) for domestic wastewater treatment. *Desalination, 243*(1-3), 251-257.

Li, J., Wee, C., & Sohn, B. (2013). Effect of Ammonium- and Potassium-Loaded Zeolite on Kale (<i>Brassica alboglabra</i>) Growth and Soil Property. American Journal of Plant Sciences, Vol.04No.10, 7, Article 37668. https://doi.org/10.4236/ajps.2013.410245

Li, J., Wee, C., & Sohn, B. (2013). Effect of ammonium-and potassium-loaded zeolite on kale (Brassica alboglabra) growth and soil property. *American Journal of Plant Sciences, 4*(10), 1976.

Li, X., Xu, Y., Shen, S., Guo, T., Dai, H., & Lu, X. (2022). Effects of dissolved organic matter on phosphorus recovery via hydroxyapatite crystallization: New insights based on induction time. *Sci Total Environ, 822*, 153618.

Li, Y., Bai, P., Yan, Y., Yan, W., Shi, W., & Xu, R. (2019). Removal of Zn2+, Pb2+, Cd2+, and Cu2+ from aqueous solution by synthetic clinoptilolite. *Microporous and Mesoporous Materials, 273*, 203-211.

Li, Z., Zhang, Y., & Li, Y. (2013). Zeolite as slow release fertilizer on spinach yields and quality in a greenhouse test. *Journal of plant nutrition, 36*(10), 1496-1505.

Liao, B.-Q., Kraemer, J. T., & Bagley, D. M. (2006). Anaerobic membrane bioreactors: applications and research directions. *Critical Reviews in Environmental Science and Technology, 36*(6), 489-530.

Lim, K. (2021). *Anaerobic membrane bioreactors for domestic wastewater treatment: Treatment performance and fouling characterization.* Kansas State University,

Lim, K., Evans, P. J., & Parameswaran, P. (2019). Long-term performance of a pilot-scale gas-sparged anaerobic membrane bioreactor under ambient temperatures for holistic wastewater treatment. *Environmental Science & Technology, 53*(13), 7347-7354.

Lim, K., Evans, P. J., & Parameswaran, P. (2019). Long-Term Performance of a Pilot-Scale Gas-Sparged Anaerobic Membrane Bioreactor under Ambient Temperatures for Holistic Wastewater Treatment. *Environmental science & technology, 53*(13), 7347-7354.

Lim, K., Evans, P., & Parameswaran, P. (2019). Long-term performance of a pilot-scale gas-sparged anaerobic membrane bioreactor under ambient temperatures for holistic wastewater treatment. *Environmental Science & Technology*.

Lin, L., Wan, C., Lee, D.-J., Lei, Z., & Liu, X. (2014). Ammonium assists orthophosphate removal from high-strength wastewaters by natural zeolite. Separation and Purification Technology, 133, 351-356.

Liu, X.-c., ZHANG, Y., Min, Y., WANG, Z.-y., & LV, W.-z. (2007). Analysis of bacterial community structures in two sewage treatment plants with different sludge properties and treatment performance by nested PCR-DGGE method. *Journal of Environmental Sciences, 19*(1), 60-66.

Liu, X., Wen, G., Hu, Z., & Wang, J. (2018). Coupling effects of pH and Mg/P ratio on P recovery from anaerobic digester supernatant by struvite formation. *Journal of Cleaner Production, 198*, 633-641.

Liu, Y., Kwag, J.-H., Kim, J.-H., & Ra, C. (2011). Recovery of nitrogen and phosphorus by struvite crystallization from swine wastewater. *Desalination, 277*(1-3), 364-369.

Ma, H., Guo, Y., Qin, Y., & Li, Y.-Y. (2018). Nutrient recovery technologies integrated with energy recovery by waste biomass anaerobic digestion. *Bioresource Technology, 269*, 520-531.

Margeta, K., Logar, N. Z., Šiljeg, M., & Farkaš, A. (2013). Natural zeolites in water treatment– how effective is their use. *Water treatment, 5*, 81-112.

Martinez, J., Dabert, P., Barrington, S., & Burton, C. (2009). Livestock waste treatment systems for environmental quality, food safety, and sustainability. *Bioresource Technology, 100*(22), 5527-5536.

Martins, T. H., Souza, T. S. O., & Foresti, E. (2017). Ammonium removal from landfill leachate by Clinoptilolite adsorption followed by bioregeneration. *Journal of Environmental Chemical Engineering, 5*(1), 63-68.

Maurer, M., Schwegler, P., & Larsen, T. (2003). Nutrients in urine: energetic aspects of removal and recovery. *Water Science and Technology, 48*(1), 37-46.

McCarty, P. L., Bae, J., & Kim, J. (2011). Domestic wastewater treatment as a net energy producer–can this be achieved? In: ACS Publications.

McInerney, M. J., Rohlin, L., Mouttaki, H., Kim, U., Krupp, R. S., Rios-Hernandez, L., . . . Campbell, J. W. (2007). The genome of Syntrophus aciditrophicus: life at the

thermodynamic limit of microbial growth. *Proceedings of the National Academy of Sciences, 104*(18), 7600-7605.

McLellan, S., Huse, S. M., Mueller-Spitz, S., Andreishcheva, E., & Sogin, M. (2010). Diversity and population structure of sewage-derived microorganisms in wastewater treatment plant influent. *Environmental Microbiology, 12*(2), 378-392.

Melia, P. M., Cundy, A. B., Sohi, S. P., Hooda, P. S., & Busquets, R. (2017). Trends in the recovery of phosphorus in bioavailable forms from wastewater. *Chemosphere, 186*, 381-395.

Metcalf, L., Eddy, H. P., & Tchobanoglous, G. (1991). *Wastewater engineering: treatment, disposal, and reuse* (Vol. 4): McGraw-Hill New York.

Mihok, F., Macko, J., Oriňak, A., Oriňaková, R., Kovaľ, K., Sisáková, K., Petruš, O., & Kostecká, Z. (2020). Controlled nitrogen release fertilizer based on zeolite clinoptilolite: Study of preparation process and release properties using molecular dynamics. Current Research in Green and Sustainable Chemistry, 3, 100030.

Milan, Z., Sanchez, E., Weiland, P., de Las Pozas, C., Borja, R., Mayari, R., & Rovirosa, N. (1997). Ammonia removal from anaerobically treated piggery manure by ion exchange in columns packed with homoionic zeolite. *Chemical Engineering Journal, 66*(1), 65-71.

Milan, Z., Sánchez, E., Weiland, P., de Las Pozas, C., Borja, R., Mayari, R., & Rovirosa, N. (1997). Ammonia removal from anaerobically treated piggery manure by ion exchange in columns packed with homoionic zeolite. *Chemical Engineering Journal, 66*(1), 65-71.

Min, B., Kim, J., Oh, S., Regan, J. M., & Logan, B. E. (2005). Electricity generation from swine wastewater using microbial fuel cells. *Water Research, 39*(20), 4961-4968.

Monballiu, A., Ghyselbrecht, K., Crabeels, X., & Meesschaert, B. (2019). Calcium phosphate precipitation in nitrified wastewater from the potato-processing industry. *Environ Technol, 40*(17), 2250-2266.

Monballiu, A., Ghyselbrecht, K., Pinoy, L., & Meesschaert, B. (2020). Phosphorus reclamation by end-of-pipe recovery as calcium phosphate from effluent of wastewater treatment plants of agroindustry. *Journal of Environmental Chemical Engineering, 8*(5), 104280.

Mondor, M., Masse, L., Ippersiel, D., Lamarche, F., & Massé, D. I. (2008). Use of electrodialysis and reverse osmosis for the recovery and concentration of ammonia from swine manure. *Bioresource Technology, 99*(15), 7363-7368.

Montégut, G., Michelin, L., Brendlé, J., Lebeau, B., & Patarin, J. (2016). Ammonium and potassium removal from swine liquid manure using clinoptilolite, chabazite and faujasite zeolites. *Journal of Environmental Management, 167*, 147-155.

Mulder, A. (2003). The quest for sustainable nitrogen removal technologies. *Water Science and Technology, 48*(1), 67-75.

Mullen, P., Venkiteshwaran, K., Zitomer, D. H., & Mayer, B. K. (2019). Ion exchange nutrient recovery from anaerobic membrane bioreactor permeate. *Water Environment Research, 91*(7), 606-615.

Muller, M., Yelden, T., & Schoonover, H. (2007). Food versus fuel in the United States: can both win in the era of ethanol? *Institute for Agriculture and Trade Policy (IATP) Environment and Agriculture Program. Minneapolis, MN*.

Narihiro, T., Nobu, M. K., Kim, N. K., Kamagata, Y., & Liu, W. T. (2015). The nexus of syntrophy-associated microbiota in anaerobic digestion revealed by long-term enrichment and community survey. *Environmental Microbiology, 17*(5), 1707-1720.

Naz, M. Y., & Sulaiman, S. A. (2016). Slow release coating remedy for nitrogen loss from conventional urea: a review. Journal of Controlled Release, 225, 109-120.

Nelson, M. C., Morrison, M., & Yu, Z. (2011). A meta-analysis of the microbial diversity observed in anaerobic digesters. *Bioresource Technology, 102*(4), 3730-3739.

Nelson, N. O., Mikkelsen, R. L., & Hesterberg, D. L. (2003). Struvite precipitation in anaerobic swine lagoon liquid: effect of pH and Mg:P ratio and determination of rate constant. *Bioresource Technology, 89*(3), 229-236.

Nobu, M. K., Narihiro, T., Kuroda, K., Mei, R., & Liu, W.-T. (2016). Chasing the elusive Euryarchaeota class WSA2: genomes reveal a uniquely fastidious methyl-reducing methanogen. *The ISME journal, 10*(10), 2478.

Omwene, P. I., Kobya, M., & Can, O. T. (2018). Phosphorus removal from domestic wastewater in electrocoagulation reactor using aluminium and iron plate hybrid anodes. *Ecological Engineering, 123*, 65-73.

Ong, Y. H., Chua, A. S. M., Fukushima, T., Ngoh, G. C., Shoji, T., & Michinaka, A. (2014). High-temperature EBPR process: The performance, analysis of PAOs and GAOs and the fine-scale population study of Candidatus "Accumulibacter phosphatis". *Water Research, 64*, 102-112.

Oren, A. (2014). The family Methanospirillaceae. *The Prokaryotes: Other Major Lineages of Bacteria and the Archaea*, 283-290.

Palazzo, B., Walsh, D., Iafisco, M., Foresti, E., Bertinetti, L., Martra, G., Bianchi, C. L., Cappelletti, G., & Roveri, N. (2009). Amino acid synergetic effect on structure, morphology and surface properties of biomimetic apatite nanocrystals. *Acta Biomaterialia, 5*(4), 1241-1252.

Park, M., Kim, J. S., Choi, C. L., Kim, J.-E., Heo, N. H., Komarneni, S., & Choi, J. (2005). Characteristics of nitrogen release from synthetic zeolite Na-P1 occluding NH4NO3. Journal of Controlled Release, 106(1-2), 44-50.

Parsons, S., & Doyle, J. (2004). Struvite scale formation and control. *Water Science and Technology, 49*(2), 177-182.

Perera, M. K., Englehardt, J. D., & Dvorak, A. C. (2019). Technologies for recovering nutrients from wastewater: A critical review. *Environmental Engineering Science, 36*(5), 511-529.

Perrin, T. S., Boettinger, J. L., Drost, D. T., & Norton, J. M. (1998). Decreasing Nitrogen Leaching from Sandy Soil with Ammonium-Loaded Clinoptilolite. Journal of Environmental Quality, 27(3), 656-663. https://doi.org/https://doi.org/10.2134/jeq1998.00472425002700030024x

Perrin, T. S., Drost, D. T., Boettinger, J. L., & Norton, J. M. (1998). Ammonium-loaded clinoptilolite: a slow-release nitrogen fertilizer for sweet corn. Journal of plant nutrition, 21(3), 515-530.

Petzet, S., & Cornel, P. (2012). Prevention of Struvite Scaling in Digesters Combined With Phosphorus Removal and Recovery—The FIX-Phos Process. *Water Environment Research, 84*(3), 220-226.

Pierzynski, J., & Hettiarachchi, G. M. (2018). Reactions of phosphorus fertilizers with and without a fertilizer enhancer in three acidic soils with high phosphorus-fixing capacity. *Soil Science Society of America Journal, 82*(5), 1124-1139.

Ping, Q., Li, Y., Wu, X., Yang, L., & Wang, L. (2016). Characterization of morphology and component of struvite pellets crystallized from sludge dewatering liquor: Effects of total

suspended solid and phosphate concentrations. *Journal of Hazardous Materials, 310*, 261-269.

Plugge, C. M., Zhang, W., Scholten, J., & Stams, A. J. (2011). Metabolic flexibility of sulfate-reducing bacteria. *Frontiers in microbiology, 2*, 81.

Praveckova, M., Brennerova, M. V., Holliger, C., De Alencastro, F., & Rossi, P. (2016). Indirect evidence link PCB dehalogenation with Geobacteraceae in anaerobic sediment-free microcosms. *Frontiers in microbiology, 7*, 933.

Pretel, R., Shoener, B. D., Ferrer, J., & Guest, J. S. (2015). Navigating environmental, economic, and technological trade-offs in the design and operation of submerged anaerobic membrane bioreactors (AnMBRs). *Water Research, 87*, 531-541.

Prieto, A. L., Futselaar, H., Lens, P. N. L., Bair, R., & Yeh, D. H. (2013). Development and start up of a gas-lift anaerobic membrane bioreactor (Gl-AnMBR) for conversion of sewage to energy, water and nutrients. *Journal of Membrane Science, 441*, 158-167.

Prot, T., Wijdeveld, W., Eshun, L. E., Dugulan, A. I., Goubitz, K., Korving, L., & Van Loosdrecht, M. C. M. (2020). Full-scale increased iron dosage to stimulate the formation of vivianite and its recovery from digested sewage sludge. *Water Research, 182*, 115911.

Qiu, M., Singh, A., Wang, D., Qu, J., Swihart, M., Zhang, H., & Prasad, P. N. (2019). Biocompatible and biodegradable inorganic nanostructures for nanomedicine: Silicon and black phosphorus. *Nano Today, 25*, 135-155.

Rabinovich, A., Rouff, A. A., Lew, B., & Ramlogan, M. V. (2018). Aerated fluidized bed treatment for phosphate recovery from dairy and swine wastewater. *ACS Sustainable Chemistry & Engineering, 6*(1), 652-659.

Razon, L. F. (2014). Life cycle analysis of an alternative to the haber-bosch process: Non-renewable energy usage and global warming potential of liquid ammonia from cyanobacteria. *Environmental Progress & Sustainable Energy, 33*(2), 618-624.

Rech, I., Withers, P. J., Jones, D. L., & Pavinato, P. S. (2018). Solubility, diffusion and crop uptake of phosphorus in three different struvites. *Sustainability, 11*(1), 134.

Regueiro, L., Veiga, P., Figueroa, M., Alonso-Gutierrez, J., Stams, A. J., Lema, J. M., & Carballa, M. (2012). Relationship between microbial activity and microbial community structure in six full-scale anaerobic digesters. *Microbiological research, 167*(10), 581-589.

Riviere, D., Desvignes, V., Pelletier, E., Chaussonnerie, S., Guermazi, S., Weissenbach, J., . . . Sghir, A. (2009). Towards the definition of a core of microorganisms involved in anaerobic digestion of sludge. *The ISME journal, 3*(6), 700.

Ronteltap, M., Maurer, M., & Gujer, W. (2007). The behaviour of pharmaceuticals and heavy metals during struvite precipitation in urine. *Water Research, 41*(9), 1859-1868.

Rotaru, A.-E., Shrestha, P. M., Liu, F., Shrestha, M., Shrestha, D., Embree, M., . . . Lovley, D. R. (2014). A new model for electron flow during anaerobic digestion: direct interspecies electron transfer to Methanosaeta for the reduction of carbon dioxide to methane. *Energy & Environmental Science, 7*(1), 408-415.

Ryu, H.-D., & Lee, S.-I. (2016). Struvite recovery from swine wastewater and its assessment as a fertilizer. *Environmental Engineering Research, 21*(1), 29-35.

Saliu, T., & Oladoja, N. (2021). Nutrient recovery from wastewater and reuse in agriculture: a review. *Environmental Chemistry Letters*, 1-18.

Sampat, A. M., Martín-Hernández, E., Martín, M., & Zavala, V. M. (2018). Technologies and logistics for phosphorus recovery from livestock waste. *Clean Technologies and Environmental Policy, 20*(7), 1563-1579.

Seib, M., Berg, K., & Zitomer, D. (2016a). Influent wastewater microbiota and temperature influence anaerobic membrane bioreactor microbial community. *Bioresource Technology, 216*, 446-452.

Seib, M., Berg, K., & Zitomer, D. (2016b). Low energy anaerobic membrane bioreactor for municipal wastewater treatment. *Journal of Membrane Science, 514*, 450-457.

Seiple, T. E., Coleman, A. M., & Skaggs, R. L. (2017). Municipal wastewater sludge as a sustainable bioresource in the United States. *Journal of Environmental Management, 197*, 673-680.

Sengupta, S., Nawaz, T., & Beaudry, J. (2015). Nitrogen and Phosphorus Recovery from Wastewater. *Current Pollution Reports, 1*(3), 155-166.

Seo, H., Cho, K., Shin, J., Lee, M., Park, J., Lee, B. C., & Song, K. G. (2019). Linking process performances and core microbial community structures in anaerobic membrane bioreactor with rotary disk (ARMBR) system fed with high-strength food waste recycling wastewater. *Bioresource Technology, 291*, 121918.

Shih, K., & Yan, H. (2016). Chapter 26 - The Crystallization of Struvite and Its Analog (K-Struvite) From Waste Streams for Nutrient Recycling. In M. N. V. Prasad & K. Shih (Eds.), *Environmental Materials and Waste* (pp. 665-686): Academic Press.

Smith, A. L., Skerlos, S. J., & Raskin, L. (2013). Psychrophilic anaerobic membrane bioreactor treatment of domestic wastewater. *Water Research, 47*(4), 1655-1665.

Smith, A. L., Stadler, L. B., Love, N. G., Skerlos, S. J., & Raskin, L. (2012). Perspectives on anaerobic membrane bioreactor treatment of domestic wastewater: A critical review. *Bioresource Technology, 122*, 149-159.

Smith, A., Skerlos, S., & Raskin, L. (2015). Anaerobic membrane bioreactor treatment of domestic wastewater at psychrophilic temperatures ranging from 15 C to 3 C. *Environmental Science: Water Research & Technology, 1*(1), 56-64.

Song, Y., Hahn, H. H., & Hoffmann, E. (2002). The effect of carbonate on the precipitation of calcium phosphate. *Environ Technol, 23*(2), 207-215.

Sorathiya, L. M., Fulsoundar, A. B., Tyagi, K. K., Patel, M. D., & Singh, R. R. (2014). Eco-friendly and modern methods of livestock waste recycling for enhancing farm profitability. *International Journal of Recycling of Organic Waste in Agriculture, 3*(1), 50.

Sousa, D. Z., Smidt, H., Alves, M. M., & Stams, A. J. (2009). Ecophysiology of syntrophic communities that degrade saturated and unsaturated long-chain fatty acids. *FEMS microbiology ecology, 68*(3), 257-272.

Souza, I. M. S., Gurgel, G. C. S., Medeiros, A. M., Zonta, E., Ruiz, J. A. C., Paskocimas, C. A., Motta, F. V., & Bomio, M. R. D. (2018). The use of clinoptilolite as carrier of nitrogened fertilizer with controlled release. Journal of Environmental Chemical Engineering, 6(4), 4171-4177.

Sparks, D. L., Page, A., Helmke, P., & Loeppert, R. H. (2020). Methods of soil analysis, part 3: Chemical methods (Vol. 14): John Wiley & Sons.

Stolzenburg, P., Capdevielle, A., Teychené, S., & Biscans, B. (2015). Struvite precipitation with MgO as a precursor: Application to wastewater treatment. *Chemical Engineering Science, 133*, 9-15.

Stuart, P. (2006). The advantages and disadvantages of anaerobic digestion as a renewable energy source. *Loughborough University*.

Sullivan, D. M., LaHue, D. G., Dari, B., Bary, A. I., & Cogger, C. G. (2018). Worksheet for Calculating Biosolids Application Rates in Agriculture. Oregon State University.

Sun, Y., Xia, G., He, Z., Wu, Q., Zheng, J., Li, Y., Wang, Y., Chen, T., & Chi, D. (2019). Zeolite amendment coupled with alternate wetting and drying to reduce nitrogen loss and enhance rice production. Field Crops Research, 235, 95-103.

Szogi, A. A., Vanotti, M. B., & Shumaker, P. D. (2018). Economic recovery of calcium phosphates from swine lagoon sludge using Quick Wash process and geotextile filtration. *Frontiers in Sustainable Food Systems, 2*, 37.

Szymańska, M., Szara, E., Wąs, A., Sosulski, T., van Pruissen, G. W. P., & Cornelissen, R. L. (2019). Struvite—An Innovative Fertilizer from Anaerobic Digestate Produced in a Bio-Refinery. *Energies, 12*(2), 296.

Tabak, M., Lepiarczyk, A., Filipek-Mazur, B., & Lisowska, A. (2020). Efficiency of Nitrogen Fertilization of Winter Wheat Depending on Sulfur Fertilization. Agronomy, 10(9), 1304.

Takai, K., & Horikoshi, K. (2000). Rapid detection and quantification of members of the archaeal community by quantitative PCR using fluorogenic probes. *Appl. Environ. Microbiol., 66*(11), 5066-5072.

Tao, Q., Zhou, S., Luo, J., & Yuan, J. (2015). Nutrient removal and electricity production from wastewater using microbial fuel cell technique. *Desalination, 365*, 92-98.

Tavafoghi, M., & Cerruti, M. (2016). The role of amino acids in hydroxyapatite mineralization. *Journal of the Royal Society, Interface, 13*(123), 20160462.

Tervahauta, T., van der Weijden, R. D., Flemming, R. L., Hernández Leal, L., Zeeman, G., & Buisman, C. J. (2014). Calcium phosphate granulation in anaerobic treatment of black water: a new approach to phosphorus recovery. *Water Res, 48*, 632-642.

Tilman, D., Cassman, K. G., Matson, P. A., Naylor, R., & Polasky, S. (2002). Agricultural sustainability and intensive production practices. *Nature, 418*(6898), 671-677.

Tilman, D., Cassman, K. G., Matson, P. A., Naylor, R., & Polasky, S. (2002). Agricultural sustainability and intensive production practices. *Nature, 418*(6898), 671-677.

Valsami-Jones, E. (2001). Mineralogical controls on phosphorus recovery from wastewaters. *Mineralogical magazine, 65*(5), 611-620.

Van Der Houwen, J. A. M., & Valsami-Jones, E. (2001). The Application of Calcium Phosphate Precipitation Chemistry to Phosphorus Recovery: The Influence of Organic Ligands. *Environmental technology, 22*(11), 1325-1335.

van Haandel, A., De Vrieze, J., Verstraete, W., & dos Santos, V. S. (2014). Methanosaeta dominate acetoclastic methanogenesis during high-rate methane production in anaerobic reactors treating distillery wastewaters. *Journal of Chemical Technology & Biotechnology, 89*(11), 1751-1759.

Van Lier, J. B., Mahmoud, N., & Zeeman, G. (2008). Anaerobic wastewater treatment. *Biological wastewater treatment: principles, modelling and design*, 415-456.

Vandenberg, O., Dediste, A., Houf, K., Ibekwem, S., Souayah, H., Cadranel, S., . . . Vandamme, P. (2004). Arcobacter species in humans. *Emerging infectious diseases, 10*(10), 1863.

Vasenko, L., & Qu, H. (2017). Effect of NH4-N/P and Ca/P molar ratios on the reactive crystallization of calcium phosphates for phosphorus recovery from wastewater. *Journal of Crystal Growth, 459*, 61-66.

Vasenko, L., & Qu, H. (2019). Enhancing the recovery of calcium phosphates from wastewater treatment systems through hybrid process of oxidation and crystallization. *Journal of Environmental Chemical Engineering, 7*(1), 102828.

Vasudevan, S., Sozhan, G., Ravichandran, S., Jayaraj, J., Lakshmi, J., & Sheela, M. (2008). Studies on the removal of phosphate from drinking water by electrocoagulation process. *Industrial & engineering chemistry research, 47*(6), 2018-2023.

Viancelli, A., Kunz, A., Fongaro, G., Kich, J. D., Barardi, C. R. M., & Suzin, L. (2015). Pathogen Inactivation and the Chemical Removal of Phosphorus from Swine Wastewater. *Water, Air, & Soil Pollution, 226*(8), 263.

Vogel, T., Eichler-Löbermann, B., & Nelles, M. (2017). Phosphorus effects of recycled products from municipal wastewater on crops in a field experiment. *Plant, Soil and Environment, 63*(10), 475-482.

Wang, H., Kimberley, M. O., & Schlegelmilch, M. (2003). Biosolids-Derived Nitrogen Mineralization and Transformation in Forest Soils. Journal of Environmental Quality, 32(5), 1851-1856. https://doi.org/https://doi.org/10.2134/jeq2003.1851

Wang, S., & Peng, Y. (2010). Natural zeolites as effective adsorbents in water and wastewater treatment. *Chemical Engineering Journal, 156*(1), 11-24.

Wang, S., & Peng, Y. (2010). Natural zeolites as effective adsorbents in water and wastewater treatment. *Chemical Engineering Journal, 156*(1), 11-24.

Watanabe, Y., Yamada, H., Tanaka, J., & Moriyoshi, Y. (2005). Hydrothermal modification of natural zeolites to improve uptake of ammonium ions. *Journal of Chemical Technology & Biotechnology: International Research in Process, Environmental & Clean Technology, 80*(4), 376-380.

Watson, M. (1998). pH and lime requirement. Recommended chemical soil test procedures for the North Central Region.

Weatherley, L., & Miladinovic, N. (2004). Comparison of the ion exchange uptake of ammonium ion onto New Zealand clinoptilolite and mordenite. *Water Research, 38*(20), 4305-4312.

Weeks Jr, J. J., & Hettiarachchi, G. M. (2020). Source and formulation matter: New insights into phosphorus fertilizer fate and transport in mildly calcareous soils. *Soil Science Society of America Journal, 84*(3), 731-746.

Weeks Jr, J. J., & Hettiarachchi, G. M. (2020). Source and formulation matter: New insights into phosphorus fertilizer fate and transport in mildly calcareous soils. Soil Science Society of America Journal, 84(3), 731-746.

Wilkins, D., Lu, X.-Y., Shen, Z., Chen, J., & Lee, P. K. (2015). Pyrosequencing of mcrA and archaeal 16S rRNA genes reveals diversity and substrate preferences of methanogen communities in anaerobic digesters. *Appl. Environ. Microbiol., 81*(2), 604-613.

Wu, X., & Modin, O. (2013). Ammonium recovery from reject water combined with hydrogen production in a bioelectrochemical reactor. *Bioresource Technology, 146*, 530-536.

Xie, Z., Wang, Z., Wang, Q., Zhu, C., & Wu, Z. (2014). An anaerobic dynamic membrane bioreactor (AnDMBR) for landfill leachate treatment: performance and microbial community identification. *Bioresource Technology, 161*, 29-39.

Yamashita, T., Ishida, M., Asakawa, S., Kanamori, H., Sasaki, H., Ogino, A., . . . Yokoyama, H. (2016). Enhanced electrical power generation using flame-oxidized stainless steel anode in microbial fuel cells and the anodic community structure. *Biotechnology for biofuels, 9*(1), 62.

Yargeau, V. (2012). 17 - Water and wastewater treatment: chemical processes. In F. Zeman (Ed.), *Metropolitan Sustainability* (pp. 390-405): Woodhead Publishing.

Yetilmezsoy, K., & Sapci-Zengin, Z. (2009). Recovery of ammonium nitrogen from the effluent of UASB treating poultry manure wastewater by MAP precipitation as a slow release fertilizer. *Journal of Hazardous Materials, 166*(1), 260-269.

Yin, Q., Miao, J., Li, B., & Wu, G. (2017). Enhancing electron transfer by ferroferric oxide during the anaerobic treatment of synthetic wastewater with mixed organic carbon. *International Biodeterioration & Biodegradation, 119*, 104-110.

Zamorano-López, N., Borrás, L., Giménez, J. B., Seco, A., & Aguado, D. (2019). Acclimatised rumen culture for raw microalgae conversion into biogas: Linking microbial community structure and operational parameters in anaerobic membrane bioreactors (AnMBR). *Bioresource Technology, 290*, 121787.

Zang, G.-L., Sheng, G.-P., Li, W.-W., Tong, Z.-H., Zeng, R. J., Shi, C., & Yu, H.-Q. (2012). Nutrient removal and energy production in a urine treatment process using magnesium ammonium phosphate precipitation and a microbial fuel cell technique. *Physical Chemistry Chemical Physics, 14*(6), 1978-1984.

Zarcinas, B. A., McLaughlin, M. J., & Smart, M. K. (1996). The effect of acid digestion technique on the performance of nebulization systems used in inductively coupled plasma spectrometry. *Communications in Soil Science and Plant Analysis, 27*(5-8), 1331-1354.

Zebarth, B. J., Drury, C. F., Tremblay, N., & Cambouris, A. N. (2009). Opportunities for improved fertilizer nitrogen management in production of arable crops in eastern Canada: A review. Canadian Journal of Soil Science, 89(2), 113-132.

Zhalnina, K. V., Dias, R., Leonard, M. T., Dorr de Quadros, P., Camargo, F. A., Drew, J. C., Farmerie, W. G., Daroub, S. H., & Triplett, E. W. (2014). Genome sequence of Candidatus Nitrososphaera evergladensis from group I. 1b enriched from Everglades soil reveals novel genomic features of the ammonia-oxidizing archaea. PLos one, 9(7), e101648.

Zhang, F., Cui, Z., Fan, M., Zhang, W., Chen, X., & Jiang, R. (2011). Integrated soil–crop system management: reducing environmental risk while increasing crop productivity and improving nutrient use efficiency in China. *Journal of Environmental Quality*, *40*(4), 1051-1057.

Zhang, H., Banaszak, J. E., Parameswaran, P., Alder, J., Krajmalnik-Brown, R., & Rittmann, B. E. (2009). Focused-Pulsed sludge pre-treatment increases the bacterial diversity and relative abundance of acetoclastic methanogens in a full-scale anaerobic digester. *Water Research, 43*(18), 4517-4526.

Zhang, W., Zhou, Z., An, Y., Du, S., Ruan, D., Zhao, C., Ren, N., & Tian, X. (2017). Optimization for zeolite regeneration and nitrogen removal performance of a hypochlorite-chloride regenerant. *Chemosphere, 178*, 565-572.

Zhang, W., Zhou, Z., An, Y., Du, S., Ruan, D., Zhao, C., Ren, N., & Tian, X. (2017). Optimization for zeolite regeneration and nitrogen removal performance of a hypochlorite-chloride regenerant. *Chemosphere, 178*, 565-572.

Zhou, Z., Hu, D., Ren, W., Zhao, Y., Jiang, L.-M., & Wang, L. (2015). Effect of humic substances on phosphorus removal by struvite precipitation. *Chemosphere, 141*, 94-99.

Zinder, S. (1984). Microbiology of anaerobic conversion of organic wastes to methane: recent developments. *Am. Soc. Microbiol. News;(United States), 50*(7).
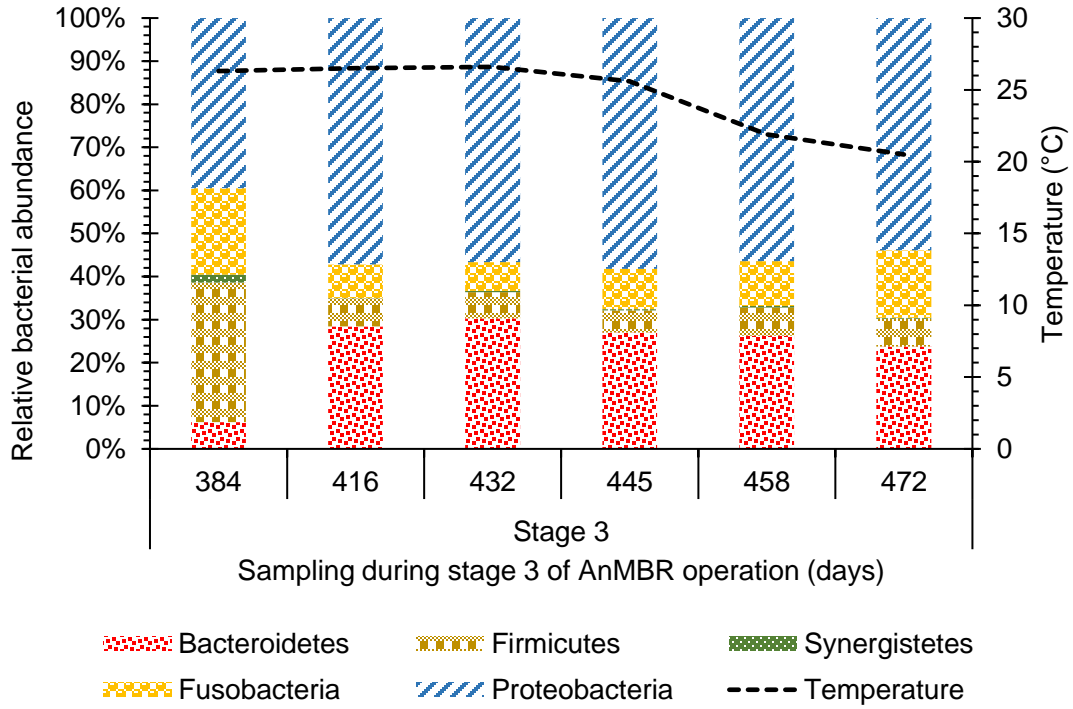
Appendix A

Appendix Table A1. Chemical composition of clinoptilolite as per the product information provided by the vendor

| Component	XRF Results %
SiO	67
Al_2O_3	10.7
CaO	1.52
MgO	0.47
Na_2O	2.55
K_2O	3.65
Fe_2O_3	0.96
MnO	0.03
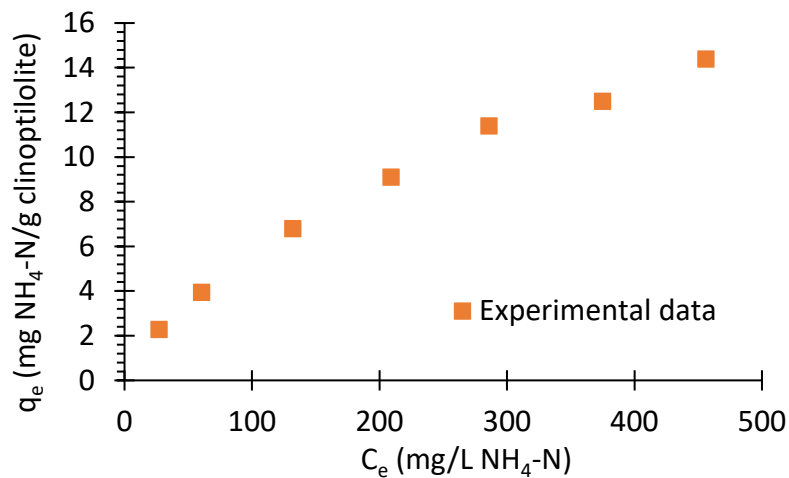
Appendix Figure A.1 Ammonia uptake data at an equilibrium concentration range of 27.2 - 456 mg/L NH_4-N in synthetic swine permeate solution only (The reported experimental data is the average of duplicate runs). The ammonia removal capacity in synthetic swine permeate was lower than DI water based NH_4Cl solution.
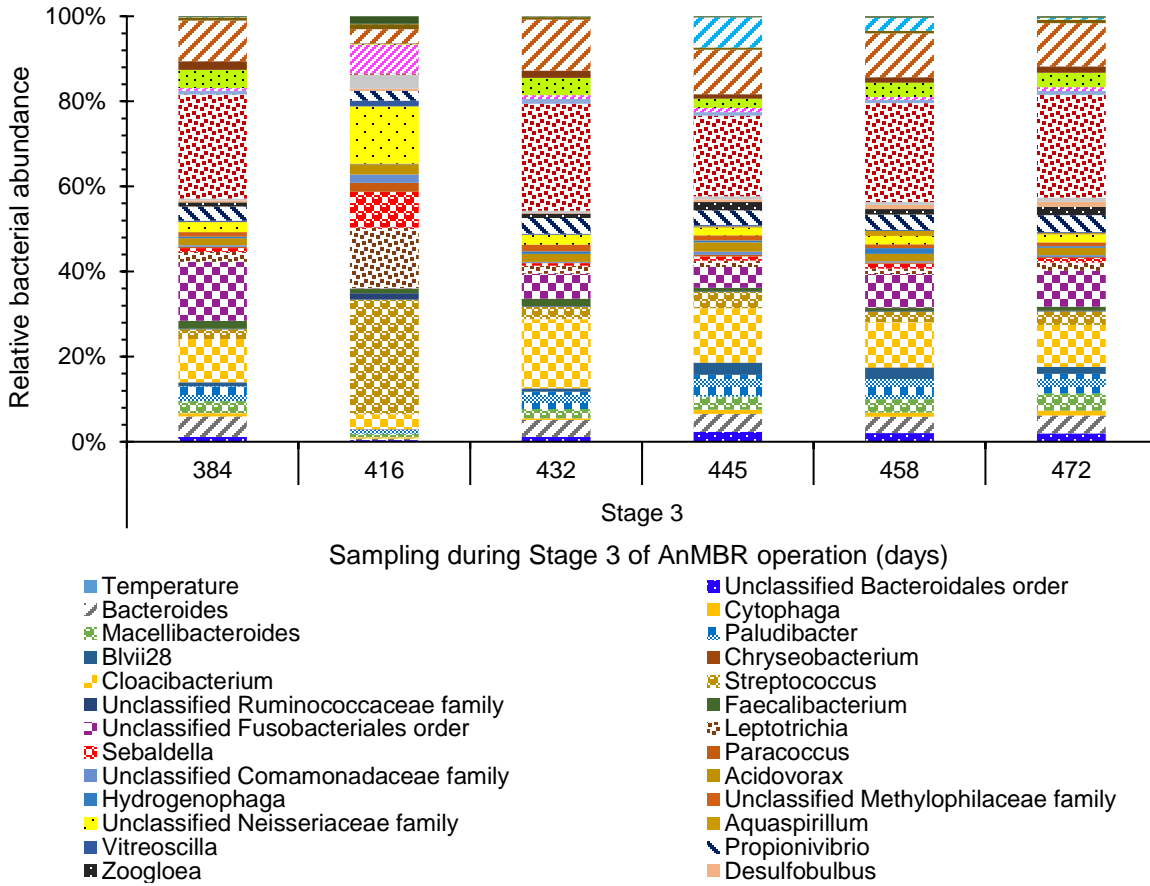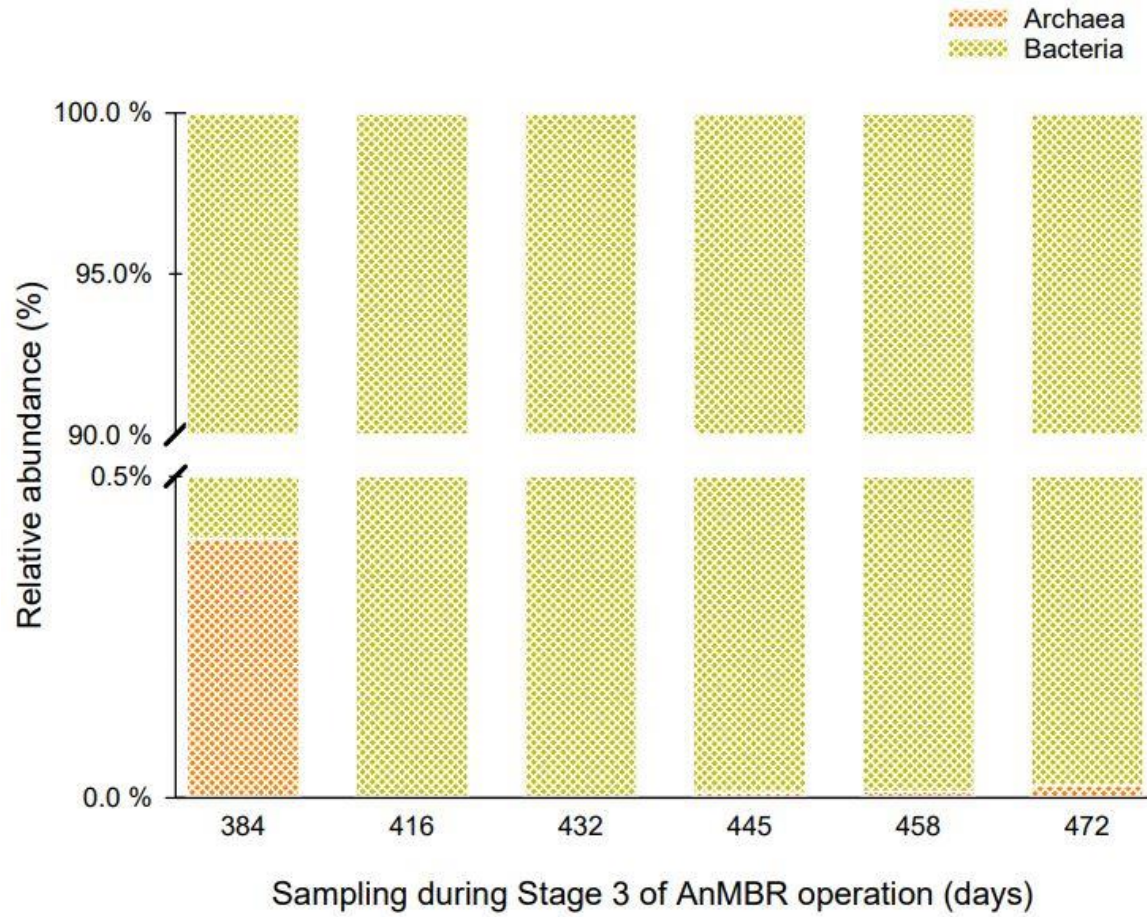
Appendix B

Appendix Figure B.1: Distribution of phylum level bacteria with ≥ 1% relative bacterial abundance in influent sample
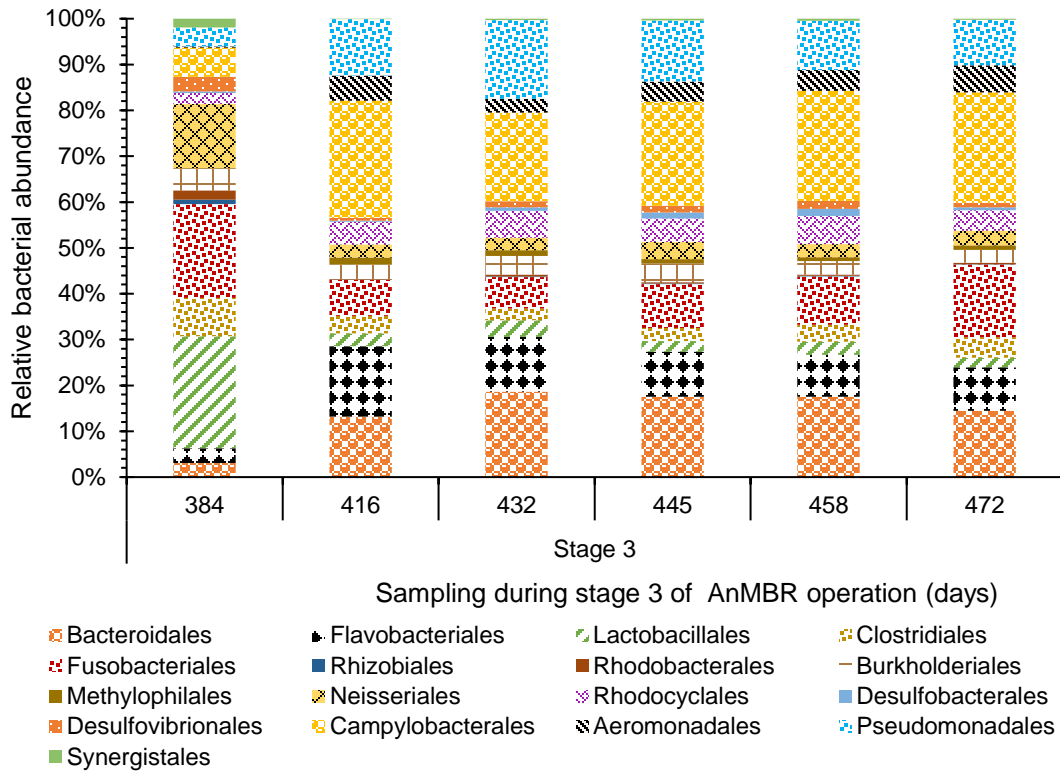
Appendix Figure B.2 Distribution of order level bacteria with ≥ 1% relative bacterial abundance in influent samples
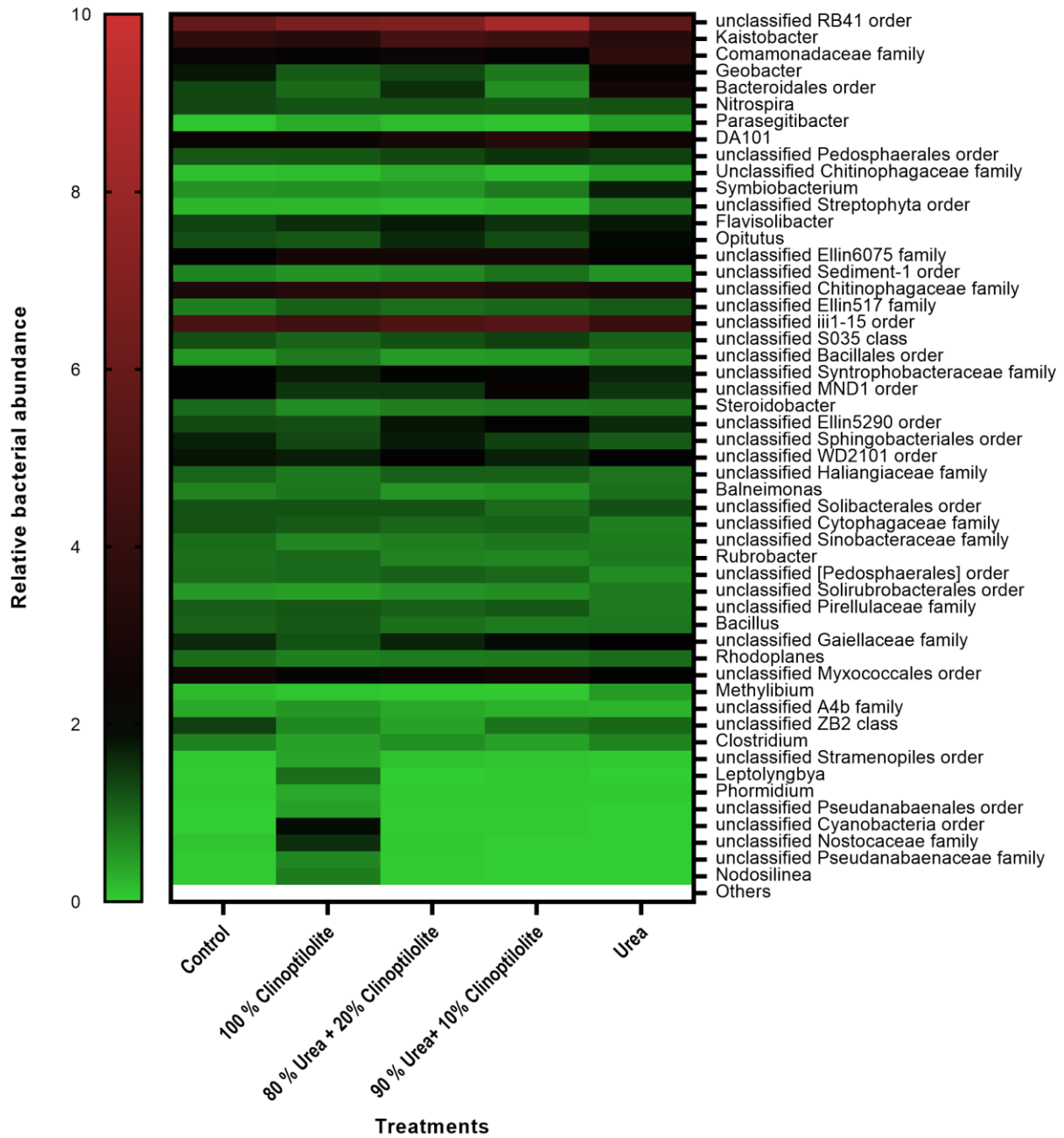
Appendix Figure B.3 Distribution of genus level bacteria with ≥ 1% relative bacterial abundance in influent samples
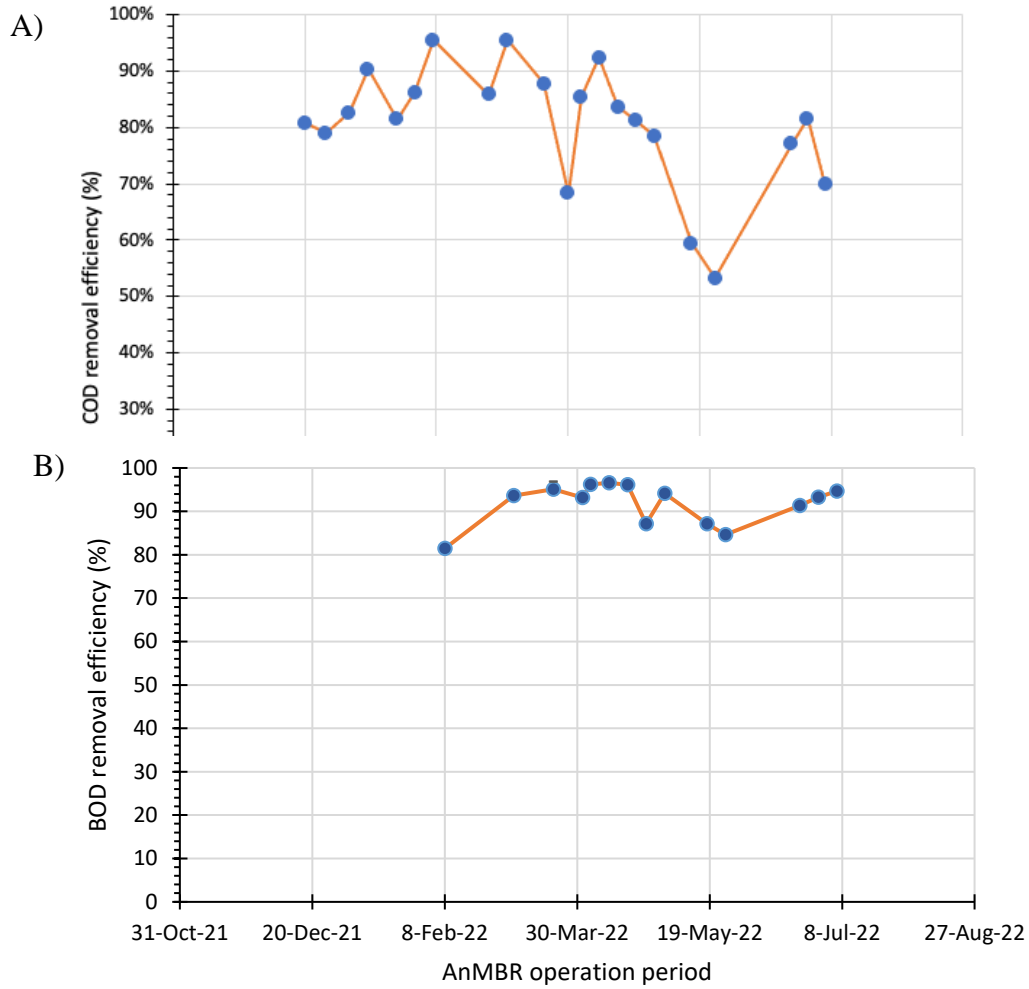
Appendix Figure B.4 Distribution of total relative abundance of archaea and bacteria in influent samples

Appendix C

Appendix Figure C.1 Genus level relative bacterial abundance in the different treatments. The mean value of three replicates for each treatment was used in the relative bacterial abundance calculation.
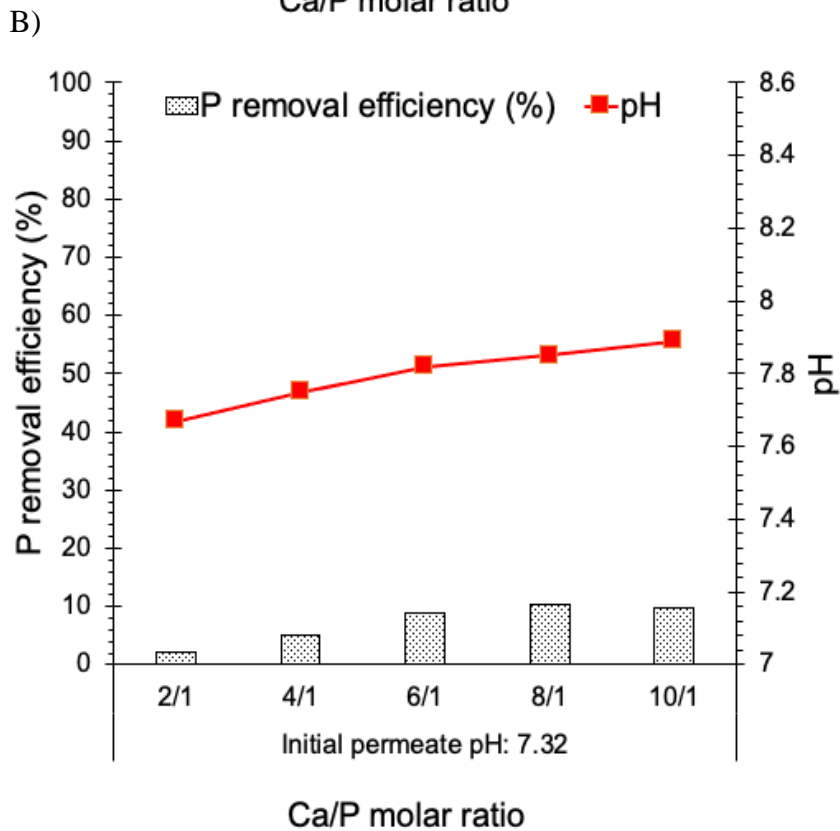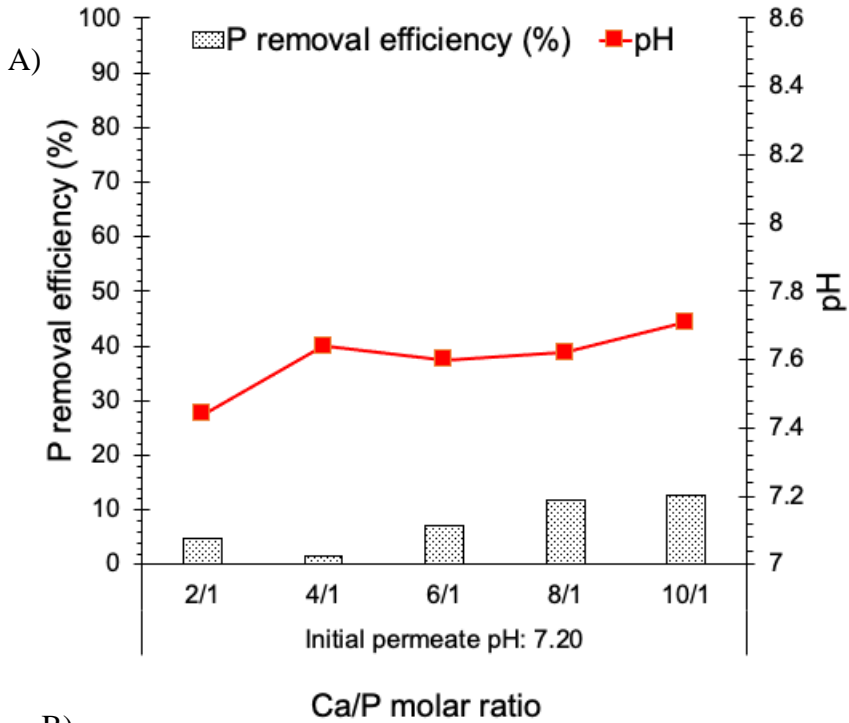
Appendix D

Appendix Figure D.1 A) COD removal efficiency and B) BOD removal efficiency under steady state operation of the Lab scale AnMBR system treating swine wastewater

Bench Scale Jar test protocol

The coagulation experiments were performed by mixing 1 L beakers filled with the swine

permeate solution using a Phipps & Bird 6-paddle jar Stirrer (model 7790-910). Incremental

dosage of calcium coagulant targeting multiple molar ratios of Ca/P were added during rapid

mixing at 100 rpm for 2 min, followed by slow mixing at 30 rpm for 20 min and a final

sedimentation step for 30 minutes which was performed by decanting the solution mixture to 1 L

graduated cylinders for analyzing sludge settleability.

Appendix Figure D.2 Phosphorus removal efficiency and final solution/product pH in AnMBR treated real swine permeate: A) Trial 1 and B) Trial 2, at varying Ca:P ratios using 100% calcium oxide.

Appendix Table D.1 EEM data table summarizing the measured intensity of Tyrosine and Tryptophan- like fluorescence in samples collected after coagulation using CaO in the altered swine permeate.

Ca/P molar ratio	Peak B – Tyrosine Intensity (Raman Intensity units)	% Tyrosine intensity reduction	Peak T – Tryptophan Intensity (Raman Intensity units)	% Tryptophan intensity reduction
Fresh permeate control	0.29	-	0.32	-
2:1	0.27	7.66	0.29	10.15
4:1	0.25	14.68	0.27	14.66
6:1	0.23	19.11	0.26	16.83
8:1	0.22	23.43	0.26	17.56
10:1	0.11	60.66	0.22	29.39